NASA Contractor Report 198363

The Effect of Interface Properties on Nickel Base Alloy Composites

M. Groves, T. Grossman, M. Sensmeier, and K. Wright
GE Aircraft Engines
Cincinnati, Ohio

July 1995

Prepared for
Lewis Research Center
Under Contract NAS3–26501

National Aeronautics and
Space Administration

FOREWORD

The contributions of several persons toward this program should be recognized here: Dr. Steve Arnold served as Program Monitor at NASA LeRC and provided helpful insight to modeling. Dr. Jeff Eldridge performed fiber pushout measurements of the samples fabricated in this program, and Dr. Ajay Misra provided guidance on interface coating selections.

TABLE OF CONTENTS

1. SUMMARY

This program was performed to assess the extent to which mechanical behavior models can predict the properties of sapphire fiber/nickel aluminide matrix composites and help guide their development by defining improved combinations of matrix and interface coating. The program consisted of four tasks: 1) selection of the matrices and interface coating constituents using a modeling-based approach; 2) fabrication of the selected materials 3) testing and evaluation of the materials; and 4) evaluation of the behavior models to develop recommendations. Ni-50Al and Ni-20Al-30Fe (a/o) matrices were selected which gave brittle and ductile behavior, respectively, and an interface coating of PVD YSZ was selected which provided strong bonding to the sapphire fiber. Significant fiber damage and strength loss was observed in the composites which made straightforward comparison of properties with models difficult. Nevertheless, the models selected generally provided property predictions which agreed well with results when fiber degradation was incorporated. The presence of a strong interface bond was felt to be detrimental in the NiAl MMC system where low toughness and low strength were observed.

2.0 INTRODUCTION

2.1 Background

The continuing drive for improved performance and durability from aircraft gas turbine engines requires improved light weight high strength high temperature materials. Such materials will enable turbine engines to operate at higher temperatures, improving efficiency, or to be more durable under current conditions. Fiber reinforcement offers one method for improving the high temperature strength (and stiffness) of materials without sacrificing weight because most high creep strength fibers are also lighter than the metals they reinforce. In principle, reinforcement of current high strength oxidation resistant superalloys would give large increases in creep and rupture capability with little or no loss in oxidation resistance. In addition, even lighter matrices, such as nickel aluminide intermetallics of either NiAl or mixed Ni_3Al-NiAl composition may be possible. These have excellent oxidation resistance due to their high aluminum content. However, these alloys tend to be brittle, and in addition to strengthening the matrix, the fibers may be required to provide toughening of the composite.

Potential reinforcing fibers for such high temperature systems (from 650C up to as high as 1200C) are limited principally to SiC (SCS-6) and single crystal oxides, since other fibers creep excessively above 900C. Because SiC reacts readily with potential Ni, Co, or Fe-base matrices, attention has been focused primarily on single crystal sapphire fibers (Saphikon) as the reinforcement of choice for high temperature MMC. In addition to good creep resistance, the thermal expansion coefficient of sapphire is relatively large for a ceramic, reducing the thermal stresses which develop due to the thermal expansion mismatch between fiber and matrix.

The range of matrix alloy compositions of interest are determined by a combination of properties: oxidation resistance, creep strength (for loading directions other than the fiber direction) and compatibility with the fibers during fabrication and high temperature service. Attention has focused primarily on Ni-base superalloys and aluminides due to their high strength, excellent oxidation resistance, and good chemical compatibility with sapphire. Such systems have been under development for several years now, first under NASA HITEMP funding (Petrasek, 1988) and later under HSCT-EPM.

At the present time, the major technical issues facing the development of such high temperature MMC's are:

1) Good load transfer from the matrix to the fibers in order to fully utilize the fiber strength;

2) Good off-axis (transverse and shear) strength, a primarily non-fiber-dominated property;

3) Resistance to thermal cyclic fatigue caused by thermal expansion mismatch between the fiber and matrix; and

4) Balancing strength against composite toughness.

While there are many potential solutions to solving these challenges, the present program was designed to focus on the role of the interface and interface coatings in controlling key composite properties, with the aim of identifying improved composite interfaces. Such improved composite interface coatings would be beneficial in several ways:

1) The bonding between many Ni-base alloys, especially NiAl, and sapphire is relatively weak and primarily frictional (Bowman, et al., 1991). This leads to poor high temperature longitudinal strength where the thermal clamping stresses relax and load transfer to the fiber becomes poor. A good interface coating should provide a degree of chemical bonding between the fiber and matrix which is less temperature dependent and stronger at high temperatures.

2) The weak interface bond in current Ni-base MMC also leads to poor off-axis composite strengths. Improving the bond strength will permit raising the off-axis strengths from a fraction (approximately half) of the matrix strength to a level close to or even exceeding the matrix strength (Cooper and Kelly, 1968).

3) The thermal cycling and oxidation resistance of the composite can be improved by improving interface strength because a good bond inhibits the transport of oxygen down the interface. This transport of oxygen has been shown to increase internal oxidation especially under thermal cycling conditions where the interfaces are subject to stress (Bowman, et al., 1991).

4) Improving the interface strength would also influence composite toughness, since toughening mechanisms such as fiber pullout and crack deflection are influenced by interface strength. For brittle matrices especially, like NiAl, too strong an interface may prevent toughening and lead to brittle behavior.

5) Interface coatings are also important in controlling high temperature reactions between the fiber and matrix. Thermodynamic aspects of interfaces in these materials have been considered by Misra, 1988.

Thus a careful balance of interface properties is required, and different matrix systems may have different needs. In view of the difficulty and expense of identifying good interfaces empirically by fabricating and testing many different coated MMC systems, an analytical approach was adopted, whereby interface dependent property models were

selected and evaluated to give guidance toward improved coatings. A few coated systems were selected for testing to provide data to check the validity of these models, and the models were re-evaluated in light of these results to assess their usefulness in guiding material development.

2.2 Objectives

The objectives of this program were to assess the extent to which mechanical behavior models can predict the properties of nickel base alloy matrix composites and to help guide the development of these composites by defining improved combinations of matrix and interface coating.

2.3 Approach

The program consisted of four tasks as shown in Figure 1 and described below:

Task 1 - Selection of Systems

Two nickel-aluminide-base composite systems were selected in consultation with NASA LeRC. One brittle matrix (NiAl base) and one ductile matrix (NiAlFe base) were selected to provide a range of matrix properties. The matrices were reinforced with sapphire fibers and fiber/matrix interface properties were controlled by applying a coating on the fibers. Coating selection was based on the predictions of the models using existing property data (extrapolated or approximated where necessary) and consideration of the metallurgical stability of the coatings in contact with the matrices and the fiber. The coated systems were to be compared with existing data on similar uncoated fiber reinforced systrems.

Task 2 - Fabrication of Materials

The sapphire fibers were coated and consolidated into composites. Panels of both the selected composites and the monolithic matrix alloys (without fiber reinforcement) were fabricated using powder cloth processing.

Task 3 - Testing and Evaluation

This task provided the experimental data base against which to evaluate the analytical models. Both composite and constituent (model input) mechanical properties were obtained. The composite tests included room temperature longitudinal and transverse tensile tests, elevated temperature longitudinal tensile tests, and room temperature fracture toughness. The matrix properties measured were matrix stress-strain response as a function of temperature, matrix toughness, and coefficient of thermal expansion. Similar data for the fiber were taken from the literature. Shear strength of the interfaces were measured by fiber pushout tests.

Task 4 - Evaluation of Behavior Models

The models selected and evaluated in Task 1 were re-calculated using the matrix and interface data developed in Task 3. These calculations were compared to the experimental results on composites also developed in Task 3. Validation of the models or determination of their deficiencies was conducted.

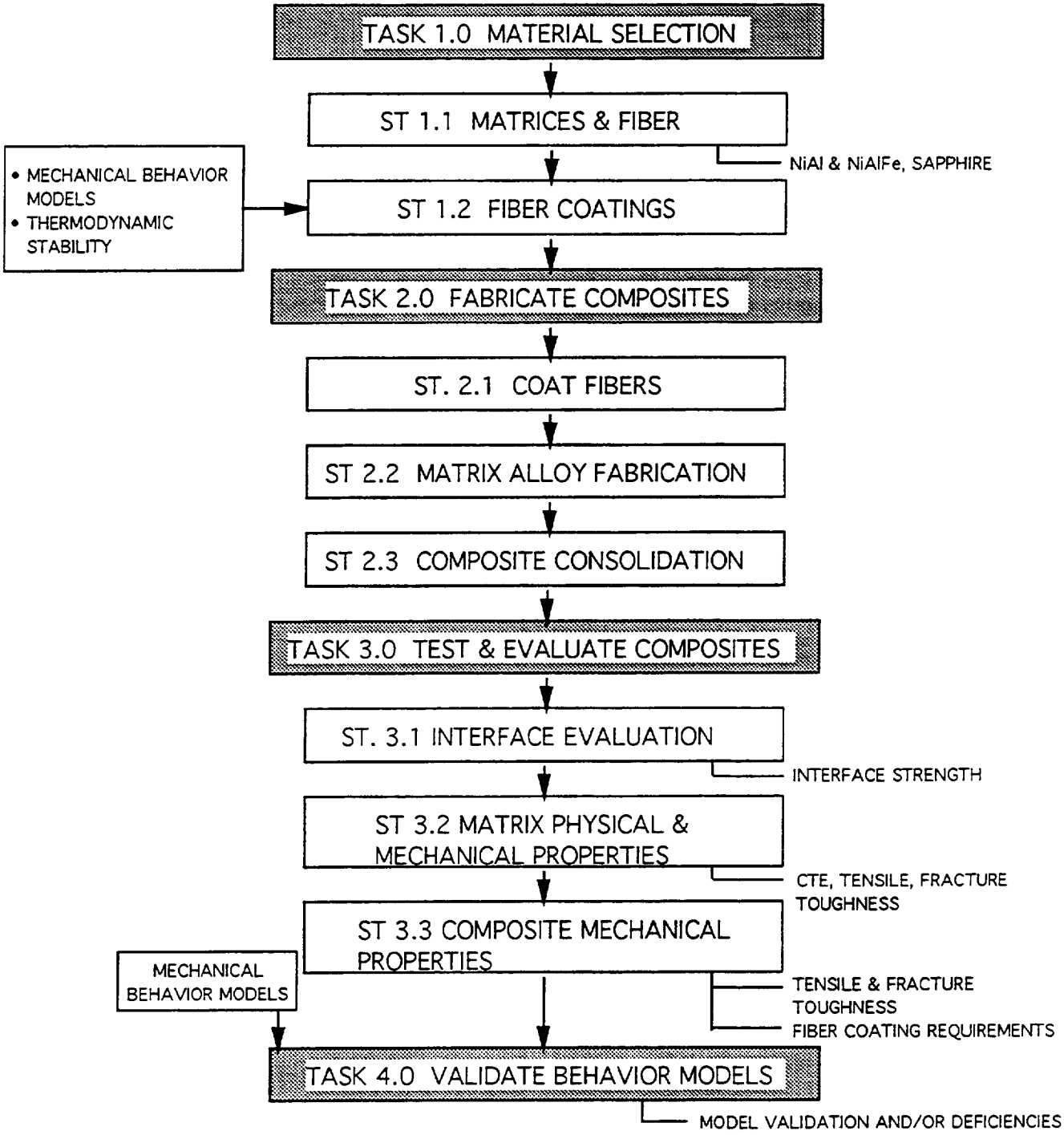

Figure 1 - Outline of Program Plan

3. RESULTS

3.1 Task 1 - Selection of Systems

The system of sapphire reinforced nickel-aluminide base alloys was selected for study based on the reasons presented in the Introduction. The steps in selecting the specific matrix alloys and coatings to be studied was as follows: First, property models were selected for each key composite mechanical property to be studied. Next, the potential (but realisitic) range of matrix and interface coating properties were assessed and defined from the literature and in-house data. Then the models were executed with a range of these property values, and finally the results of the modeling were evaluated to select a limited number of materials for study and confirmation of the modeling in Tasks 2 through 4.

The types of models required for this study were determined to be those which related to basic composite mechanical properties that were typically evaluated in composite material development programs, namely, longitudinal and transverse tensile strength at room and elevated temperture, as well as a measure of composite toughness. While other properties such as fatigue and creep resistance are required for actual application of these materials to gas turbine components, this program was primarily intended at aiding material development. It was felt that if good progress could be achieved in improving some of the "simpler" composite properties, then the more complex life properties would probably improve as well.

Therefore, the following mechanical properties were selected for study and modeling:

- longitudinal tensile strength,
- transverse tensile strength, and
- toughness in the presence of a notch perpendicular to the fibers.

Because of the ever-present nature of thermal residual stresses in MMC, and their demonstrated importance to mechanical properties, analytical modeling for thermal residual stresses was also included as a first step in applying the other models. As part of the thermal and mechanical loading evaluation, a model to analyze for the presence of matrix cracking was also included, since the presence of matrix cracks will determine in part whether a brittle (cracks present) or ductile (cracks absent) modeling approach should be used.

3.1.1 Analytical Model Selection

The behavior models were selected using the following criteria:

- The models must reasonably represent the physical processes occurring in the composite.
- The models must be usable for studying the effect of interfaces and coatings on composite behavior.
- The models must be available "off the shelf" for immediate use on this program.
- The models should be relatively simple (closed form if possible) so that a large number of iterations on different material combinations could be performed.

These criteria effectively eliminated finite element models which, though powerful, tend to be computationally intensive and awkward to incorporate interface sliding effects.

The models used in the analyses are described below, including the references and a description of the basic principles of each model.

3.1.1.1 Residual Stress Model

The residual stress state in both the fiber and the matrix was analyzed using the concentric cylinder model used by Wright, et al (1993). To enable the inclusion of matrix plasticity in the analysis, the matrix portion of the concentric cylinder is divided into a number of "sub-rings" (see Figure 2).

The nonlinear problem of predicting elasto-plastic residual stresses during cooldown is modeled using an incremental procedure. The total temperature change from processing temperature to room temperature is divided into small increments ΔT. For each increment, a linear thermal elasticity problem is solved. A brief summary of this procedure is presented here (for full details, see Hecker, 1968).

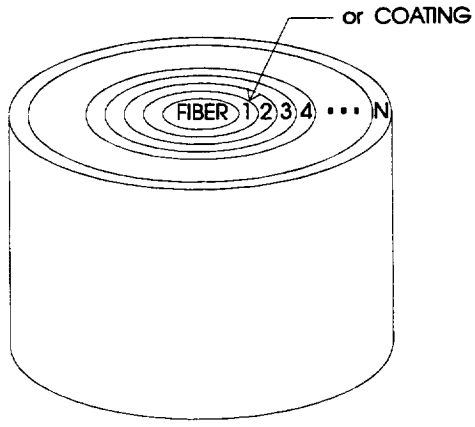

Figure 2 - Schematic of concentric cylinder model

For a concentric cylinder model with a fiber embedded in N rings of matrix (or coating), the equilibrium of forces is given by

$$\frac{d\sigma_r}{dr} + \frac{\sigma_r - \sigma_\theta}{r} = 0 \tag{1}$$

and the axisymmetric strains are given by

$$\varepsilon_z = \frac{dw}{dz}, \quad \varepsilon_r = \frac{du}{dr}, \quad \varepsilon_\theta = \frac{u}{r} \tag{2}$$

where u, w are the radial and axial deflections, respectively. Using Hooke's Law for an elastic material (or a linear increment of a plastic material), the equilibrium equation becomes

$$\frac{d^2u}{dr^2} + \frac{1}{r}\frac{du}{dr} - \frac{u}{r^2} = 0 \tag{3}$$

The solution to this equation within ring i is of the form

$$u_i = C_1^i r + \frac{C_2^i}{r} \tag{4}$$

So the total solution of the problem is known if the coefficients C_1 and C_2 are known for each layer. Also, the total axial strain ε_z, which is constant, is an unknown to be determined. Thus, the total number of unknowns in the problem is 2N+3.

Enforcing continuity of radial displacements at the ring interfaces provides N equations, and the continuity of radial tractions provides an additional N+1 equations. Requiring displacements to be finite forces C_2 for the fiber to be zero. This makes a total of 2N+2 equations. The final equation is obtained by setting the resultant force integrated over all the rings to be zero, or

$$\sum_{i=0}^{N} \sigma_z^i \, 2\pi r dr = 0 \tag{5}$$

This results in a system of 2N+3 linear equations in 2N+3 unknowns, which are then solved using a linear solver subroutine. Once the coefficients are known, the stresses in each layer i are given by

$$\begin{aligned}
\sigma_r &= K^i\left[C_1^i - \frac{C_2^i}{r^2}(1-2\nu^i) + \nu^i\varepsilon_z - (1+\nu^i)\alpha^i\Delta T\right] \\
\sigma_\theta &= K^i\left[C_1^i + \frac{C_2^i}{r^2}(1-2\nu^i) + \nu^i\varepsilon_z - (1+\nu^i)\alpha^i\Delta T\right] \\
\sigma_z &= K^i\left[C_1^i 2\nu^i + (1-\nu^i)\varepsilon_z - (1+\nu^i)\alpha^i\Delta T\right]
\end{aligned} \tag{6}$$

and the strains in layer i are given by

$$\varepsilon_\theta = C_1^i + \frac{C_2^i}{r^2}, \quad \varepsilon_r = C_1^i - \frac{C_2^i}{r^2} \tag{7}$$

Matrix plasticity in each ring is implemented using the incremental stress-strain relations of the form:

$$d\varepsilon_1 = \frac{1}{p}[d\sigma_1 - m(d\sigma_2 + d\sigma_3)]$$

$$d\varepsilon_2 = \frac{1}{p}[d\sigma_2 - m(d\sigma_1 + d\sigma_3)]$$

$$d\varepsilon_3 = \frac{1}{p}[d\sigma_3 - m(d\sigma_1 + d\sigma_2)] \tag{8}$$

where $d\varepsilon$, $d\sigma$ are the total (elastic+plastic) strain and stress increments, respectively, p is the instantaneous tangent modulus, and m is the instantaneous Poisson's ratio (p and m are equivalent to E and ν in the elastic region). The constitutive relationships utilize the temperature-dependent effective stress-strain curves, where effective stress and strain increments are defined by

$$d\bar{\varepsilon} = \frac{\sqrt{2}}{2(1+m)}\left[(d\varepsilon_1 - d\varepsilon_2)^2 + (d\varepsilon_2 - d\varepsilon_3)^2 + (d\varepsilon_1 - d\varepsilon_3)^2\right]^{\frac{1}{2}}$$

$$d\bar{\sigma} = \frac{1}{\sqrt{2}}\left[(d\sigma_1 - d\sigma_2)^2 + (d\sigma_2 - d\sigma_3)^2 + (d\sigma_1 - d\sigma_3)^2\right]^{\frac{1}{2}} \tag{9}$$

It has been noted that predictions of residual stress made by this implementation of the concentric cylinder model tend to be about 10 to 15% higher (more conservative) than those from elastic-plastic finite element models (Nimmer, 1990) or the NASA-sponsored MCCM (Williams and Pindera, 1994). This discrepancy should be kept in mind when comparing results between models. However, it was felt that this difference was small enough (and consistent enough) to make satisfactory conclusions for guidelines for materials development directions.

3.1.1.2 Matrix Cracking Model

To predict the effect of the cooldown from processing temperature on the integrity of the composite systems, the matrix cracking criterion presented by Lu, et al (1991) was applied. This analysis was used to predict whether either system, particularly the brittle matrix system, would contain matrix cracks upon fabrication but prior to mechanical loading. This method includes both large macrocracks perpendicular to the fibers as well as smaller radial microcracks around the fibers (see Figure 3).

The cracking criteria in this model are based on a non-dimensional group $\Re$, defined as

$$\Re = R(E_m \varepsilon_T / K_m)^2 \tag{10}$$

where R is the fiber radius, K_m the matrix toughness, E_m the matrix modulus, and ε_T the misfit strain. Matrix cracking (of either type) is predicted to occur when $\Re$ is greater than some critical value $\Re_C$. The critical value, $\Re_C$, depends on the properties of the constituents, the fiber volume fraction, and the interfacial friction. This value also differs

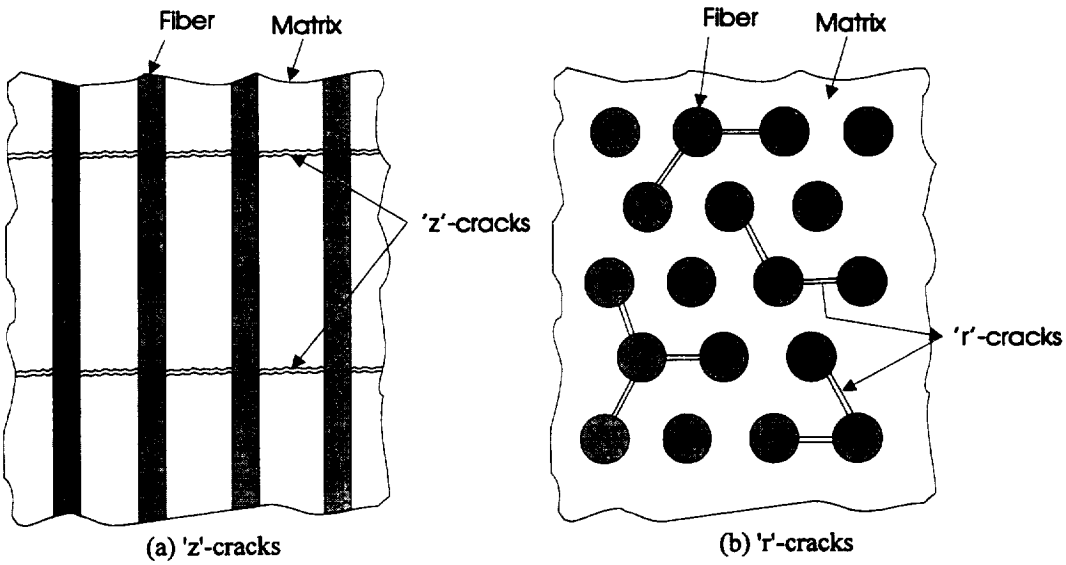

Figure 3 - Types of cracks considered by matrix cracking model of Lu, et al.

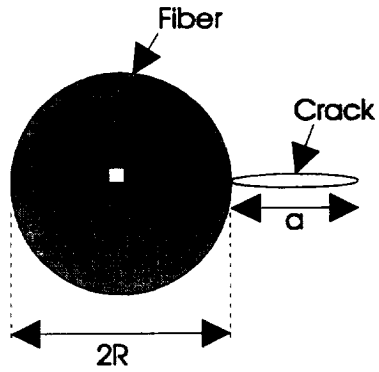

Figure 4 - Radial 'r'-crack at isolated fiber

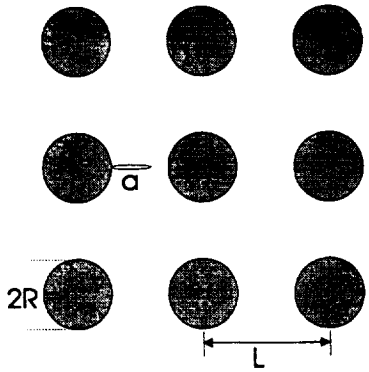

Figure 5 - Multi-fiber problem for 'r'-cracks

depending on which type of cracking is being considered.

'Z'-cracks (Figure 3a) - For a well-bonded interface, a good approximation for $\Re_c$ is presented by Lu, et al (where here the elastic moduli are assumed the same for both the fiber and matrix) as

$$\Re_c = \sqrt{6}B^2(1-\nu)^3(1+\nu)^{\frac{2}{2}}/f(1-f) \tag{11}$$

where B is a coefficient between 0.8 and 1, f is the fiber volume fraction, and ν is the composite Poisson's ratio.

For an interface which is poorly bonded or completely unbonded, the critical value $\Re_c$ is then given by

$$\Re_c = 3\mu(1-\nu)/f \tag{12}$$

where μ is the friction coefficient of the debonded surface.

'r'-cracks (Figure 3b) - The critical value $\Re_c$ for the radial crack case is obtained through a stress intensity calculation. First, if one considers a radial crack at an isolated fiber (Figure 4), the cracking number for a well-bonded composites is found to be

$$\Re_c = 17.5(1-\nu)^2 \tag{13}$$

For a crack which debonds along the interface rather than arrest there, a lower bound for $\Re_c$ is given by

$$\Re_c = 4(1-\nu)^2 \tag{14}$$

To include the effect of neighboring fibers, the stress intensity factor can easily be calculated for the multi-fiber problem shown in Figure 5. The results of this type of analysis are presented in Lu, et al. (1991).

3.1.1.3 Constitutive Response Model

The stress-strain responses of the composite materials were predicted using the method of cells presented by Aboudi (1986). The Aboudi model considers a regularly spaced array of rectangular (for simplicity) fibers (Figure 6). The approach for this model is to first define a unit cell of the composite (Figure 7). The equations of equilibrium are then applied to this 4-cell model. Additionally, displacement continuity and traction continuities between the appropriate subcells are enforced. This results in a closed-form set of equations to solve for the average response of the composite given the properties of the constituents.

Matrix plasticity is incorporated into the matrix subcells using the unified theory of plasticity of Bodner (1986). This theory reduces to five material parameters which are considered inputs to the Aboudi model. These parameters are:

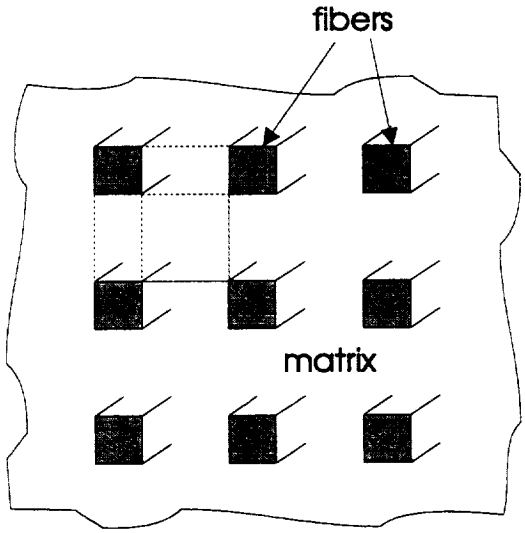

Figure 6 - Cross-section of composite considered by Aboudi model

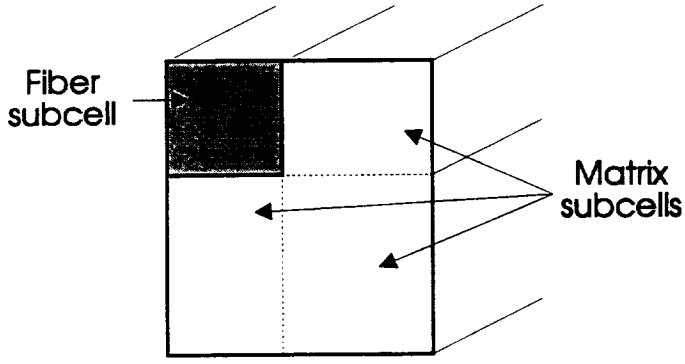

Figure 7 - Definition of unit cell of composite for Aboudi model.

- Z_0 related to the uniaxial yield stress
- Z_1 related to the uniaxial ultimate stress
- m rate of work-hardening
- n rate sensitivity
- D_0 limiting strain rate

The effects of imperfect fiber-matrix bonding are incorporated through two bonding efficiency parameters R_n and R_t., where the subscripts n and t denote, respectively, normal and tangential. These parameters describe the jump of normal or tangential displacement across the fiber/matrix interface. Thus, a bonding parameter value of zero indicates a perfect bond, while a value of ∞ (or some large number, say 50) indicates a complete disbond.

The effect of imperfect bonding has little or no effect on longitudinal stress-strain, but can have a quite large effect on transverse behavior. Based on experience with titanium matrix composites, one would expect transverse stress-strain to exhibit a kind of bi-linear behavior. While the radial residual stresses are still in force, the composite behaves as if the fiber and matrix were well-bonded. However, when enough transverse stress is applied, the residual clamping is overcome and the composite behaves as if the fiber and matrix were imperfectly bonded.

Experience with the SiC/Ti composites suggests that when the transverse stress in the subcell directly beside the fiber subcell reaches a tensile value equal to the compressive residual stress, separation will occur. Thus, the method used in this effort was to model the composite response two times, once with a perfect bond and once with an imperfect bond (R_n=R_t=0.00001). The two curves are then patched together at the point where separation is expected.

3.1.1.4 Longitudinal Strength Models

The simplest model for predicting composite strength is rule-of-mixtures. This model predicts the fiber-direction strength by

$$\sigma_1^u = f\sigma_f^u + (1-f)\sigma_m^y \tag{15}$$

where f is again the fiber volume fraction, σ_f^u is the ultimate tensile strength of the fiber, and σ_m^y is the matrix yield strength. Here, the matrix yield is used rather than the ultimate strength. This is because the strain to failure of the sapphire fibers is fairly low compared to the total elongation of either matrix, so the stress which develops in the matrix is not likely to greatly exceed its yield stress.

The rule-of-mixtures model often does not predict well the strength of composites with brittle matrices or fiber/matrix sliding. Curtin (1993) has presented a theory for ultimate strength of fiber-reinforced ceramics and metals which incorporates interfacial sliding as well as the statistical nature of the fiber strengths. The ultimate strength

expression presented by Curtin for a brittle-matrix composite is

$$\sigma_1^u = f\bar{\sigma}\left[\left(\frac{1}{m+2}\right)^{1/(m+1)}\left(\frac{m+1}{m+2}\right)\right]\left[\frac{2\tau L_0}{r\bar{\sigma}\ln 2}\right]^{1/(m+1)} \tag{16}$$

where σ is the mean fiber strength (50% failure probability) at gauge length L_0, m is the Weibull modulus of fiber strength, τ is the interfacial sliding friction, and r is the fiber radius. For a ductile-matrix system with a fairly strong matrix, Curtin presents the following expression for ultimate strength

$$\sigma_1^u = f\bar{\sigma}\left[\left(\frac{1}{m+2}\right)^{1/(m+1)}\left(\frac{m+1}{m+2}\right)\right]\left[\frac{2\tau L_0}{r\bar{\sigma}\ln 2}\right]^{1/(m+1)} + (1-f)\sigma_m^y \tag{17}$$

3.1.1.5 Transverse Strength Models

Although the Aboudi model is effective for predicting transverse stress-strain response of a composite with matrix plasticity and imperfect interfacial bonding, it has been less successful for predicting transverse strength. For the current program, strength expressions presented by Cooper and Kelly (1968) were used.

For a system with a weak fiber-matrix bond, failure is expected to occur at locations where the matrix ligaments are smallest. The resulting expression for ultimate transverse strength is then given by

$$\sigma_2^u = \sigma_m\left(1-\sqrt{\left(\frac{4f}{\pi}\right)}\right) \tag{18}$$

where σ_m is the matrix strength and f is again the fiber volume fraction.

A second case could exist where the interface debonding strength (for normal mode I debonding) has a non-zero strength, but still less than the matrix strength. For this system, Cooper and Kelly present a "law of mixtures" approach expressed as

$$\sigma_2^u = \sigma_m\left(1-\sqrt{\left(\frac{4f}{\pi}\right)}\right)+\sigma_i'\left(\sqrt{\frac{4f}{\pi}}\right) \tag{19}$$

where σ'_i is the average tensile stress necessary to cause fiber-matrix separation during transverse loading.

3.1.1.6 Fracture Toughness Models

A simple approach for predicting the fracture toughness of a composite would be to apply a rule-of-mixtures method similar to that used for predicting longitudinal strength. That is, the composite toughness would be given by

$$K_c = fK_c^f + (1-f)K_c^m \tag{20}$$

where K_c^f and K_c^m are the fracture toughness of the fiber and matrix, respectively. However, for the current program (and for most composites), the fiber fails in a brittle manner, thus contributing only negligibly to the composite toughness. Only the matrix portion would then contribute to the composite fracture toughness.

However, other fracture mechanisms have been observed in these types of composites which contribute to the energy absorption during fracture. In this study, we considered two mechanisms which were considered to be potentially important:

1. Fiber bridging - matrix crack propagates leaving unbroken fibers in its wake which inhibit the stress intensity at the crack tip
2. Matrix plasticity - brittle fibers fail ahead of propagating matrix crack, matrix ligaments then fail in a ductile manner

The proposed expression for the composite toughness which was used in this program is

$$K_c = (1-f)K_c^m + \Delta K_c \tag{21}$$

where ΔK_c is the toughness contribution due to either fiber bridging or local matrix plasticity. If the actual fracture mechanism is known, the appropriate relationship can be chosen. If not, then the two values can give bounds for the expected toughness.

Two different fiber bridging relationships were selected for this analysis. The first is a method presented by Marshall and Cox (1987), which is based on a stress intensity approach for bridged cracks. The simplified expression for the influence of fiber bridging on composite toughness is

$$\Delta K_c = (1-f)K_c^m \left\{ \left[1 + 4\left(\sigma_f^u f/\sigma_n\right)^3 \right]^{\frac{1}{2}} - 1 \right\} \tag{22}$$

where

$$\sigma_n = \left[3\alpha^2 (1-f)^2 (K_c^m)^2 (1-\nu^2)/E_c \right]^{\frac{1}{3}} \tag{23}$$

and

$$\alpha = \left[\frac{4\tau f^2 E_f E_c}{R E_m (1-f)} \right]^{\frac{1}{2}} \tag{24}$$

where τ is the interfacial sliding friction, ν is the composite Poisson's ratio, R is the fiber radius, and E_f, E_m, and E_c are the fiber, matrix, and composite moduli, respectively.

A second approach for predicting the effect of fiber bridging on composite toughness was presented by Phillips and Tetelman (1972). They presented a number of

expressions for theoretical models of energy absorption. For fiber bridging, the predicted effect on composite toughness is given by

$$\Delta K_c = \left[\frac{2fR(\sigma_f^u)^3 E_c(1+\nu_f)(1-2\nu_f)}{12\tau E_f(1-\nu_f)} \right]^{\frac{1}{2}} \tag{25}$$

where ν_f is the Poisson's ratio of the fiber.

For the effect on composite toughness of local matrix plastic deformation, Phillips and Tetelman give the following expression

$$\Delta K_c = \left[\frac{(1-f)^2 \sigma_m^u R (K_c^m)^2 E_c}{f \tau_m^u E_m} \right]^{\frac{1}{2}} \tag{26}$$

where $\sigma_m{}^u$ and $\tau_m{}^u$ are the ultimate normal and shear strengths of the matrix material.

3.1.1.7 Crack Growth Direction

Buczek and Herakovich (1983) have presented a model for predicting the growth direction for a crack in an arbitrarily loaded and arbitrarily oriented composite (see Figure 8). The model is based on the assumption that crack extension will occur in the direction ϕ which maximizes the normal stress ratio, defined as

$$R(r_0, \phi) = \frac{\sigma_{\phi\phi}}{T_{\phi\phi}} \tag{27}$$

where $\sigma_{\phi\phi}$ is the normal stress acting on the radial plane at a given distance r_O from the crack tip (see Figure 9), and $T_{\phi\phi}$ is the tensile strength on the ϕ plane. $T_{\phi\phi}$ is taken as

$$T_{\phi\phi} = \sigma_1^u \sin^2\beta + \sigma_2^u \cos^2\beta \tag{28}$$

where β is the angle from the plane of interest to the fiber direction. Equation (28) satisfies the three conditions:

1. $T_{\phi\phi}$ is equal to the longitudinal tensile strength $\sigma_1{}^u$ for crack growth perpendicular to the fibers
2. $T_{\phi\phi}$ is equal to the transverse tensile strength $\sigma_2{}^u$ for crack growth along the fibers
3. $T_{\phi\phi}$ is independent of ϕ for an isotropic material

To apply the normal stress ratio criterion for crack extension to an anisotropic composite, one must solve for the crack tip stresses. This can be done by using Lekhnitskii's

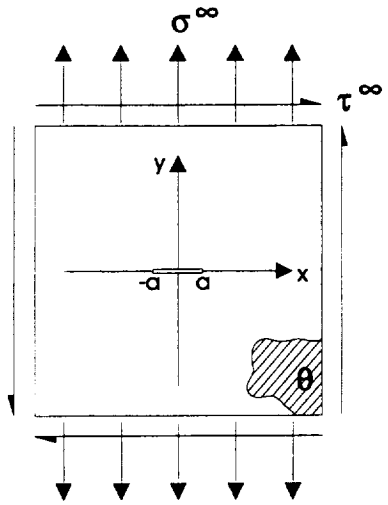

Figure 8 - Composite geometry considered by Buczek & Herakovich

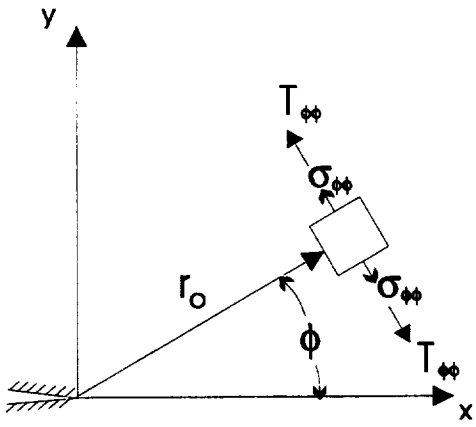

Figure 9 - Schematic definition of Normal Stress Ratio (NSR)

complex variable solution (Lekhnitskii, 1963) for an elliptic hole in an anisotropic plate and reducing the minor axis dimension to zero.

3.1.2 Material Systems Chosen for Analysis

All composites analyzed were assumed to be unidirectionally reinforced with continuous single crystal alumina (sapphire) fibers, approximately 150 microns in diameter.

The composite systems that were modeled at this stage of the program encompassed combinations of three matrix alloys and three classes of coating materials. The three matrix alloys were:

- Ni-50Al (a/o)
- NiCrAlY (Ni-10.2Cr-9.3Al-6.0Ta-0.22Hf-0.43Y) (w/o)
- NiCoCrAlY (Ni-20.8Co-17.8Cr-12.5Al-0.73Hf-0.61Y) (w/o)

The NiAl alloy represents a low ductility, low strength composition with good oxidation resistance and low density. The latter two alloys represented a range of properties that could be obtained with ductile alloys. NiCrAlY has a higher stiffness than NiCoCrAlY (207 GPa compared to 138 GPa) and a higher yield strength (1030 MPa compared to 830 MPa at 25^{o}C). It was intended to select the NiAl alloy as a brittle matrix composition and either NiCrAlY or NiCoCrAlY as a ductile matrix composition for the experimental part of the program.

The three classes of interface coatings which were studied in the modeling effort were:

- Carbides, as represented by TiC
- Oxides, as represented by 8 Yttria-stabilized Zirconia (YSZ) (w/o)
- Metallic, as represented by Ni-32Al-20Fe (a/o)

These coatings were selected to investigate a wide range of potential coating behavior, to indicate the best final coating(s) to select. Carbides, especially SiC, represent a class of coating previously shown to produce weak interfaces in Ni-base MMC. However, their metallurgical stability with nickel alloys is not good. Oxides also are expected to prodice a weak interface since their fracture energy is low. Their stability with nickel alloys and sapphire fiber should be good. Metallic coatings were investigated because they can provide a ductile, tough interface. An additional diffusion barrier coating was considered to be needed for the NiAlFe coating to prevent excessive interdiffusion between it and the matrix alloys. The final coating selected for the experimental portion of the program was included in the modeling in Task 4.

3.1.3 Analytical Model Predictions

3.1.3.1 Residual Stress Predictions

Residual stresses were calculated for all three matrix alloys with various thicknesses of YSZ coating. The system was assumed to be stress-free at 1260C (2300F) with 25 v/o sapphire fibers. Figures 10 and 11 show the predicted radial clamping stress at the interface as a function of coating thickness. Varying the fiber coating thickness had the largest effect on the higher stiffness NiCrAlY matrix composite and a the least effect on the NiAl matrix composite. Varying the fiber coating thickness in the NiCrAlY (and NiCoCrAlY) system can dramatically influence the clamping stress which in turn can influence the interface sliding stress.

3.1.3.2 Matrix Cracking Model Predictions

The calculations for $\Re$ and $\Re_c$ for axial and radial matrix cracking for the three material systems are presented in Table 1. These were all performed assuming fully elastic behavior. For the NiAl system, as shown above, this assumption is conservative because this matrix yields on cooldown, reducing the stresses or energy available for cracking.

Table 1 - Matrix Cracking Predictions for MMC

Material System	**Axial (z) Cracking**			**Radial (r) Cracking**		
	$\Re$	$\Re_c$	Cracking?	$\Re$	$\Re_c$	Cracking?
Sapphire/ NiAl	4.77	3.27	expected	4.77	11.6/2.7*	expected
Sapphire/ NiCoCrAlY	0.59	3.27	no	0.59	11.6/2.7*	no
Sapphire/ NiCrAlY	0.17	3.27	no	0.17	11.6/2.7*	no

* well-bonded interface/unbonded interface

$\Re$ is the non-dimension cracking parameter from Equation (10) and $\Re_c$ (Equations 11 through 14) is the critical level of $\Re$ below which cracking should not occur. Two levels of $\Re_c$ are displayed for radial cracking: the larger one for a well-bonded interface and the smaller one for and unbonded interface (i.e., it is easier for a system with an unbonded interface to crack). Comparison of the $\Re$ and $\Re_c$ values shows that both axial and radial cracking are expected in the Sapphire/NiAl system (if no yielding occurs), but that cracking is not expected in the other two matrices.

3.1.3.3 Transverse Strength Model Predictions

The predicted stress-strain behavior for NiAl and NiCrAlY matrices are shown in Figures 12 and 13. The transverse strength of the NiAl composite is predicted to be much lower than the transverse strength of the NiCrAlY (as well as the NiCoCrAlY) system.

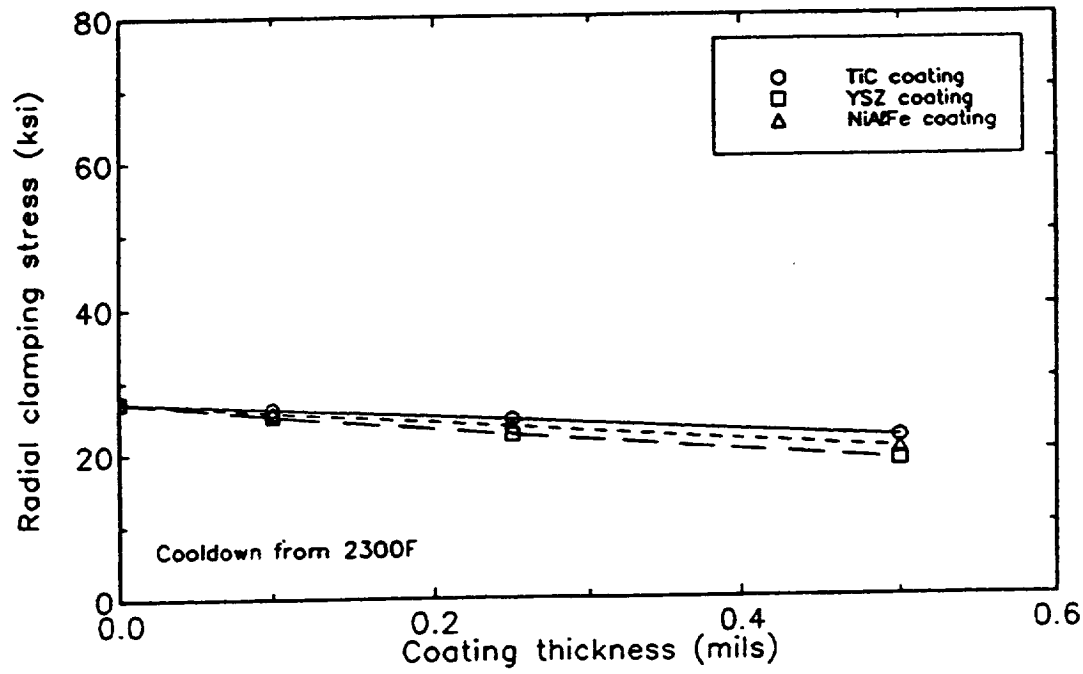

Figure 10 - Predicted Effects of Fiber Coating Thickness on Residual Clamping Stresses. in 25 v/o Sapphire Fiber/NiAl Matrix Composites

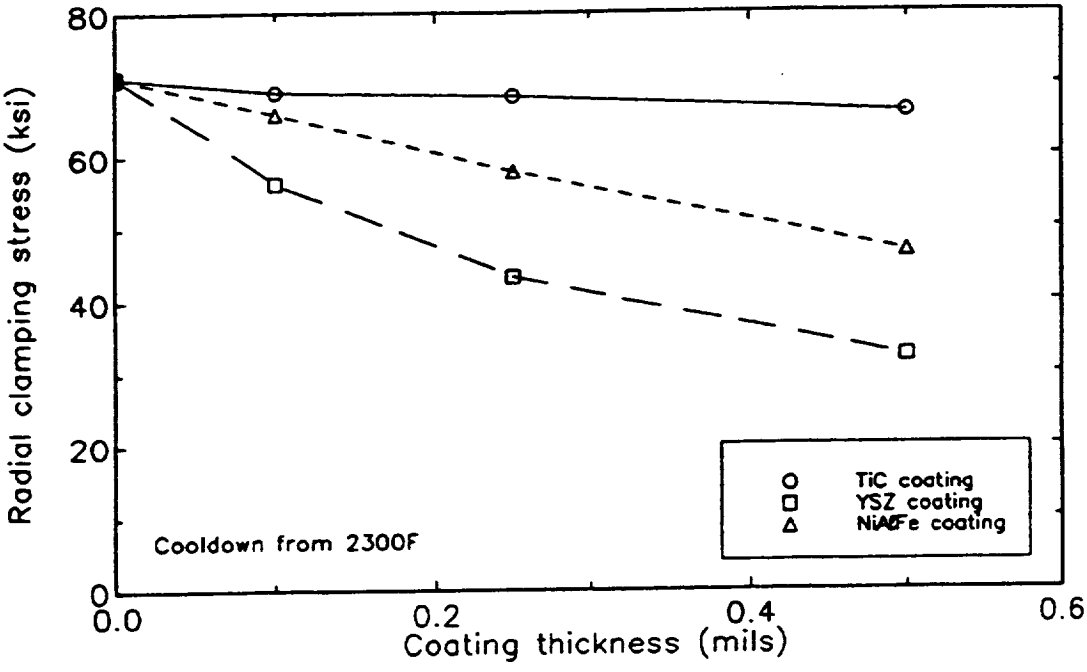

Figure 11 - Predicted Effects of Fiber Coating Thickness on Residual Clamping Stresses. in 25 v/o Sapphire Fiber/NiCrAlY Matrix Composites

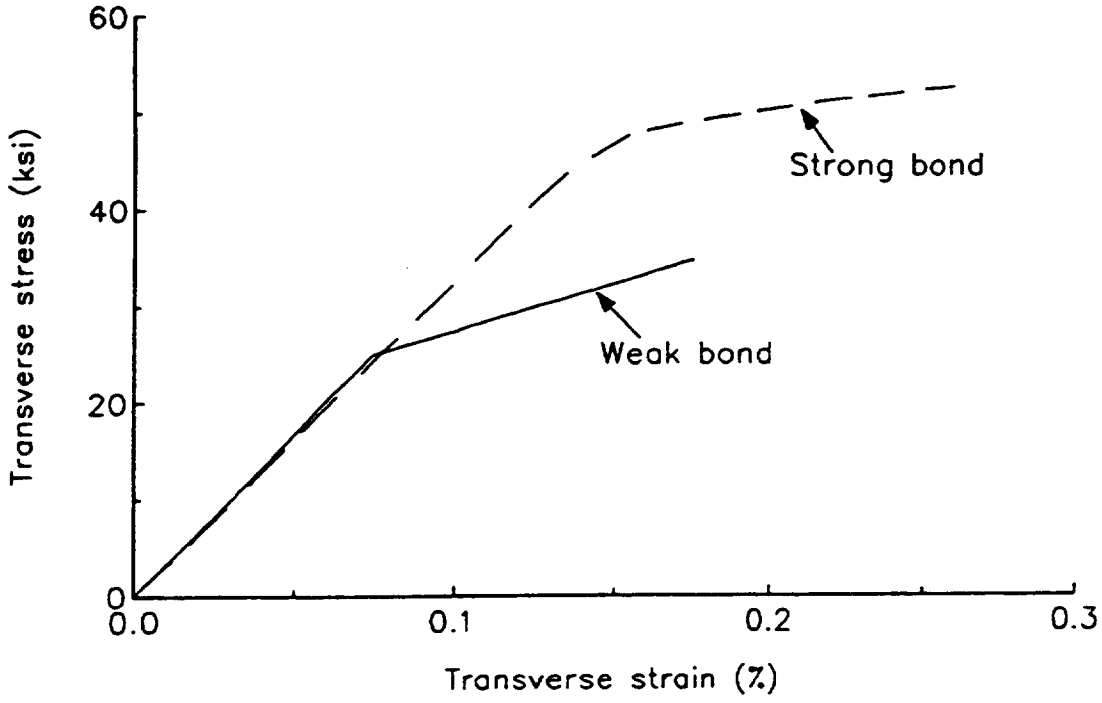

Figure 12 - Predicted Transverse Behavior of 25 v/o Sapphire Fiber/NiAl Matrix Composite

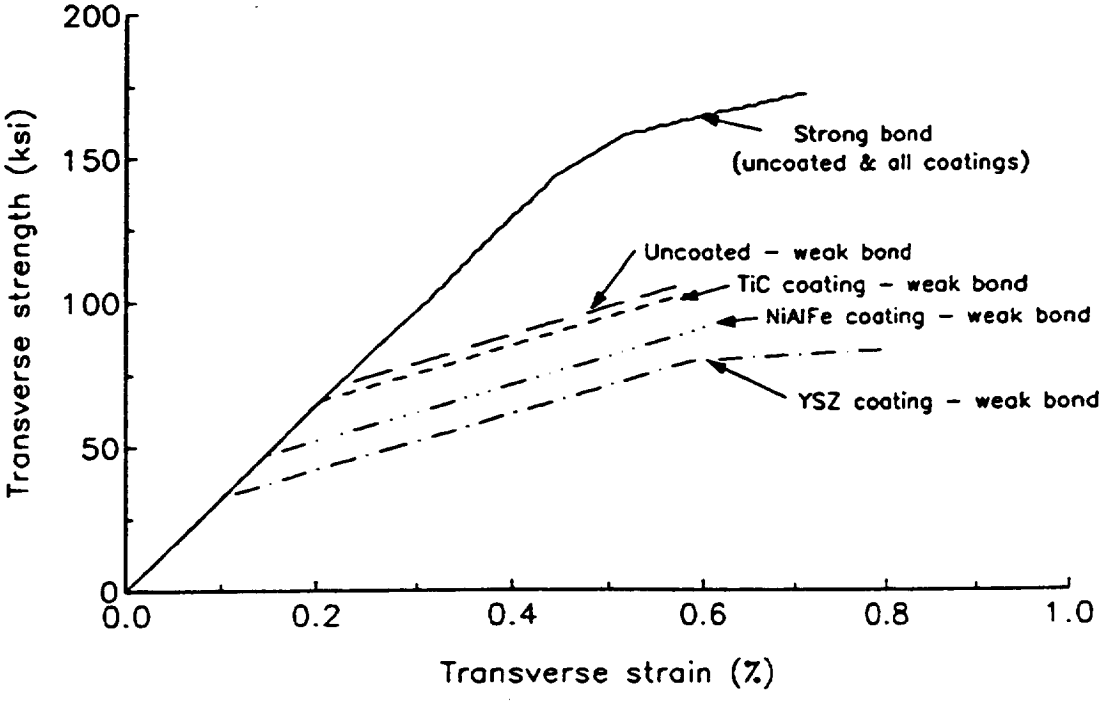

Figure 13 - Predicted Transverse Behavior of 25 v/o Sapphire Fiber/NiCrAlY Matrix Composite

For all of the composites systems, strong bonding at the fiber-matrix interface leads to higher transverse strengths because it inhibits separation of the matrix from the fiber. When there is a weak bond between the fiber and matrix, higher residual clamping stresses will lead to higher transverse strengths. Therefore, the YSZ and NiFeAl coatings which were shown to reduce residual stresses for the NiCrAlY (and NiCoCrAlY) systems will reduce the transverse strengths as shown in Figure 13 if they are weakly bonded. These coatings did not reduce the residual stresses in the NiAl composites and therefore all of the NiAl systems would be expected to show similar transverse strength behavior.

3.1.3.4 Composite Toughness Model Predictions

Figures 14 through 16 show the work of fracture calculated as a function of the interface sliding coefficient of friction for the three matrices with an assumed coating thickness of 12 microns. For equivalent bonding, the toughness of the composites with an NiAl matrix is predicted to be higher than the toughness of the composites with either ductile matrix studied. This is due to the lower frictional stresses at the interface (due to the lower residual clamping stresses) in NiAl which results in longer fiber pull-out lengths. Fiber coatings which reduce the residual clamping stresses should result in higher toughness in the composite. Systems with a high clamping stresses result in composites with little pullout, a more planar fracture surface and thus lower toughness. Therefore YSZ and NiAlFe coatings should increase toughness significantly in the NiCoCrAlY and NiCrAlY systems as shown in Figures 15 and 16.

3.1.3.5 Crack Direction Model Predictions

Figure 17 shows the predicted angle for crack growth for the three composites systems using the Normal Stress Ratio model. The longitudinal and transverse strengths predicted from the strength models described above were used as inputs to this model. The transverse strengths of the NiAl systems are predicted to be always low enough to cause cracks to deflect along the fibers. However, if the transverse strength is sufficiently high, as in well-bonded NiCoCrAlY and NiCrAlY systems, the crack growth direction will change from along the fiber-matrix interface (parallel to the loading) to through the fibers (perpendicular to the loading).

3.1.3.6 Summary of Predictions

Table 2 summarizes the results form calculations of all the models in terms of improvement or degradation for each aspect of composite behavior that was considered by the models. In this table, + indicates property improvement, - indicates property degradation, and 0 indicates no change, as shown in the key. For the NiAl matrix, the models predict that if all of the coatings provided a strong bond between the fiber and matrix the behavior of all three composite systems would be similar. The coatings would improve the crack resistance and transverse strength while degrading composite toughness. The degree of improvement or degradation would be the same order of magnitude for all three of the coating compositions, Crack deflection behavior would not be affected by any of the coatings. If the coatings provided weak bonds, they would also not affect crack deflection behavior. However, they would affect the remainder of

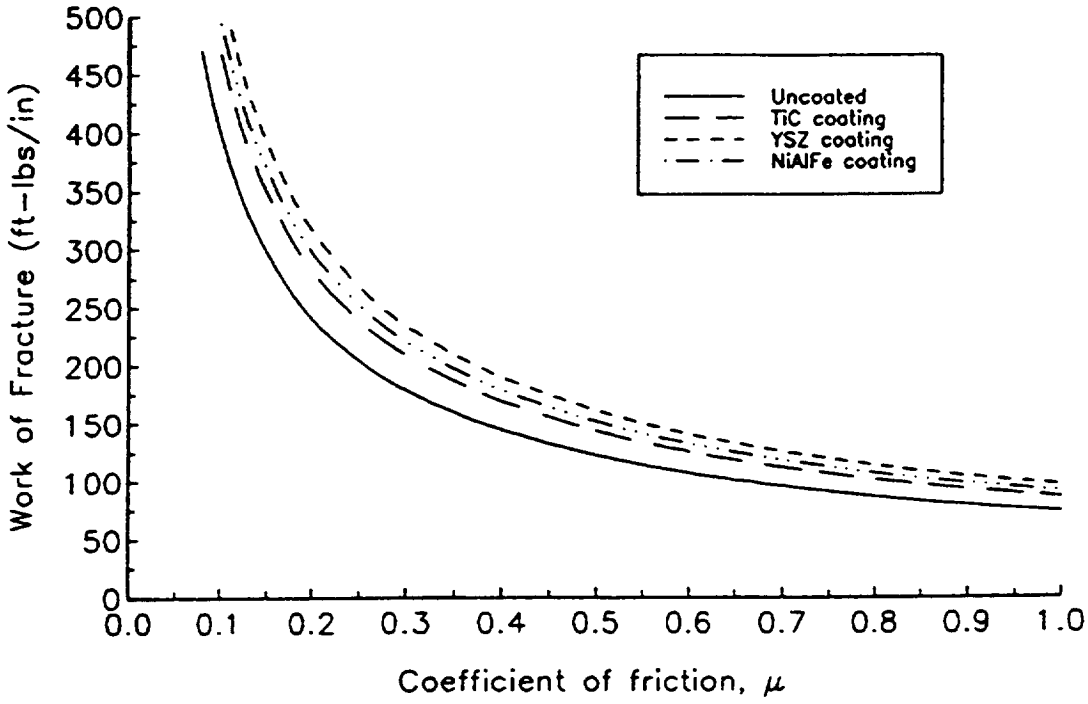

Figure 14 - Predicted Work of Fracture of 25 v/o Sapphire Fiber/NiAl Matrix Composite

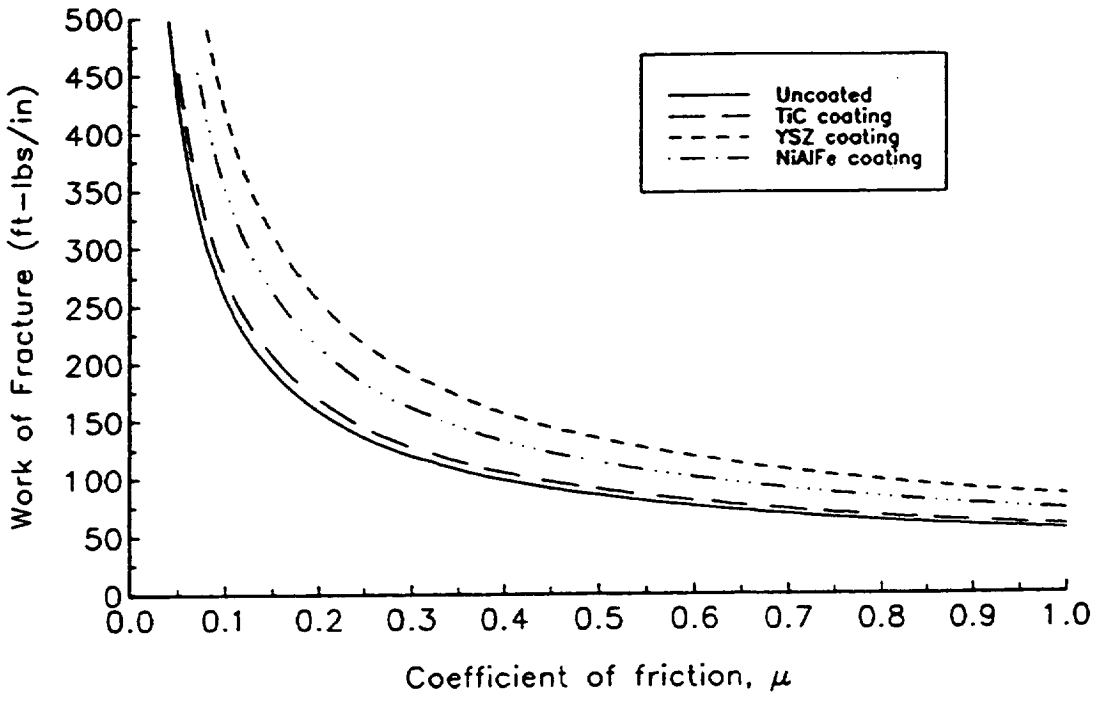

Figure 15 - Predicted Work of Fracture of 25 v/o Sapphire Fiber/NiCoCrAlY Matrix Composite

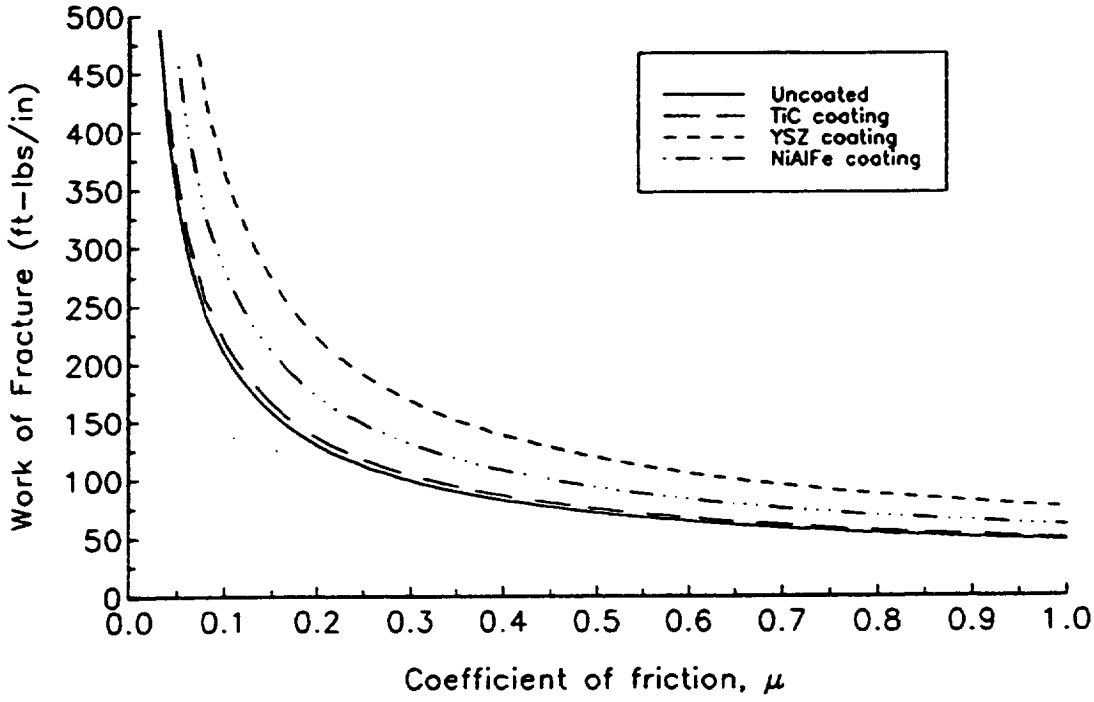

Figure 16 - Predicted Work of Fracture of 25 v/o Sapphire Fiber/NiCrAlY Matrix Composite

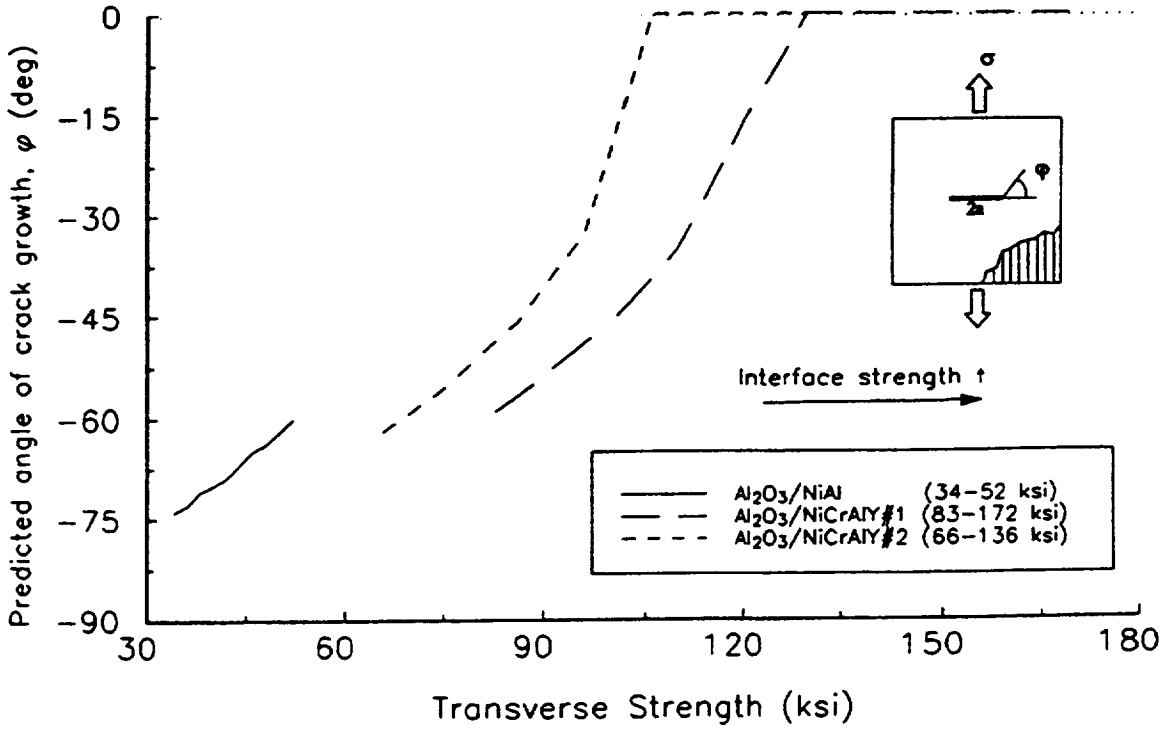

Figure 17 - Predicted Crack Growth Directions in Sapphire Reinforced/Nickel Base Alloy Composites

the composite properties opposite to the effect of coating that provide strong bonds. Thermal stress cracking resistance and transverse strength would be degraded while composite toughness would be improved by coatings providing a weak bond. In addition, the degree of improvement in composite toughness would depend upon coating composition with the YSZ coating providing the most improvement.

Table 2 - Summary of Model Predictions of Interface Effects on Ni-base Matrix Composites

Property	TiC Coating		YSZ Coating		NiAlFe Coating	
	weak bond	strong bond	weak bond	strong bond	weak bond	strong bond
NiAl Matrix (brittle)						
Matrix Cracking	-	+	-	+	-	+
Transverse Strength	-	+	-	+	-	+
Toughness	+	-	++	-	++	-
Crack Deflection	0	0	0	0	0	0
NiCoCrAlY Matrix (ductile)						
Matrix Cracking	0	0	0	0	0	0
Transverse Strength	-	+	--	+	--	+
Toughness	+	-	++	-	++	-
Crack Deflection	+	-	++	-	++	-
NiCrAlY Matrix (ductile)						
Matrix Cracking	0	0	0	0	0	0
Transverse Strength	-	+	--	+	--	+
Toughness	+	-	++	-	++	-
Crack Deflection	+	-	++	-	++	-

KEY

large degradation	small degradation	no effect	small improvement	large improvement
--	-	0	+	++

The effects of the fiber coatings on composite systems with either the NiCoCrAlY or NiCrAlY matrix would be similar. Unlike the systems using the NiAl matrix, crack resistance would not be affected but crack deflection would be affected by coating composition and bond strength. Again, weak and strong bonds would have opposite effects. Strong bonds would improve transverse strength but degrade composite toughness and crack deflection. Weak bonds would degrade transverse strength but improve composite toughness and crack deflection. The degree of improvement in these latter properties would be dependent on coating composition with YSZ offering the largest improvement.

3.1.4 Selection of Materials

Based on the results of the analytical modeling, the first four composite systems listed in Table 3 were initially considered for fabrication and testing.

Table 3 - Materials Considered for Fabrication

Fiber	Coating	Matrix	Final Selections
Sapphire	YSZ[1]	NiCoCrAlY[3]	-
Sapphire	NiAlFe[2]	NiCoCrAlY	-
Sapphire	YSZ	NiAl[4]	*
Sapphire	NiAlFe	NiAl	-
Sapphire	YSZ	NiAlFe	*

1) Zirconia-8Yttria (w/o)
2) Ni-20Al-30Fe (a/o)
3) Ni-20.8Co-17.8Cr-12.5Al-0.61Y-0.73Hf (w/o)
4) Ni-50Al (a/o)

Processing trials were conducted at GE to make unreinforced and uncoated sapphire reinforced NiCoCrAlY and NiAl. Satisfactory consolidation conditions could be identified for the NiCoCrAlY matrix composites, but subsequent testing of the unreinforced materials so processed showed that the matrix ductility (total elongation) was poor: approximately 1.5% elongation to failure at room temperature. Since the "ductile" matrix composite models assume a ductility of at least 6 to 8%, this was felt to be inadequate to represent a ductile matrix system. Processing trials on NiAl MMC yielded matrix cracking and delamination which were unacceptable to good composite properties.

In view of these fabrication difficulties, the material fabrication plan was altered as follows: The NiCoCrAlY matrix was replaced by Ni-20Al-30Fe (a/o), since this alloy has been previously been shown by other GE work to produce a ductile system. In addition, this eliminated the need for NiAlFe coating and its reaction barrier coating, since the coating composition was now the matrix. Only one coating composition was

selected, YSZ, for both ductile and brittle matrix systems since the NiAlFe was unnecessary in the NiAlFe matrix system and no diffusion barrier coating could be identified for the NiAl system. Finally, it was decided to fabricate the NiAl panels at NASA LeRC since they had showed good success in making sound NiAl MMC.

3.2 Task 2 - Fabrication of Materials

3.2.1 Fabrication of Materials

Sapphire fiber was obtained and coated in 25 mm (1") wide mats of 4.3 fibers/mm (110 fibers/inch) by sputtering at GE to a coating thickness of approximately 2 to 3 microns, Figure 18.

The plan for panel fabrication shown in Table 4 was carried out:

Table 4 - Fabrication Plan for Unreinforced and MMC Material

Matrix	Reinforcement	Serial Numbers	Size	Source
NiAlFe	Unreinforced	5/6/93-1 5/6/93-2 5/7/93	3" diameter x 1" thick	GE-AE
NiAlFe	YSZ-coated Sapphire	5/8/93 5/10/93 5/11/93 5/12/93	3" diameter x 0.12" thick	GE-AE
NiAl	YSZ-coated Sapphire	93-089 #1 93-089 #2 93-089 #3	2" wide x 6" long x 6 ply	NASA

No unreinforced NiAl matrix was fabricated since properties of unreinforced NiAl were obtained from prior NASA studies (Bowman et al., 1989, Noebe et al. 1990).

The unreinforced NiAlFe material was fabricated from -150 mesh powder without binder loaded into a 76 mm (3") diameter stainless steel can, evacuated, sealed, and vacuum hot pressed at 1177°C/24 MPa/2 hrs (2150F/3.5 ksi/2 hrs) followed by HIPing at 1177°C/172 MPa/2 hrs (2150F/25 ksi/2 hrs).

NiAlFe composites were fabricated by impregnating the fiber mats with matrix powder slurry and drying to a thickness of .46 mm (.018") for a target fiber volume fraction of 30%. Four 76 mm (3") long x 25 mm (1") wide fibers tapes were inserted into 76 mm (3") diameter cans as shown in Figure 19. Extra matrix powder was placed on the outside and top and bottom of the fiber reinforced region. Consolidation conditions were the same as for the unreinforced NiAlFe material.

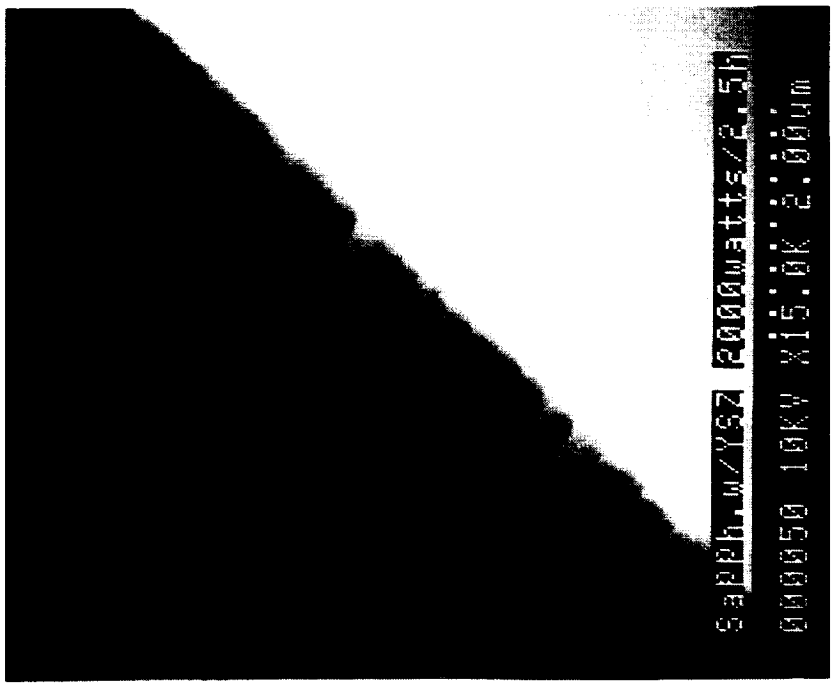

Figure 18 - Respresentative PVD-YSZ Coating Thickness and Structure as Deposited on Sapphire Fiber.

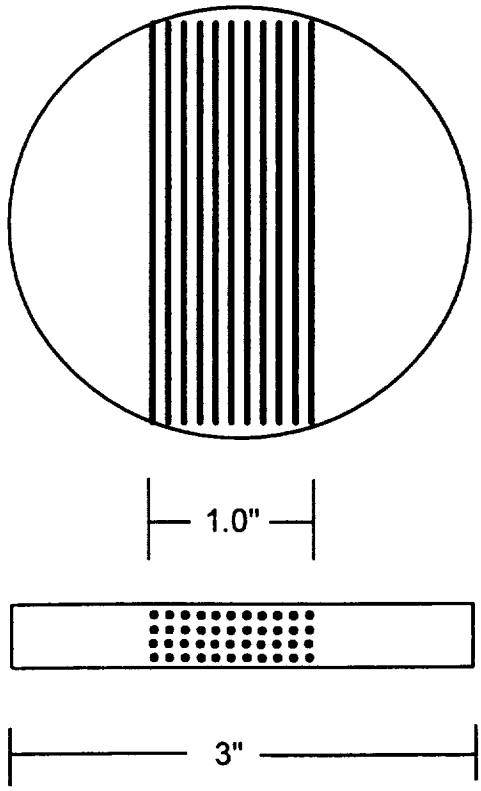

Figure 19 - Layup of NiAlFe MMC

6-ply unidirectionally reinforced YSZ-coated sapphire fiber/NiAl matrix MMC panels 25 mm (1") wide by 152 mm (6") long were fabricated by Dr. Randy Bowman at NASA LeRC by the powder cloth method (Watson et al., 1988).

3.2.2 Microstructual Evaluation of Composites

Fiber digestions, metallography, and in a few cases, ultrasonic inspections were performed on the composite panels to evaluate their quality after fabrication.

Fiber breakage was evaluated qualitatively by dissolving the matrix and exposing the fibers. The fiber condition after matrix digestion is shown in Figures 20 and 21 for the NiAl and NiAlFe composites, respectively. Considerably damage exists in both systems, with the NiAlFe system showing a higher proportion of very short fiber lengths.

In the YSZ-coated Saphikon/Ni-50Al system the two panels used for specimens (93-089 #1 and #2) were examined by metallography. 93-089 #1 could only be examined about 2 cm. from the ends because the longitudinal tensile specimens were taken from the rest of the panel. These near-end regions, however, showed evidence of matrix porosity (Figure 22) and extensive fiber breakage (Figure 23) which if typical of the specimen material, will lead to poor mechanical properties. 93-089 #2 (away from the panel ends) had significantly better features: full matrix consolidation (Figure 24) and unbroken fibers (Figure 25). The fiber coating was thick and uniform on all fibers (Figure 26).

In the YSZ-coated Saphikon/NiAlFe system metallography showed that the fibers wandered out of the intended fiber plane and resulted in the top-most ply of fibers being partially cut by the surface grinding process. Thickness machining was stopped at this point, resulting in thicker specimens and a lower fiber volume fraction than intended. Fiber distribution was fairly good near the edges of the fiber mat where samples were taken, but indications of fiber breakage could be seen, Figure 27. The fiber coating was similar to that shown in Figure 26.

As an additional check on NiAl MMC panel quality to see if it would be fruitful to machine extra tensile specimens from a third remaining panel (93-089 #3), NDE was performed on that panel as well as on one of the room temperature tensile tested coupons from panel 93-089 #2. Fine grained Xray and high resolution scanning acoustic microsopy was performed with generally inconclusive results, that is, it could not be stated with certainty that the intact panel had superior or inferior structure to the test specimen. Indications which were noted in the panel suggested the presence of porosity at the end of the panel, short cracks along one edge, and some fiber damage along a strip down the center, Figure 28. As a result, it was decided not to machine extra test specimens.

The fiber volume fractions were measured from Figures 22, 24 and 27 by counting the fibers and using an average fiber diameter of 150 microns. These measurements show that the actual fiber fractions of the NiAl Fe and NiAl MMC were

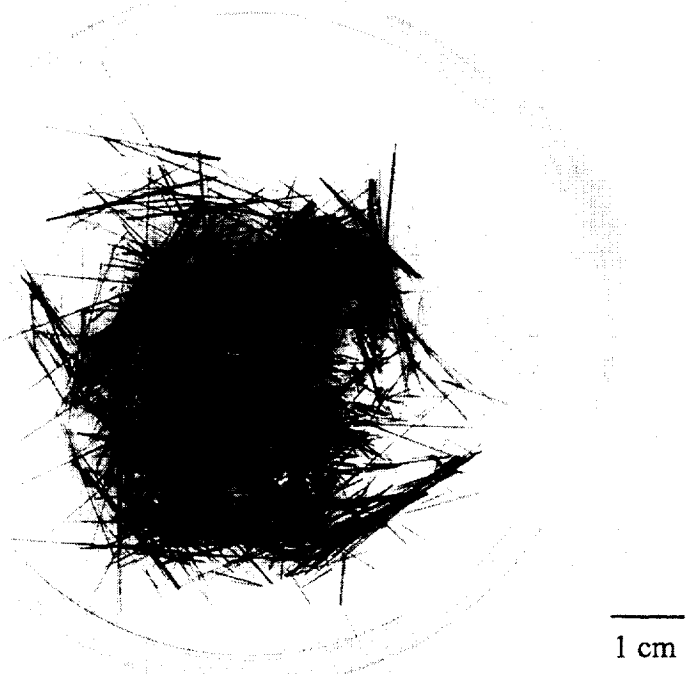

Figure 20 - Fiber Lengths after Matrix Digestion for YSZ-coated Sapphire/NiAl Composite

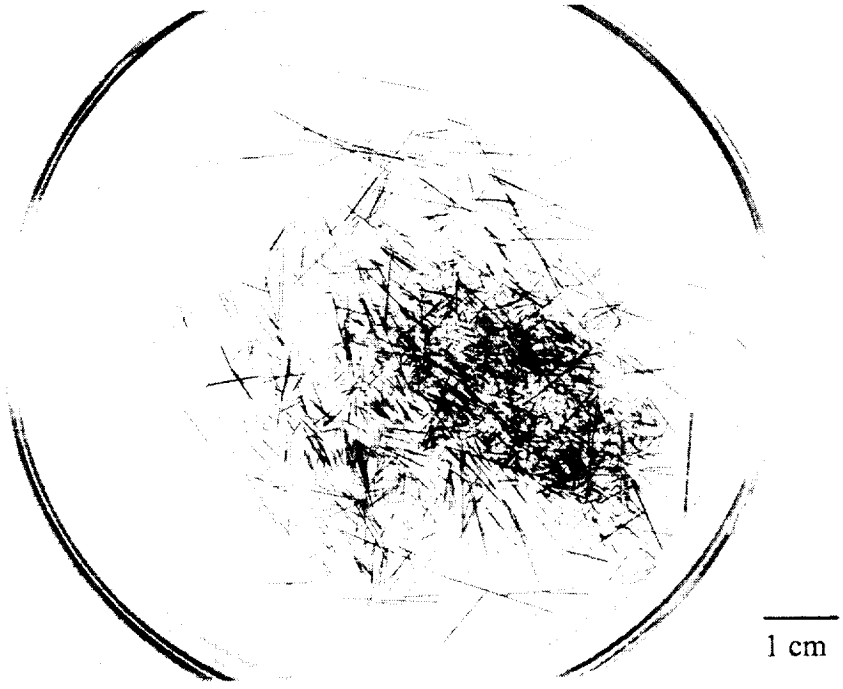

Figure 21 - Fiber Lengths after Matrix Digestion for YSZ-coated Sapphire/NiAlFe Composite

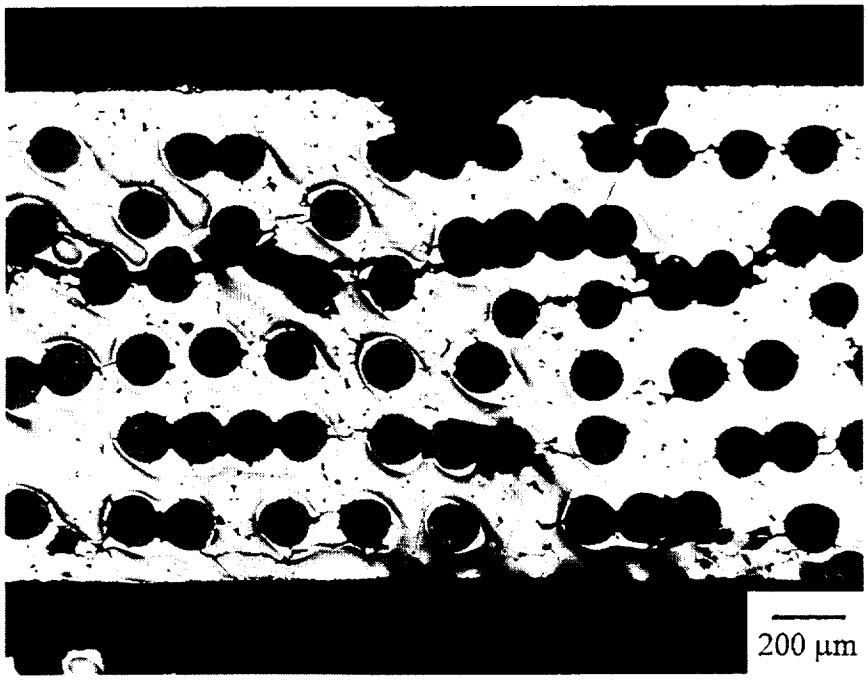

Figure 22 - Transverse Cross Section of YSZ-coated Sapphire/Ni-50Al Panel 93-089#1 Showing Incomplete Matrix Consolidation Near Panel Ends (Sample Overetched). 50X

Figure 23 - Longitudinal Cross Section of YSZ-coated Sapphire/Ni-50Al Panel 93-089#1 Showing Fiber Breakage Near Panel Ends. 50X.

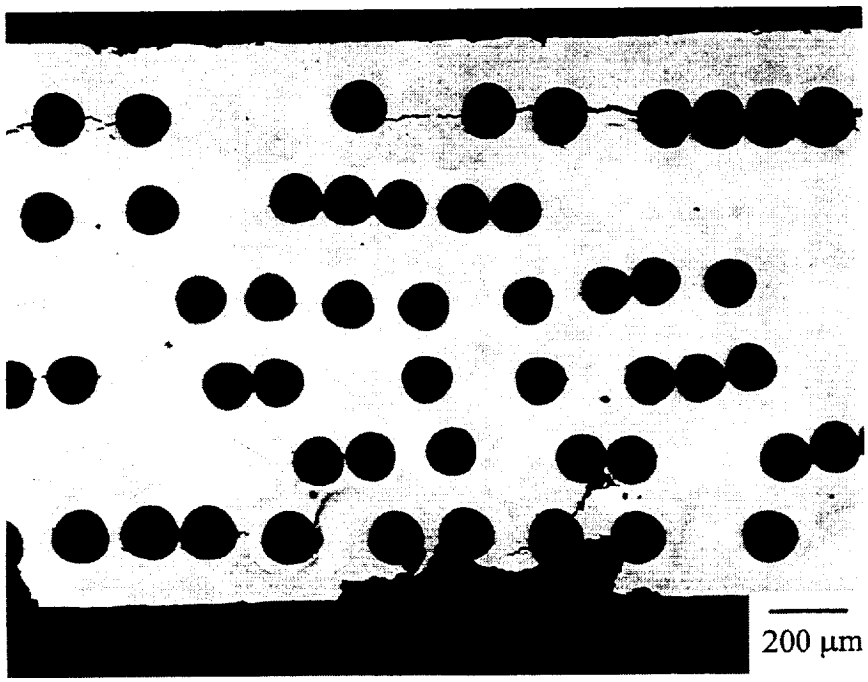

Figure 24 - Transverse Cross Section of YSZ-coated Sapphire/Ni-50Al Panel 93-089#2 Showing Dense Matrix. 50X.

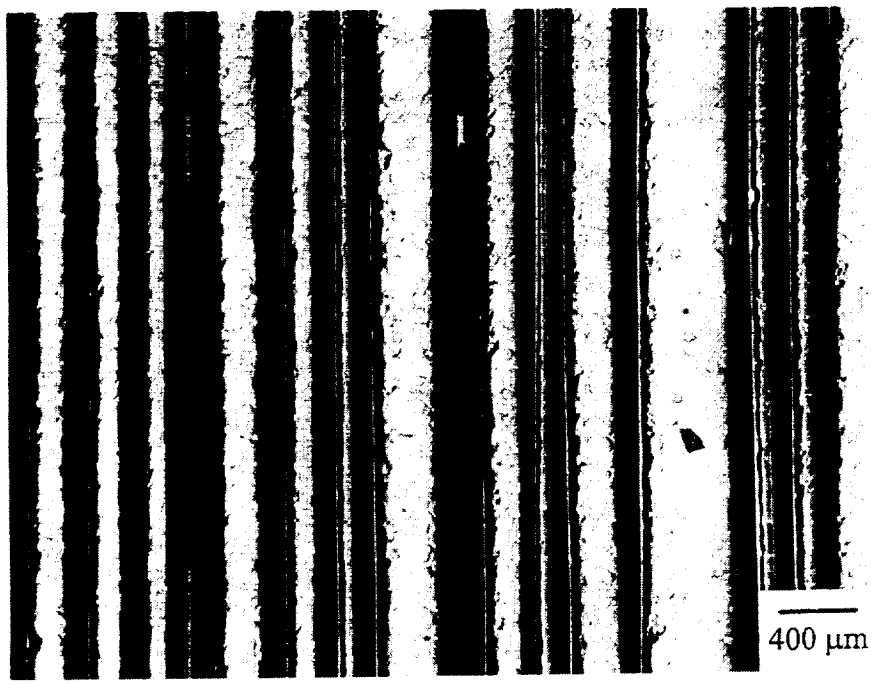

Figure 25 - Longitudinal Cross Section of YSZ-coated Sapphire/Ni-50Al Panel 93-089#2 Showing Unbroken Fibers. 50X.

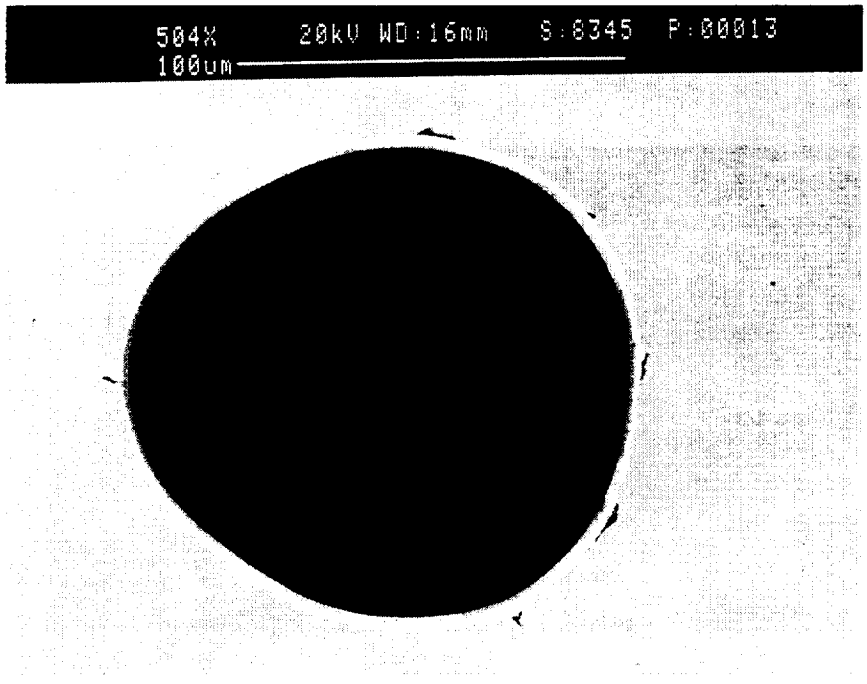

Figure 26 - PVD YSZ Coating on Sapphire Fibers (Ni-50Al matrix)

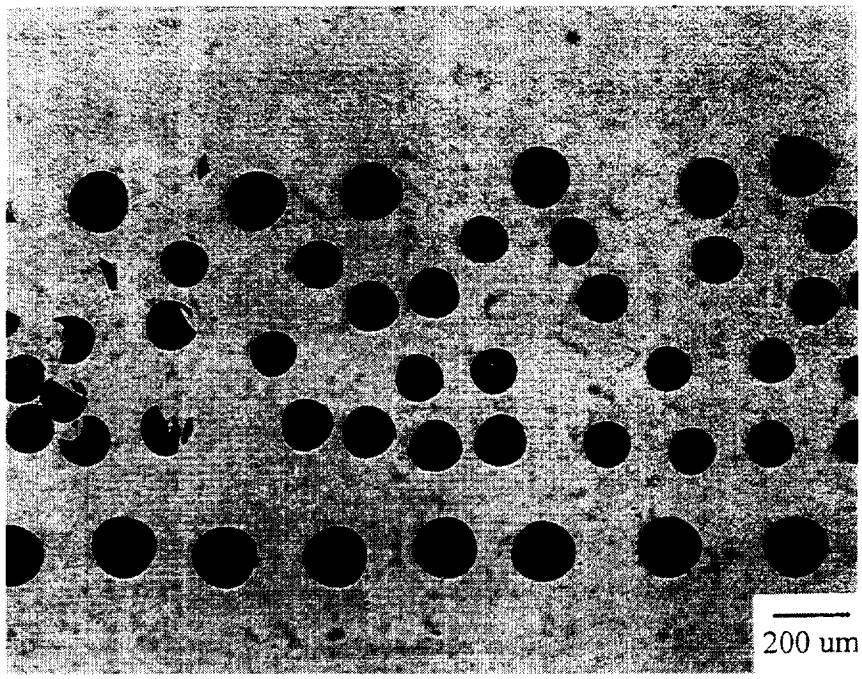

Figure 27 - Transverse Cross Section of YSZ-coated Sapphire/NiAlFe
Panel Showing Excess Matrix on Either Side of Fibers and Fiber Breakage. 50X.

Figure 28 - Ultrasonic Scan of Remaining Panel of YSZ-coated Sapphire/NiAl (93-089 #3) Showing Indications Suggesting Porosity at Panel End, Cracks Along Edge, and Fiber Bunching/Damage Along Strip in Center.

14% and 25%, respectively. The NiAl Fe MMC fiber fraction was significantly lower than the target of 30% because a large amount of matrix material had to be left on the top and bottom surfaces due to the out of plane curvature of the fibers in the as-consolidated specimens.

3.3 Task 3 - Testing and Evaluation

3.3.1 Fabrication of Specimens

Disks of unreinforced NiAlFe materials and disks and panels of YSZ-coated Sapphire reinforced NiAlFe and NiAl material were machined into tensile and toughness specimens at Cincinnati Test Laboratories, Cincinnati, OH according to the test plans shown in Tables 5 and 6.

Table 5 - Test Plan for Unreinforced NiAlFe

Test Type	Temperature, C (F)	No. of Specimens
Tensile	21 (72)	2
"	204 (400)	2
"	427 (800)	2
"	538 (1000)	2
"	650 (1200)	2
"	871 (1600)	2
Toughness	21 (72)	2
Thermal Expansion	21-1093 (72-2000)	1

Table 6 - Test Plan for MMC Systems

Test Type	Orientation	Temperature	No. of Specimens per System
Tensile	Longitudinal	RT	2
	Transverse	RT	2
	Longitudinal	ET	2
Toughness	Longitudinal	RT	2

The specimen configurations used are shown in Figures 29 through 33. These configurations were adapted from larger, standard metallic or MMC specimens to fit the material size limitations and test capabilities available. Tests were conducted at Cincinnati Test Laboratories, Cincinnati, OH, except for the NiAlFe thermal expansion measurements, which were performed at GE-EMTL.

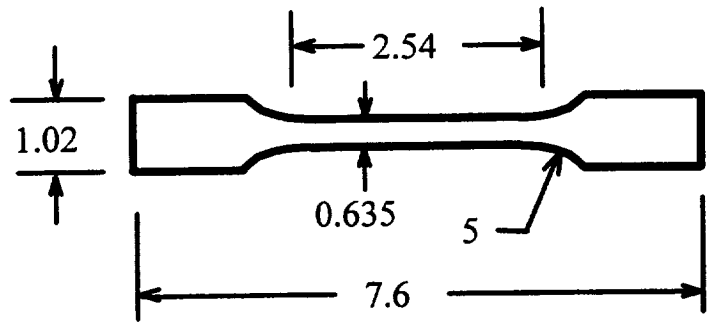

dimensions in cm.

Figure 29 - Tensile Specimen for Unreinforced NiAlFe Material

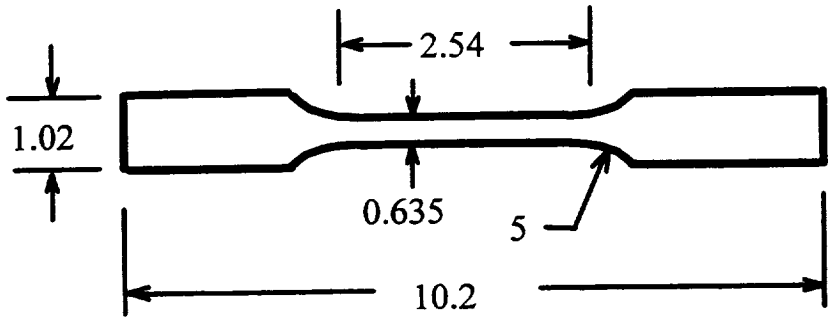

dimensions in cm.

Figure 30 - Tensile Specimen for YSZ-coated Sapphire/NiAl Composite; Longitudinal Direction

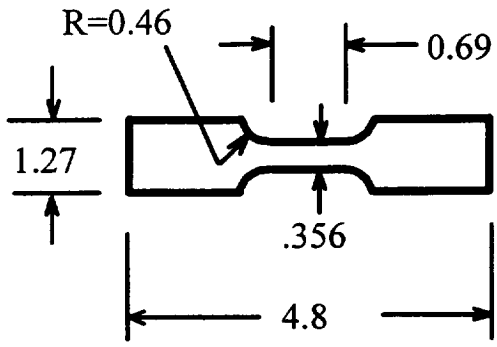

dimensions in cm.

Figure 31 - Tensile Specimen for YSZ-coated Sapphire/NiAl Composite; Transverse Direction

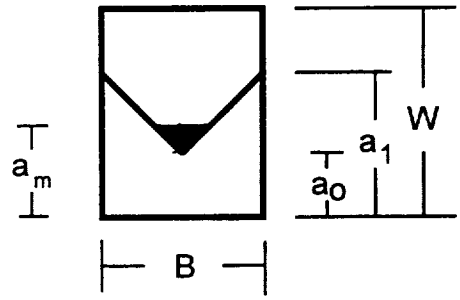

a) Cross Section Through Notch Plane

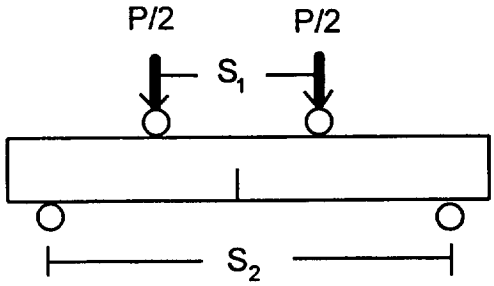

b) Side View

Figure 32 - Geometry of Chevron Notched Four Point Bend Specimen (for Unreinforced and Longitudinal Composite Materials

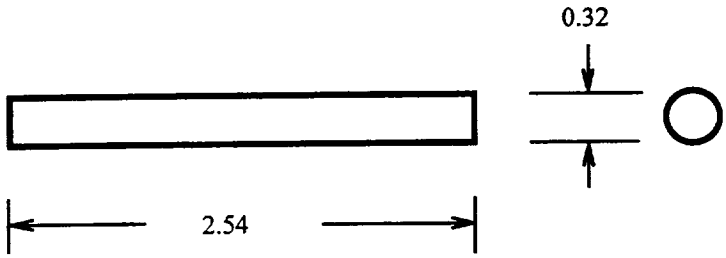

dimensions in cm.

Figure 33 - Thermal Expansion Specimen for Unreinforced NiAlFe

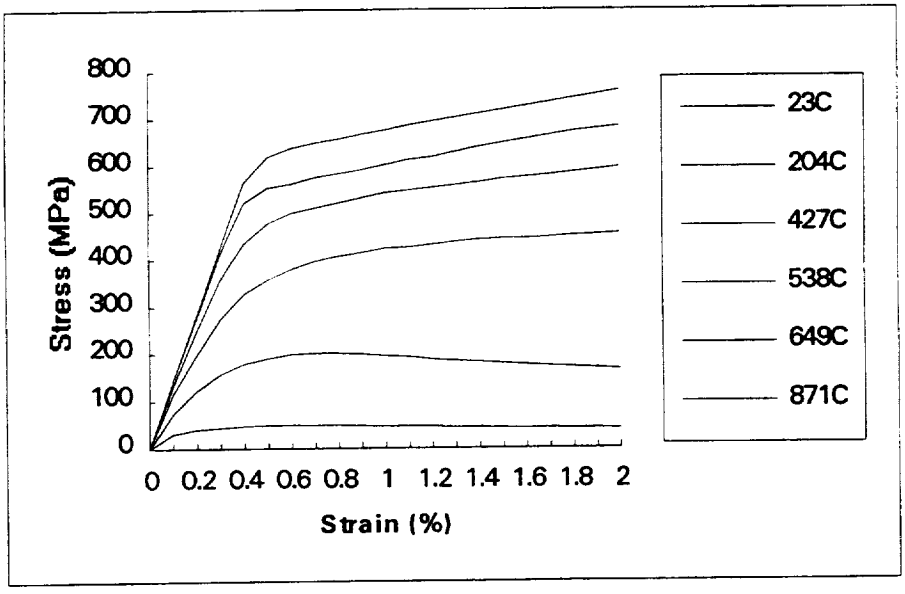

Figure 34 - Stress-Strain Behavior as a Function of Temperature for Unreinforced NiAlFe

3.3.2 Matrix Material Results

Duplicate specimens of unreinforced Ni-20Al-30Fe matrix were tensile tested at various temperatures to establish the matrix mechanical properties required for property modeling in Task 4. Tests were performed in crosshead displacement control at a rate of .063 mm/min (0025 in/min) up to yield, followed by a rate of .63 mm/min (.025 in/min). Strain was measured using with an extensometer using a 12 mm (0.5") gage length. Specimen heating was acheived using an induction coil.

Stress-strain curves were obtained at 25, 204, 427, 538, 649, and 871C (75, 400, 800, 1000, 1200, and 1600F), and the average (of two tests) Young's modulus, 0.2% yield strength, ultimate tensile strength, and plastic elongation are shown in Table 7. Typical stress-strain curves used for modeling are shown in Figure 34. The properties decrease gradually with increasing temperature to about 538C (1000F), and then fall more rapidly above that temperature. At 871C the matrix is quite weak (45 MPa/6.5 ksi yield strength).

Table 7 - Mechanical Properties of Ni-20Al-30Fe a/o Matrix Material

Temperature °C (°F)	Specimen Numbers	Modulus (GPa)	Yield Strength (MPa)	Ultimate Strength (MPa)	Elongation (%)
21 (70)	5/6/93-1-1	141	638	1163	14
	5/7/93-2	(20.4)	(92.5)	(168.7)	
204 (400)	5/6/93-2-1	141	564	1072	14
	5/6/93-1-5	(20.4)	(81.8)	(155.5)	
427 (800)	5/6/93-1-4	131	501	847	13
	5/6/93-2-3	(19.0)	(72.7)	(122.8)	
538 (1000)	5/6/93-1-2	122	367	569	8
	5/6/93-2-2	(17.7)	(53.2)	(82.5)	
649 (1200)	5/6/93-1-3	71	207	284	4
	5/7/93-3	(10.3)	(30.0)	(41.2)	
871 (1600)	5/7/93-1	35	46	88	7
	5/7/93-4	(5.1)	(6.7)	(13)	

Property data for NiAl were obtained from NASA LeRC, and are reported in Table A-2.1 of Appendix 2. The strength vs. temperature behavior of NiAl is similar to NiAlFe, but the strength levels of NiAl are uniformly lower. Based on this information, a temperature of 649°C was chosen for elevated temperature testing of the longitudinal composites.

Toughness data were obtained for NiAlFe by performing room temperature four point bend testing of the chevron notched specimens shown in Figure 32 (above). The loading was applied in a "one-third point" geometry and loading and crosshead deflection

were recorded. A typical plot is shown in Figure 35 and the maximum load and toughness are reported in Table 8. Toughness was obtained from the load and specimen geomtry through the relation:

$$K = (Y^*P)/(B\sqrt{W}) \quad (29)$$

where $Y^* = 12.0$ The derivation of this expression is described in Appendix I.

Table 8 - Fracture Load and Toughness for NiAlFe Matrix

Material	S/N	B (cm)	W (cm)	Y	P (N)	Kq (MPa-$m^{1/2}$)
NiAlFe	CG2DB	0.3820	0.637	12.0	1688	66

The NiAl toughness data were obtained from Dr. Randy Bowman, NASA LeRC.

Thermal expansion measurements were conducted on NiAlFe in a dilatometer using the specimen shown in Figure 33. The NiAl expansion behavior was taken from published values obtained from NASA-LeRC. These results, in the form of secant values (average over the temperature range from RT reference to the stated temperature), are shown in Table 9.

Table 9 - Thermal Expansion of NiAlFe Matrix

Temperature °C (°F)	Thermal Expansion 10^{-6}/°C (10^{-6}/°F)
22 (70)	4.61 (2.56)
204 (400)	11.12 (6.18)
427 (800)	14.80 (8.22)
538 (1000)	15.34 (8.52)
649 (1200)	15.88 (8.82)
871 (1600)	10.87 (6.04)
1316 (2400)	7.27 (4.04)

3.3.3 MMC Properties

The test methods used for the MMC were identical to those used for the NiAlFe matrix material, with the exception of using strain gages to measure strain in the room temperature transverse tensile tests of the NiAl MMC. This was required because the NiAl MMC panels were only 50 mm (2") wide, making the transverse specimens too short to mount a 12 mm (0.5") extensometer.

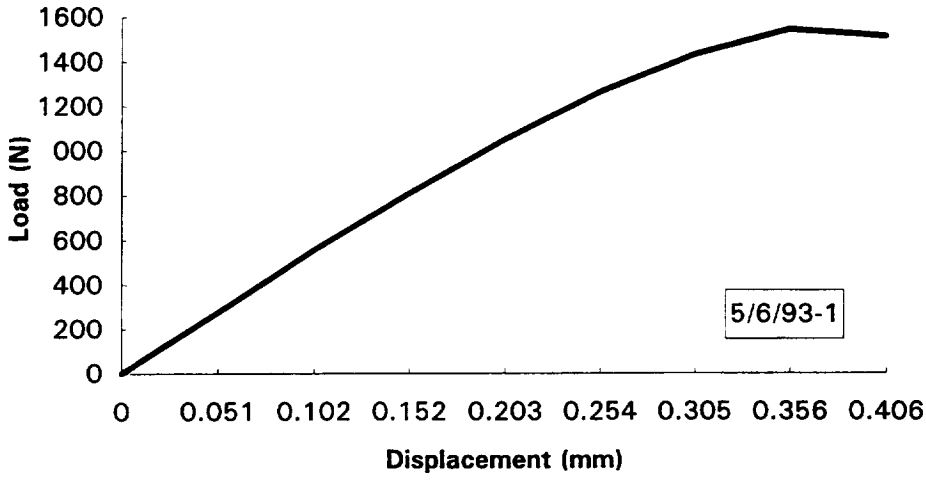

Figure 35- Representative Load-Displacement Curve for Chevron Notched Four Pont Bend Test

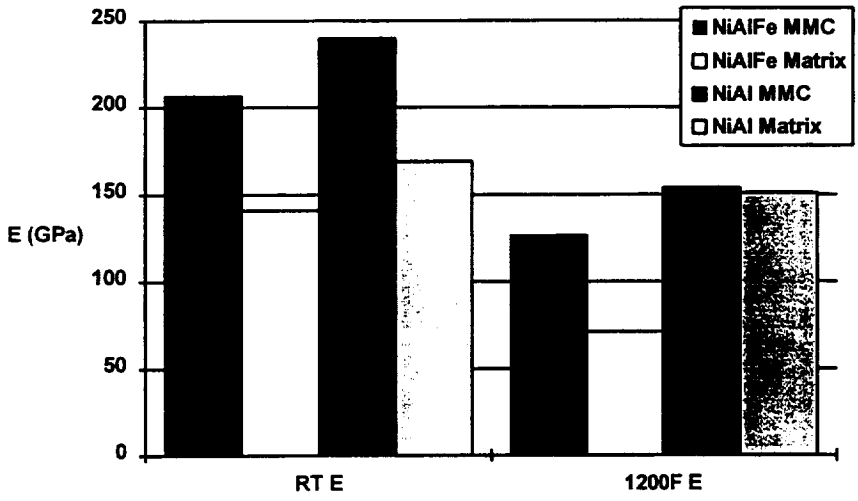

Figure 36 - Elastic Moduli of MMC and Matrix Materials in the Longitudinal Orientation

3.3.3.1 Tensile Properties

Tensile testing of the YSZ-coated Saphikon/NiAlFe (ductile matrix) and YSZ-Saphikon/NiAl (brittle matrix) systems included 2 tests for each system at room temperature in the longitudinal and transverse directions, and 2 tests for each system at 649C (1200F) in the longitudinal direction only. The test results are shown in Table 10.

Table 10 - Tensile Properties of Unidirectional YSZ-Coated Sapphire Fiber Reinforced Composites

Matrix	S/N	Orient-ation	Modulus GPa (Msi)	.2% Yield MPa (Ksi)	UTS MPa (Ksi)	Elong-ation %
RT:						
NiAlFe	5-8-93-2	L	207 (30.1)	848 (123)	979 (142)	6.8
	5-11-93-2	L	202 (29.3)	793 (115)	993 (144)	8.4
NiAl	93-089 #1-2	L	241 (35.0)	-	223 (32.3)	0.06
	93-089 #1-3	L	239 (34.6)	-	116 (16.9)	0.03
NiAlFe	5-12-93-1	T	168 (24.4)	-	470 (68.2)	0.19
	5-12-93-2	T	189 (27.4)	-	454 (65.8)	0.18
NiAl	93-089 #2-1	T	-	-	29 (4.2)	0.01
	93-089 #2-2	T	243 (35.2)	-	59 (8.6)	0.07
650C/1200F						
NiAlFe	5-8-93-1	L	103 (14.9)	-	314 (45.5)	2.1
	5-11-93-1	L	152 (22.1)	305 (44.3)	310 (44.9)	4.1
NiAl	93-089 #1-1	L	154 (22.3)	-	183 (26.6)	0.2

The longitudinal elastic moduli of the MMC's and their matrices are shown in Figure 36. In all cases the modulus was increased by the addition of fibers, as expected. Using the values of fiber fraction of the NiAl Fe and NiAl MMC as 14% and 25%, respectively, a fiber modulus of 379 GPa (55Msi), and the matrix moduli shown Table 7 in a Rule of Mixtures estimate gives the comparison shown in Table 11.

Table 11 - Estimated Rule of Mixtures vs. Observed Longitudinal Elastic Moduli for MMC

System	RT		650C (1200F)	
	Estimated GPa (Msi)	Observed GPa (Msi)	Estimated GPa (Msi)	Observed GPa (Msi)
NiAlFe MMC	174 (25.2)	205 (29.7)	114 (16.5)	127 (18.5)
NiAl MMC	221 (32.1)	240 (34.8)	208 (30.2)	154 (22.3)

Effective stiffening of the composites by the fibers appears to be occurring at all conditions except for the NiAl MMC at 650C. This condition showed the most fiber breakup combined with the weakest matrix.

Ultimate strengths of the longitudinal MMC are compared with the 0.2% yield strengths of the matrices in Figure 37. The reason for comparing to the 0.2% matrix yield strength instead of the ultimate strength is to present the matrix-only strength at a comparable strain level to that observed in the MMC. At room temperature both of the MMC's are weaker than their matrices. This is probably at least partly a result of the large amount of fiber damage in these materials. In the NiAlFe MMC, the fiber fraction is so low that little fiber strengthening is expected. The critical fiber fraction for this system (the fiber fraction below which no strengthening is expected) is predicted to be

$$V_f^* = \frac{S_m^u - S_m^y}{S_f - S_m^y} \qquad (30)$$

where at RT, S_m^u = 1163 MPa, S_m^y = 638 MPa , and S_f = 3000 MPa give V_f^* = 0.22. In the NiAl MMC, the critical volume fraction is much lower (less than 1%) since the NiAl matrix is much weaker.

At 650C some fiber strengthening is seen in both systems, but it is far less than that expected from continuous fibers based on Rule of Mixtures for undamaged fiber strengths.

Longitudinal elongation to failure for the MMC and matrices is shown in Figure 38. The NiAlFe MMC showed elongations nearly as high as the the unreinforced matrix. This is probably a result of a combination of the low fiber fraction and the fiber damage. Elongations of the NiAl MMC were quite low.

Room temperature transverse tensile properties are shown in Table 10. In both composites the transverse moduli were increased over those of the matrix. Transverse tensile strengths of the MMC were significantly lower than those of the unreinforced matrix. Experience on reinforced titanium systems shows that transverse tensile strength is not sensitive to fiber damage, so that these decreases are probably from other causes.

3.3.3.2 Toughness

Chevron-notched four-point bend tests were conducted on fiber reinforced NiAlFe and NiAl MMC using the same procedures as described for the unreinforced NiAlFe material. The test results are shown in Table 12.

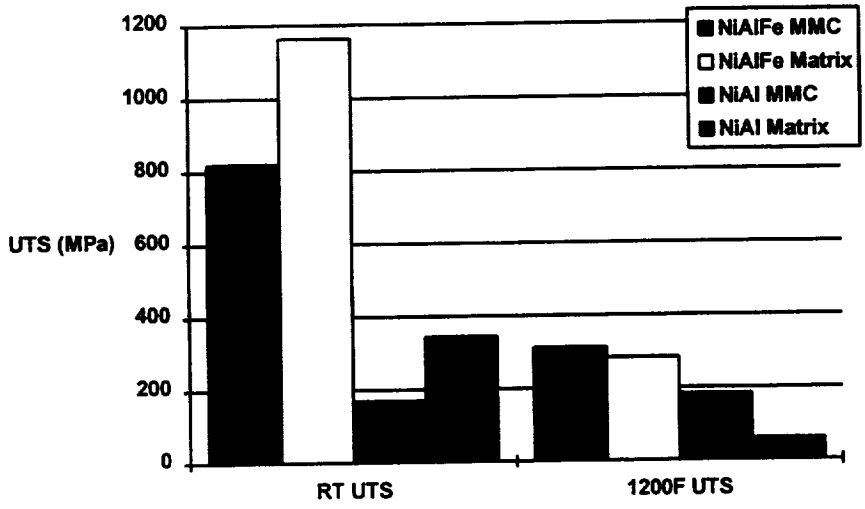

Figure 37 - Strength of MMC and Matrix Materials in the Longitudinal Direction. (UTS for MMC's; YS for Matrices)

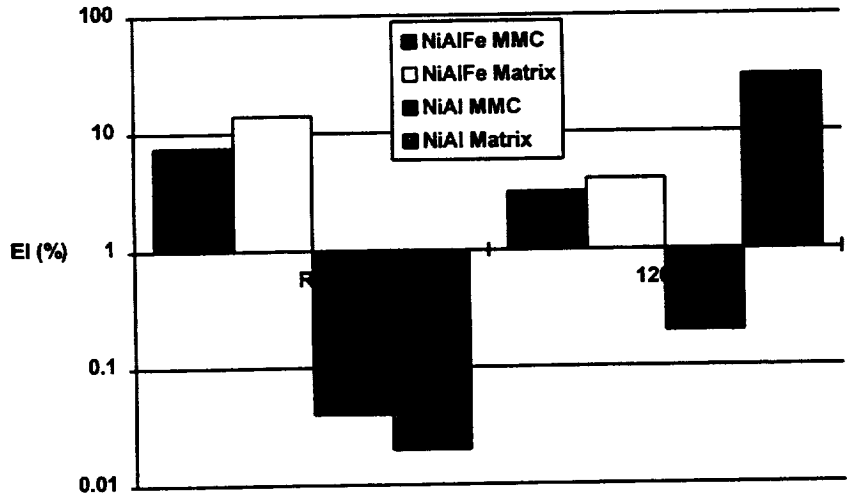

Figure 38 - Plastic Elongation at Failure for MMCs and Matrix Materials in the Longitudinal Direction

Table 12 - Fracture Toughnesses for Ni-Base MMC

Material	S/N	B (cm)	W (cm)	Y	P (N)	Kq (MPa-$m^{1/2}$)
NiAl MMC	2-3	0.145	0.637	12.0	88	9.1
"	2-4	0.146	0.637	12.0	110	11.3
NiAlFe MMC	5-6-93-1	0.382	0.631	12.0	1543	61
"	5-6-93-2	0.383	0.637	12.0	1666	65
"	5-10-93-1	0.276	0.636	12.0	1330	72
"	5-10-93-2	0.277	0..637	12.0	1335	72
NiAlFe Matrix	CG2DB-1	0.382	0.637	12.0	1688	66

Both the NiAlFe matrix and its composite were relatively tough, with the MMC being slightly tougher than the matrix alone. The NiAl MMC material, by contrast, was quite brittle. Since MMC toughness is ususally less sensitive to material defects than are tensile properties, this may be an indication that the poor tensile properties of the NiAl MMC are as much a result of poor toughness as material quality issues.

The toughness of the NiAl MMC is found to be markedly below that of the NiAlFe MMC. Reported toughnesses for NiAl are in the 4 to 7 MPa-$m^{1/2}$ (4 to 6 ksi-$in^{1/2}$) range, so that a modest amount of toughening may be occurring in these composites. The toughness for the NiAlFe matrix is essentially the same as for the NiAlFe MMC. The toughness in these systems seems to be predominately determined by the matrix toughness.

3.3.3.3 Interface Push Tests

Dr. Jeff Eldridge of NASA LeRC conducted push-out tests on samples from two panels each of the YSZ-coated Sapphire/NiAl and YSZ-coated Sapphire/NiAlFe composite used for mechanical testing. These tests were performed at RT on samples approximately 0.4 to 0.3 mm thick (parallel to the fibers). The results are given in Table 13.

Table 13- Fiber Push-out Results for Ni-Base MMC's

Material	Panel ID	Temperature °C	Debond Shear Stress (MPa)
YSZ-Sapphire/NiAl	93-089 #1	22	240 ± 80
	93-089 #2	22	170 ± 65
	93-089 #1	650	185 ± 30
YSZ-Sapphire/NiAlFe	5-8-93	22	330 ± 20
	5-10-93	22	340 ± 65
	5-8-93	650	>245

The NiAlFe-matrix MMC appears to have a somewhat higher and more uniform interfacial shear strength than does the NiAl-matrix MMC. In the NiAl-matrix MMC, the two panels had noticeably different interface strengths despite having identical processing. Metallography indicated that this panel had a much thinner coating than did 93-089 #2. At RT the pushout mode was primarily along the interface, with some fiber fracturing at the top side along the edges of the indenter. At 650°C extensive matrix yileding occured, and for the NiAlFe system, no interfacial separation was seen up to the stress reported.

3.3.3.4 Fractography

Fractographic and metallographic evaluation of selected tested MMC specimens was performed. One sample of each test condition was examined as follows:

Table 14 - Specimens Examined by Optical Metallography and SEM

Material	Test Type	Orientation	Temperature	Spec. ID.
NiAl MMC	Tension	Long.	RT	93-089 #1-2
"	"	Transv.	RT	93-089 #2-2
"	"	Long.	650°C	93-089 #2-2
"	Toughness	Long.	RT	93-089 #2-4
NiAlFe MMC	Tension	Long.	RT	5/11/93-2
"	"	Transv.	RT	5/12/93-T2
"	"	Long.	650°C	5/8/93-1
"	Toughness	Long.	RT	5/10/93-2

Fractography showed that the YSZ-coated Sapphire/NiAlFe MMC's generally had fibers asymmetrically placed with respect to the specimen centerline, as shown in Figure 39. The outer fiber ply on one side intersected the surface, while on the other side a thick layer of matrix remained. This was a result of fiber bowing out of the plane of the specimen making it impossible to machine the specimens uniformly. As a result the overall fiber volume fraction was approximately 15%. Within the fiber-containing region fiber distribution was good. Multiple fiber breaks could be seen on the exposed fibers, resulting from either machining damage or the high test elongations.

The YSZ-coated Sapphire/NiAl MMC's had a uniform layer of matrix on each side and a much higher fiber volume fraction overall, 31%, as seen in Figure 40. The fiber distribution within the MMC was not uniform, however, and some fractures seemed to originate from multiple touching fibers, Figure 41. The lack of complete consolidation of the matrix could also be seen, Figure 42. Little to no fiber pullout was seen in either material, as shown typically in Figure 42.

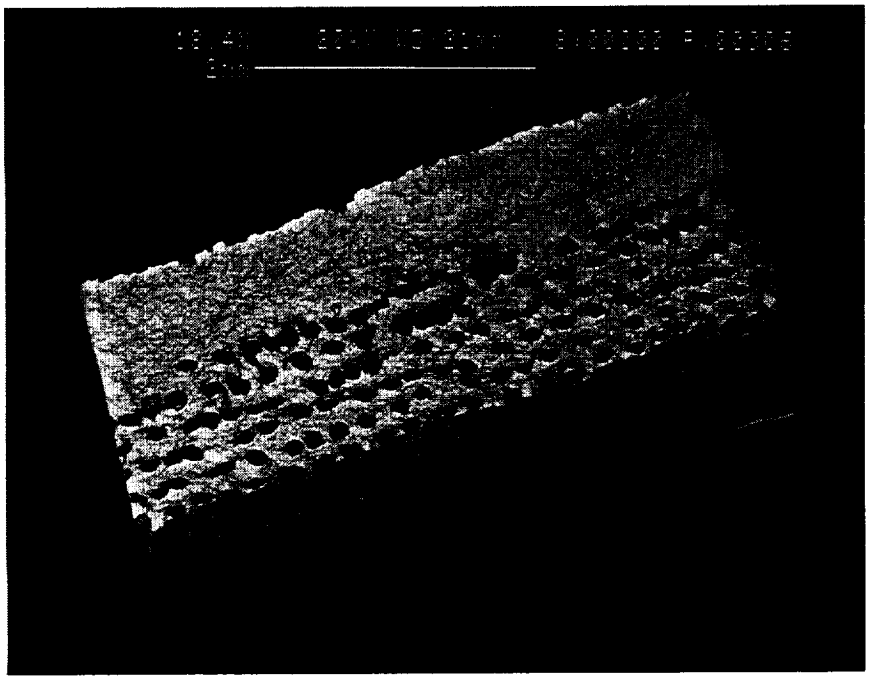

Figure 39 - Fracture Surface of Room Temperature Longitudinal Tensile Specimen of YSZ-coated Sapphire/NiAlFe (S/N 5-11-93-2) Showing Nonuniform Distribution of Matrix and Cut Fibers on Surface.

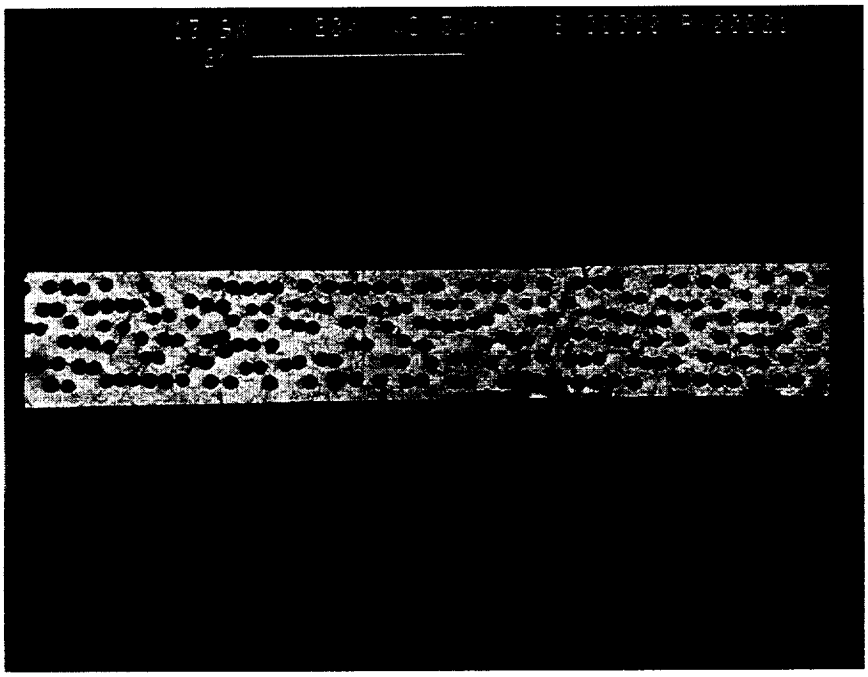

Figure 40 - Fracture Surface of Room Temperature Longitudinal Tensile Specimen of Saphikon/YSZ/NiAl (S/N 1-2) Showing Uinform Matrix Layers on Surfaces but Nonuniform Distribution of Fibers.

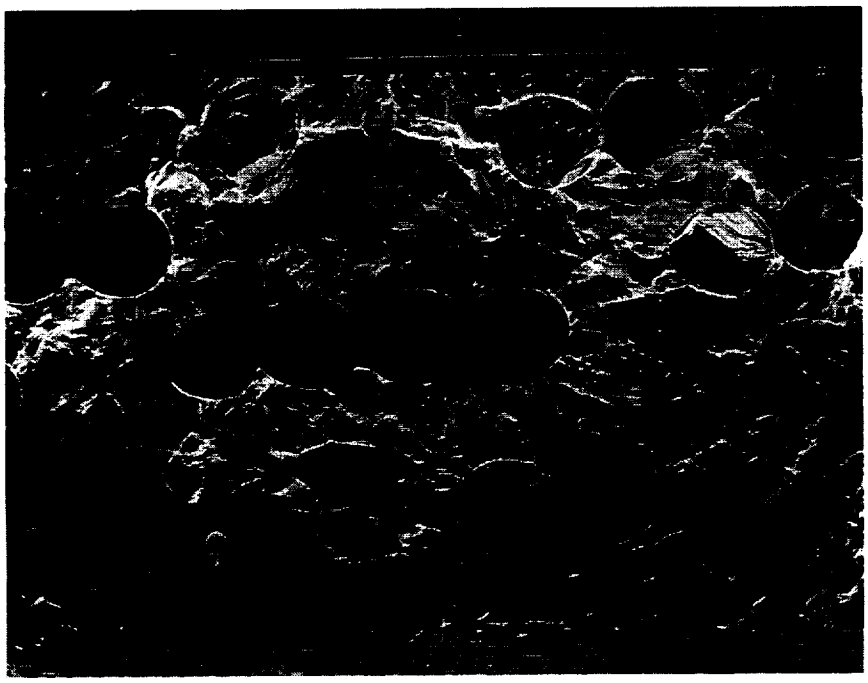

Figure 41 - Higher Magnification View of YSZ-coated Sapphire/NiAl Specimen (650C Longitudinal Tension, S/N 1-1) Showing Bunching of Fibers and Cleavage Fracture of Matrix.

Figure 42 - Room Temperature Longitudinal Tension Fracture Surface of YSZ-coated Sapphire/NiAl (S/N 1-2) Showing Low Level of Fiber Pullout and Incomplete Matrix Consolidation.

In the NiAlFe matrix composites the matrix fracture mode was ductile dimpling at room temperature, and a mixture of intergranular and dimpled fracture at 650C (Figure 43). In the NiAl matrix composites, the matrix fracture mode was cleavage at both room temperature and 650C, Figures 41 and 44. The observance of cleavage in NiAl at 650C is somewhat surprising since the ductile-brittle transition temperature of this material is expected to be about 300C.

The fiber coatings in both systems were strongly adherent to the fibers as seen in Figures 43 and 44, and when interface separation did occur, it was mostly at the coating/matrix interface.

The transverse tension samples from both MMC systems fractured through the fibers, Figure 45, with little or no interfacial debonding. This supports the observation from the longitudinal tension tests that the presence of the coating causes the interface to be well bonded. No difference in interface debonding was seen between the two different matrix systems.

The toughness specimens showed fracture features which were very similar to those in the longitudinal room temperature tension tests. Fractures appeared to start at or near the point of the chevron notch, Figure 46 and 47, and were quite flat and parallel to the notch plane. The NiAlFe matrix was ductile, while the NiAl matrix showed cleavage.

Metallographic evaluation of the same tested specimens shown in Table 12 was also conducted. In the NiAl MMC material, the features in the RT and 650C longitudinal tensile tests were indistinguishable. A low magnification view of the 650C specimen (93-089 #1-1) in Figure 48 shows irregular fiber spacing and incomplete matrix consolidation as noted earlier. Little fiber pullout has occurred. At higher magnification in Figure 49 (RT, S/N 93-089 #1-2), almost no coating (< 0.2 micron) can be seen on the fibers. The transverse tension and longitudinal toughness samples, cut from a different panel, showed more coating ($\cong$ 1 micron thick), as in Figure 50, although it appears to have flowed some during consolidation and is bunched between fibers. The transverse tension fracture has progressed through the fibers (Figure 51), indicating a strong bond between the fiber and matrix. The toughness sample (Figure 52) showed much more complete consolidation, but like the longitudinal tension samples, the fracture proceeded with little pullout or crack deflection.

Metallographic observation of the NiAlFe MMC showed that the first ply of fibers in the RT longitudinal tension sample (5/11/93-2) were badly broken up, Figure 53, due to their being machined into during specimen fabrication. Fibers in other samples in which machining did not intersect the fibers (Figure 54, RT toughness, 5/10/93-2) appeared to be unbroken. This is at odds with the evidence from fiber extraction reported earlier which indicated a large amount of fiber breakage in these panels. The rationale for this discrepancy is that the fibers aren't actually broken after consolidation, just severely weakened (possibly by twinning or chemical reactions) and when the matrix is removed

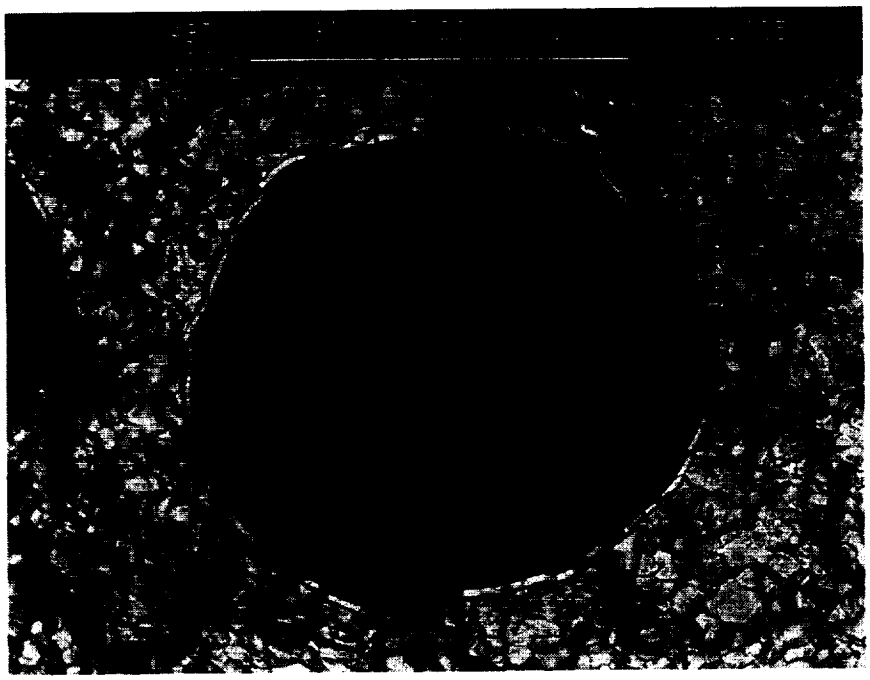

Figure 43 - High Magnification View of 650C Longitudinal Tension Test Fracture Surface for YSZ-coated Sapphire/NiAlFe (S/N 5-9-93-1) Showing Fiber Coating and Matrix Failure Mode.

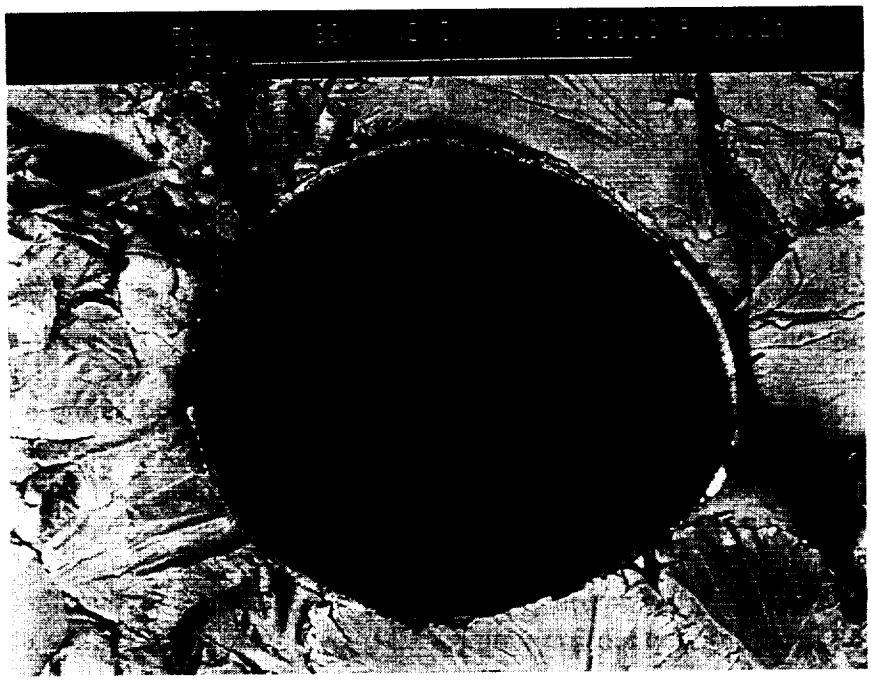

Figure 44 - High Magnification View of RT Longitudinal Tension Test Fracture Surface for YSZ-coated Sapphire/NiAl (S/N 1-2) Showing Fiber Coating and Matrix Failure Mode.

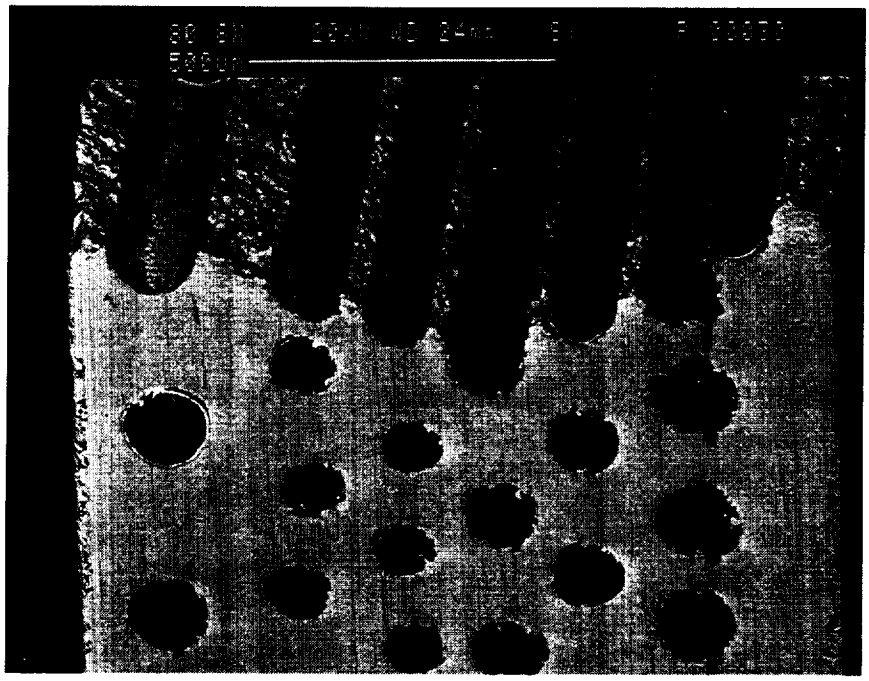

Figure 45 - Fracture Surface of RT Transverse Tension Specimen of YSZ-coated Sapphire/NiAlFe (S/N 5-12-93-T2) Showing Fracturing through the Fibers and Lack of Interface Debonding.

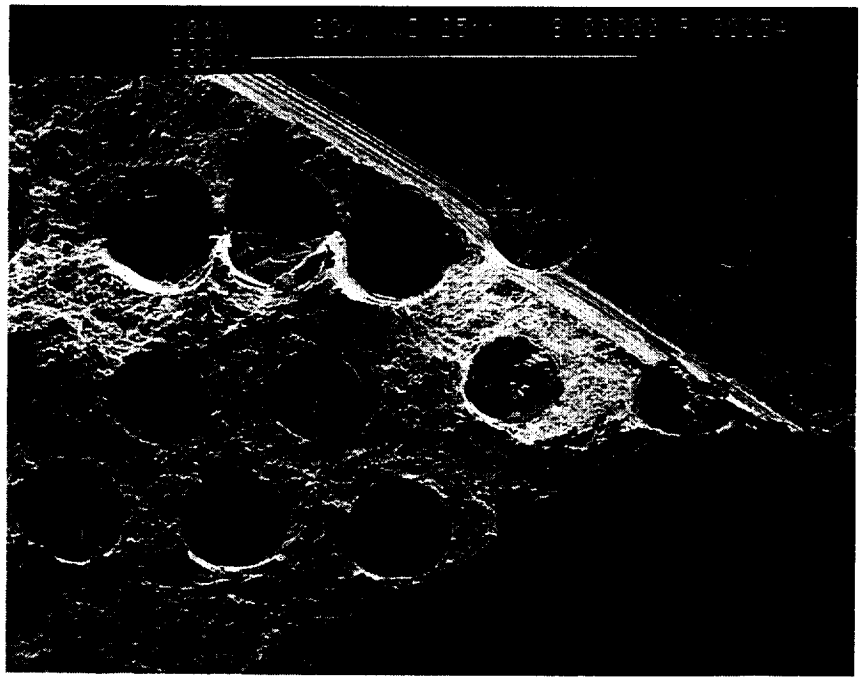

Figure 46 - Fracture Surface of Toughness Specimen of YSZ-coated Sapphire/NiAlFe (S/N 5-10-93-2) Showing Ductile Matrix Dimpling and Low Level of Fiber Pullout.

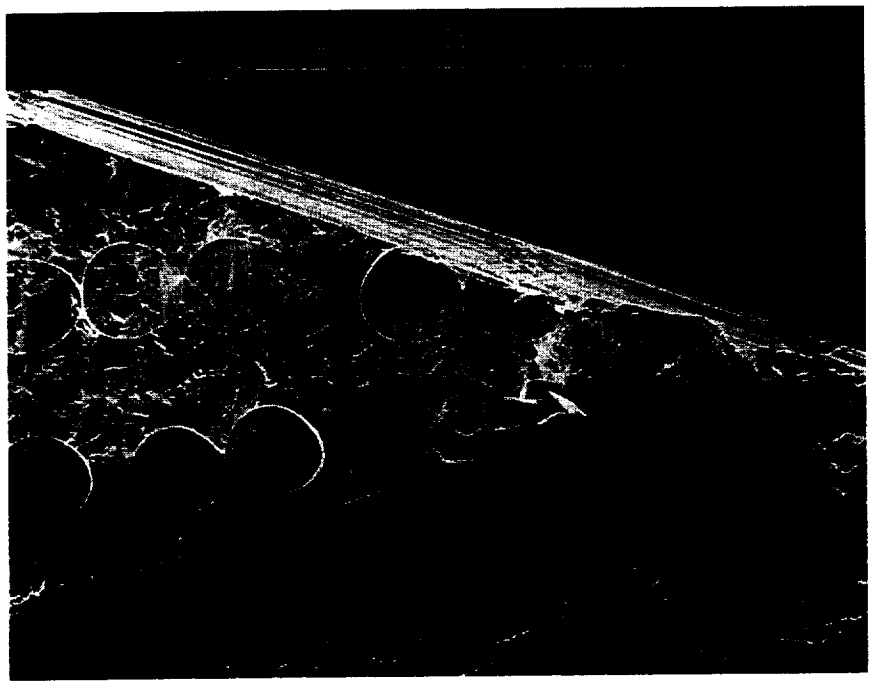

Figure 47- Fracture Surface of Toughness Specimen of YSZ-coated Sapphire/NiAl (S/N 2-4) Showing Matrix Cleavage and Low Level of Fiber Pullout.

Figure 48 -Metallographic Section of 650C Longitudinal Tensile Specimen of YSZ-coated Sapphire/NiAl (1-1) Showing Flat Fracture and Incomplete Matrix Consolidation.

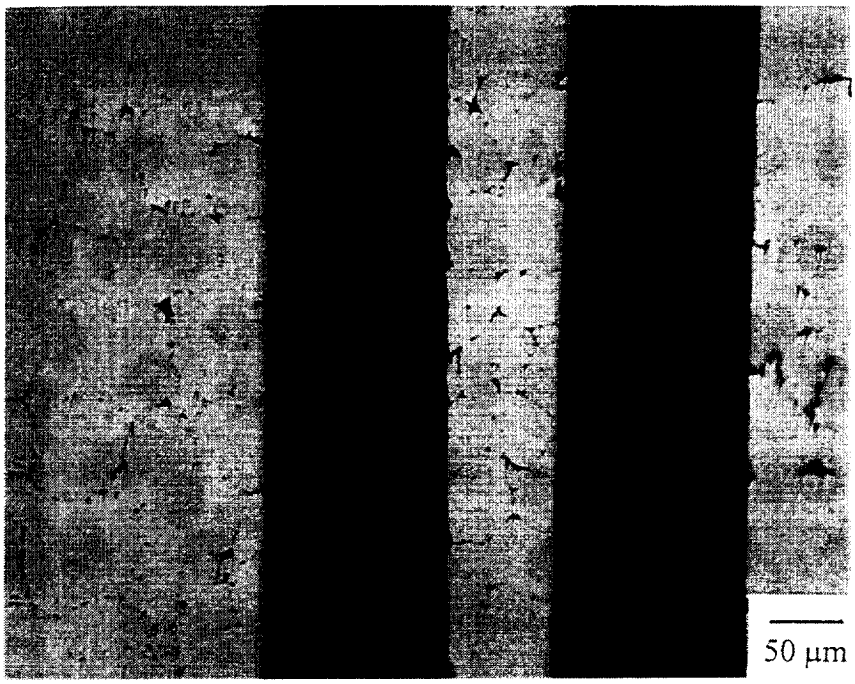

Figure 49 - Fracture Surface of Room Temperature Longitudinal Tensile Specimen of YSZ-coated Sapphire/NiAl (S/N 1-2) Showing Lack of Fiber Coating.

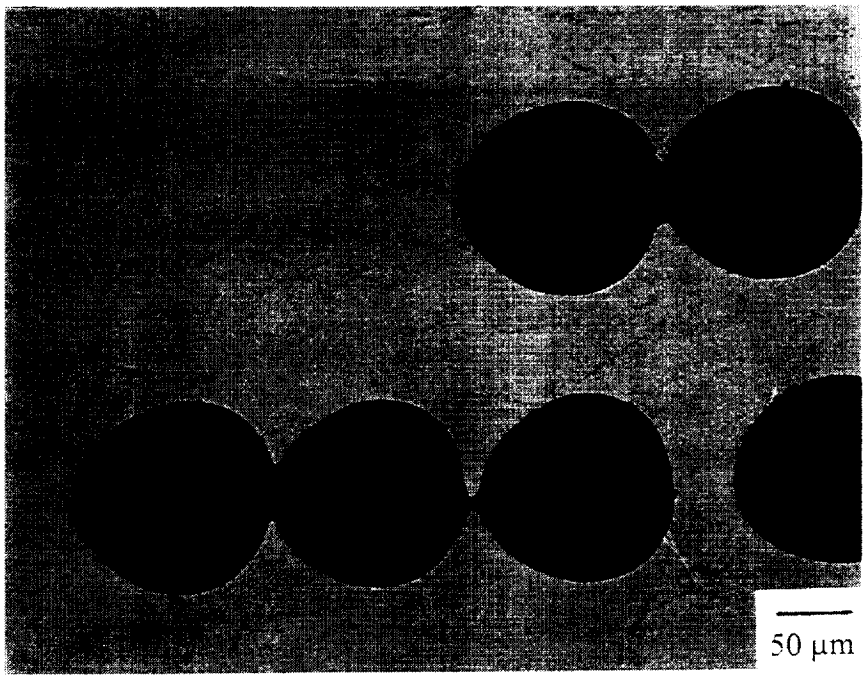

Figure 50 - YSZ-coated Sapphire/NiAl RT Transverse Tension Specimen (S/N 2-2) Showing Distribution of Coating on Fibers.

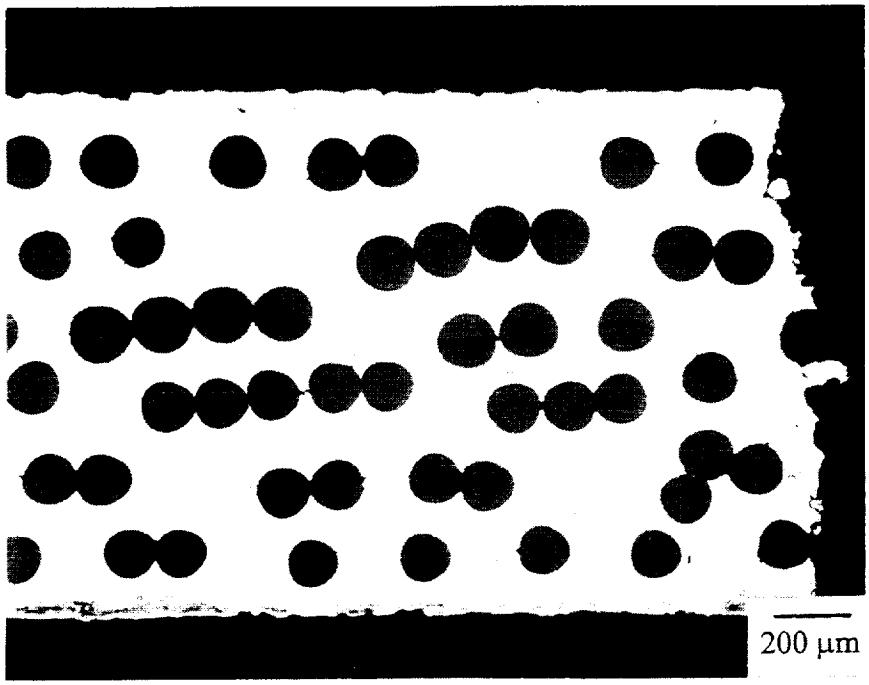

Figure 51 - Room Temperature Transverse Tension Fracture Surface of YSZ-coated Sapphire/NiAl (S/N 2-2) Showing Fracture Path Through Fibers.

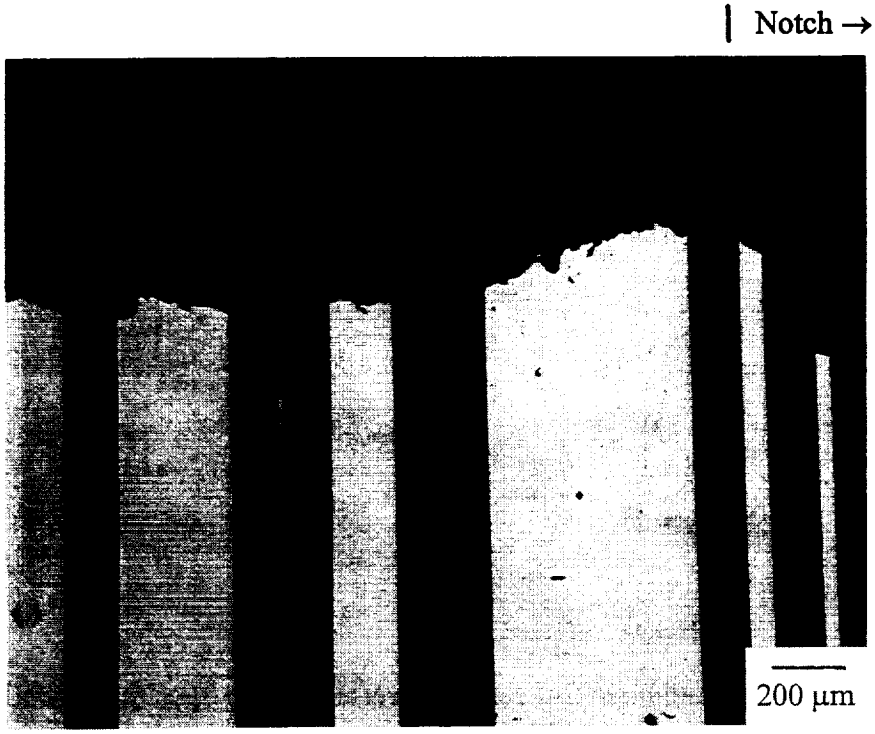

Figure 52 - RT Longitudinal Toughness Test Fracture Surface forYSZ-coated Sapphire/NiAl (S/N 2-4) Showing Flat Fracture.

Figure 53 - RT Longitudinal Tension Test Fracture Surface for YSZ-coated Sapphire/NiAlFe (S/N 5/11/93-2) Showing Fragmented Fibers and Matrix Ductility.

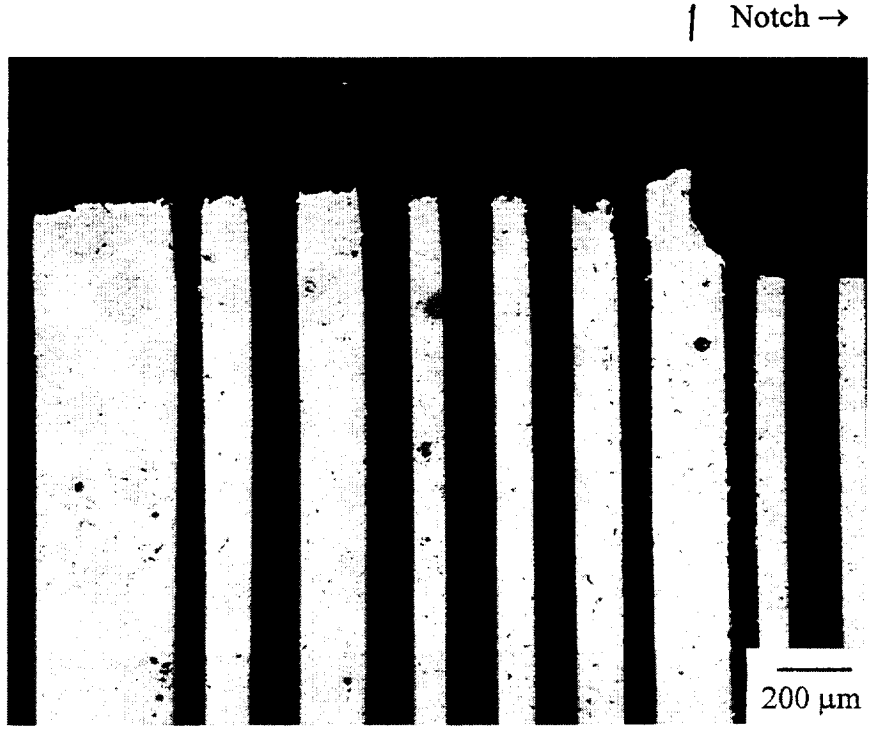

Figure 54 - Fracture Surface of RT Longitudinal Toughness Specimen of YSZ-coated Sapphire/NiAlFe (S/N 5/10/93-2) Showing Fracturing of Fibers Only Near Crack Plane.

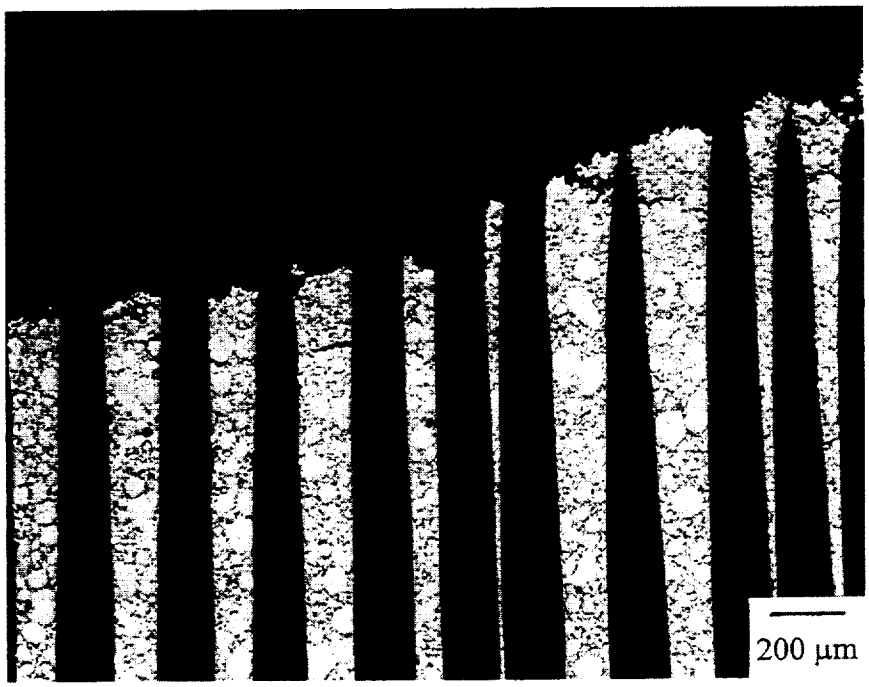

Figure 55 - 650C Longitudinal Tension Specimen of YSZ-coated Sapphire/NiAlFe (S/N 5/8/93-1).

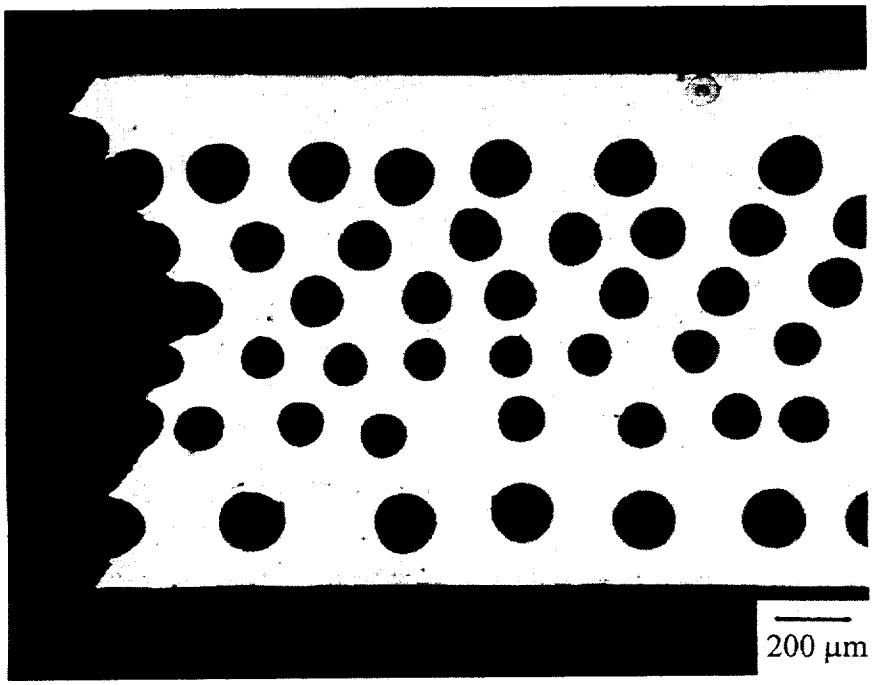

Figure 56- RT Transverse Tension Specimen of YSZ-coated Sapphire/NiAlFe (S/N 5/12/93-T2) Showing Fracture Through Fiber and Matrix.

by etching they fall apart due to the etching stresses. Some evidence of local matrix plasticity between the fibers can be seen (Figure 53) in the necking of the matrix ligaments and the large opening of the fiber cracks. Matrix plasticity seems to be slightly less at 650C, from the appearance of S/N 5/8/93-1 in Figure 55. Like the NiAl MMC, the RT transverse fracture proceeded through the fibers instead of around them, Figure 56.

3.4 Task 4 - Evaluation of Behavior Models

In this section, the models selected and described in Task 1 were re-evaluated using the experimental constituent data developed in Task 3 or obtained from NASA LeRC. Results are compared to the composite property data developed in Task 3. For the sake of clarity and readability, the input parameters for each material which were used in these computations are summarized in Appendix 2. The two unidirectional composite systems studied in Task 3 were analyzed in this task. Both systems were reinforced with YSZ-coated sapphire fibers. One system had a "ductile" matrix (NiAlFe), while the other had a "brittle" matrix (NiAl).

3.4.1. Residual Stresses

Using the concentric cylinder model, the residual stress state in each composite system was predicted. The results of this analysis are presented here.

3.4.1.1. Sapphire/NiAl System

The NiAl-matrix composites were modeled with an overall 31% fiber volume fraction, and a YSZ fiber coating with a thickness of approximately 2.5 μm (0.0001 in). For cooldown from a fabrication temperature of 1260°C (2300°F), the predicted residual stresses in the composite system are shown in Figure 57. From this plot, it is apparent that the thin YSZ coating layer had a negligible effect on the residual radial clamping stresses which affect interfacial sliding. This clamping stress was calculated to be 72.4 MPa (10.5 ksi). The model predicts a significant amount of matrix yielding during the cooldown process, due to the large mismatch in thermal expansion between the fiber and matrix.

3.4.1.2. Sapphire/NiAlFe System

The NiAlFe-matrix composites were modeled with an overall 15% fiber volume fraction, and a YSZ coating with a thickness of approximately 2.5 μm (0.0001 in). However, the cross-sections also show that the fibers were not evenly distributed through the section. In fact, the fibers are concentrated in the first two-thirds of the thickness, with a local fiber volume fraction of about 22½%. For this reason, two analyses were performed, one with a uniform 15% volume fraction and another with a uniform 22½% volume fraction. For cooldown from a fabrication temperature of 1177°C (2150°F), the predicted residual stresses in these two cases are shown in Figure 58. From these plots, it is apparent that the volume fraction had only a small effect on the residual radial clamping stresses which affect interfacial sliding. So for the purposes of subsequent

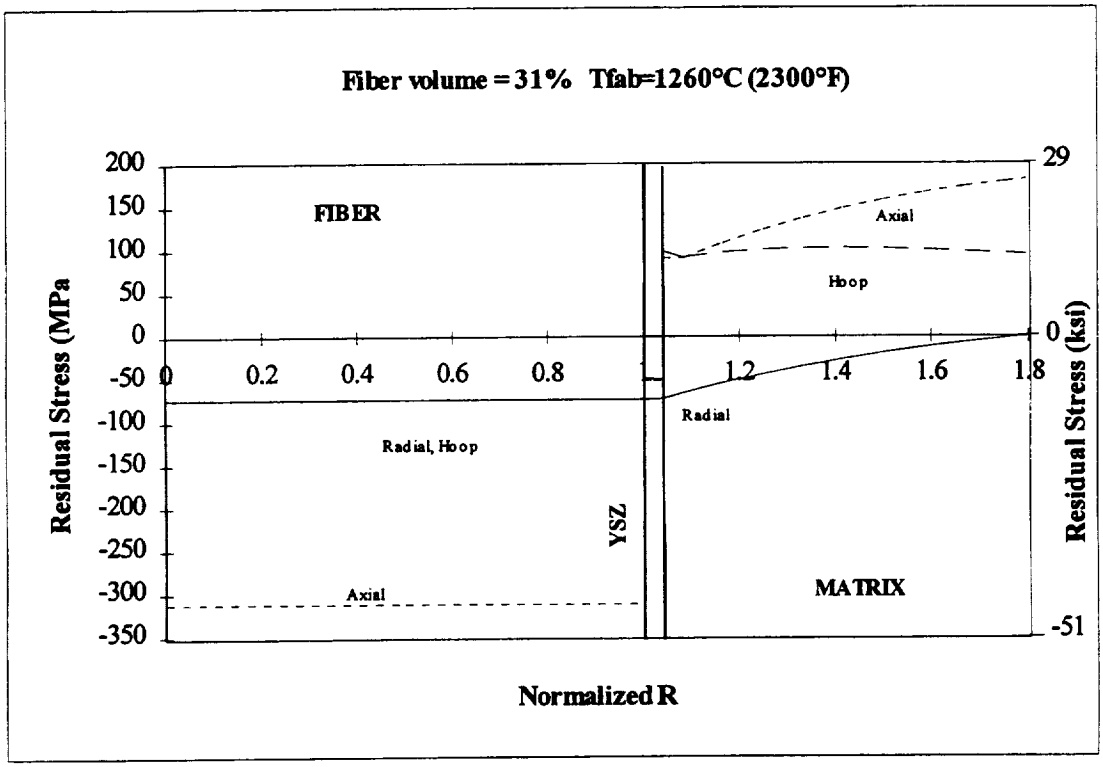

Figure 57 - Predicted residual stress state in YSZ-coated Sapphire/NiAl composite

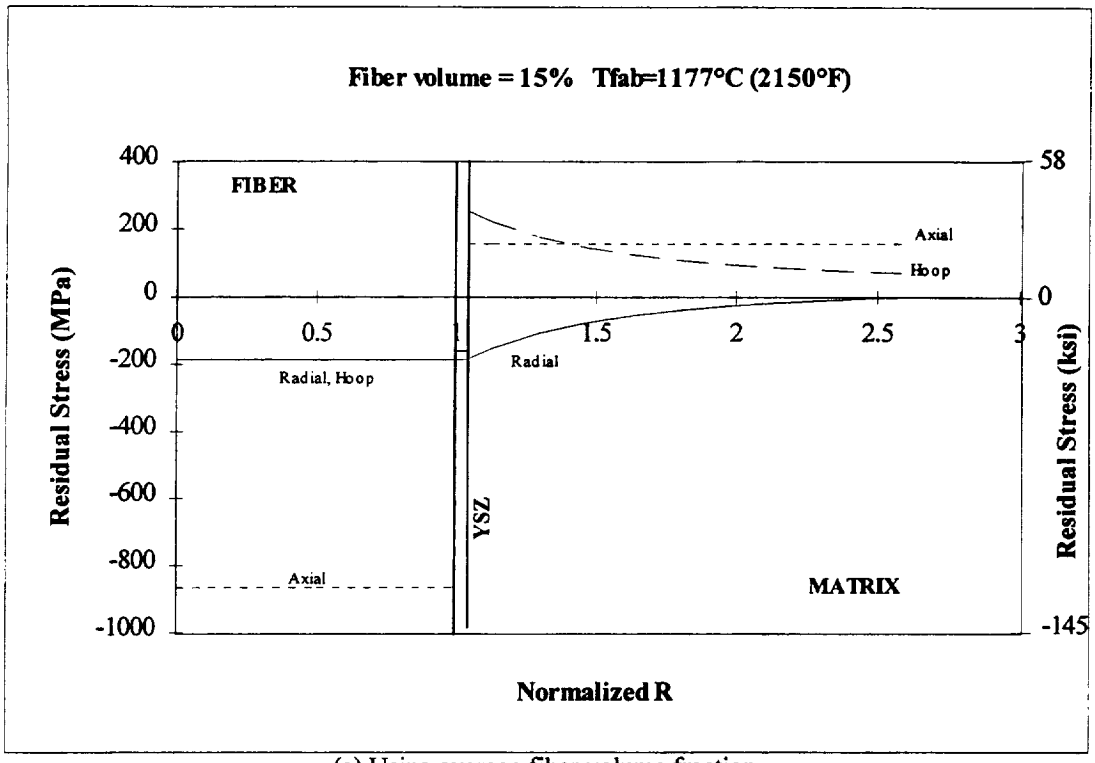

(a) Using average fiber volume fraction

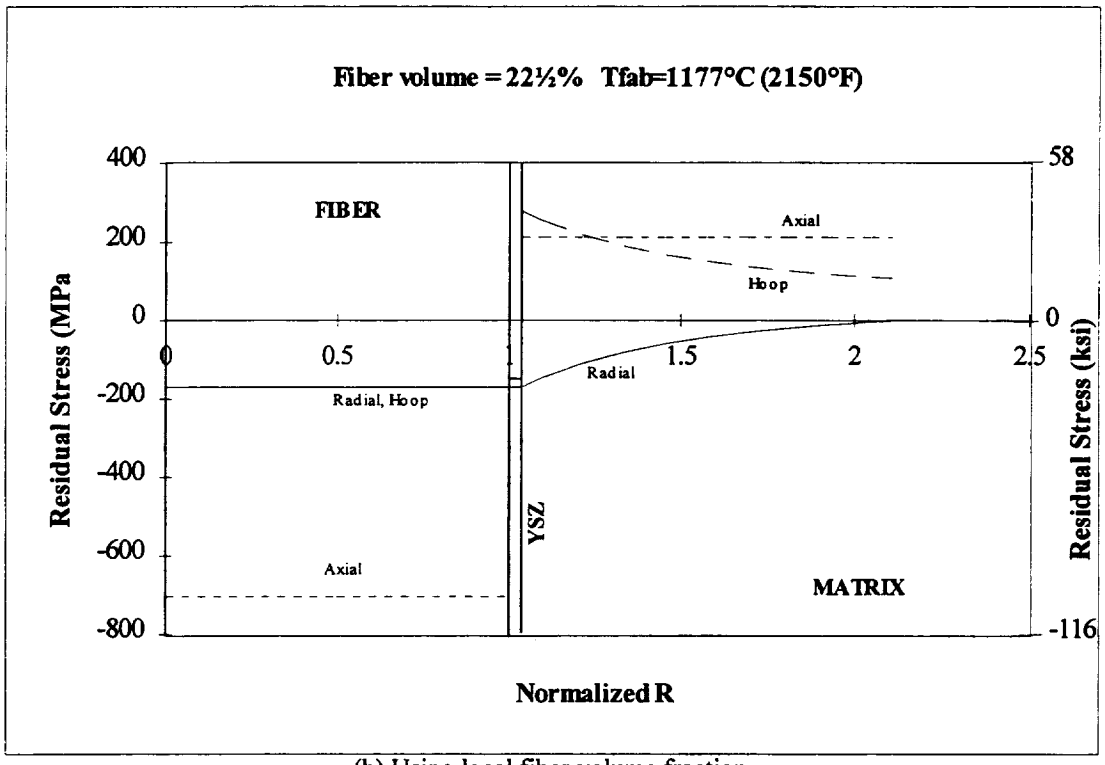

(b) Using local fiber volume fraction

Figure 58 - Predicted residual stress state in YSZ-coatedSapphire/NiAlFe composite

modeling, the uniform 15% case was used. For this case, the radial clamping stress was found to be 184.4 MPa (26.8 ksi). The model does not predict matrix yielding during the cooldown process, due to the smaller mismatch in thermal expansion between the fiber and matrix and the higher yield stress of the NiAlFe system.

3.4.2 Matrix Cracking

The matrix cracking model of Lu, et al. (1991) described in Task 1 was used to predict whether or not matrix cracks are expected to develop during cooldown in each of the systems. The results are presented here.

3.4.2.1 Sapphire/NiAl System

Due to the large degree of matrix plasticity in the NiAl-matrix system during cooldown, there is some ambiguity in applying the cracking model. Recall equation (10) for the non-dimensional cracking parameter

$$\Re = R\left(E_m \varepsilon_T / K_m\right)^2 \tag{10}$$

If we calculate the mismatch strain ε_T for this system and multiply by the room temperature modulus, we obtain

$$E_m\, \varepsilon_T = 1324 \text{ MPa}(192 \text{ ksi})$$

which is much larger than the predicted value of residual axial stress [140.2 MPa (20.3 ksi)] and substantially larger than the room-temperature yield stress! Thus, it is more physically realistic to use the predicted residual axial stress, since it represents the actual stress in the material.

If we were to use the strict version of equation (10), we would obtain for the cracking parameter (assuming the range of matrix toughness):

$$\Re \approx 2.56 - 5.76$$

This is clearly an upper bound value, and is probably very unrealistic. Using the actual predicted plastic stress, we obtain for the cracking parameter

$$\Re \approx 0.03 - 0.06$$

The critical values of $\Re_C$ were then calculated for the 31% volume fraction, and the results are summarized in Table 15. The model does not predict matrix cracking in this system (as long as our assumption of using the plastic stress is valid), which agrees with the observations of the material fabricated by GE.

Table 15 - Matrix cracking model predictions for NiAl-matrix system

Sapphire/NiAl system		
$\Re$ = 0.03 - 0.06		
Interface	$\Re_c$	**Cracking ($\Re>\Re_c$)**
'z'-cracks		
Bonded	3.46	NO
Debonded (μ=0.1)	0.73	NO
(μ=0.3)	2.18	NO
(μ=2.0)	14.52	NO
'r'-cracks		
Bonded	8.0	NO
Debonded	1.6	NO

3.4.2.2 Sapphire/NiAlFe System

Applying the matrix cracking model to the NiAlFe-matrix system was more straightforward, since there is no matrix plasticity expected to develop during cooldown. We obtain for the cracking parameter:

$$\Re \approx 0.0005$$

The critical values of $\Re$c were then calculated for the 15% volume fraction, and the results are summarized in Table 16. The model does not predict matrix cracking in this system either, which agrees with the observations of the material fabricated by GE.

Table 16 - Matrix cracking model predictions for NiAlFe-matrix system

Sapphire/NiAlFe system		
$\Re$ = 0.0005		
Interface	$\Re$c	**Cracking ($\Re>\Re$c)**
'z'-cracks		
Bonded	5.80	NO
Debonded (μ=0.1)	1.5	NO
(μ=0.3)	4.5	NO
(μ=1.0)	15.0	NO
'r'-cracks		
Bonded	9.3	NO
Debonded	2.4	NO

3.4.3 Longitudinal Behavior

The Aboudi model was used to predict the longitudinal stress-strain response of the composite systems. Attempts were made to predict the ultimate longitudinal strength using both rule-of-mixtures and the Curtin model. For both models, the degraded fiber properties were utilized (see Appendix 2). The results of these analyses are presented in this section.

3.4.3.1 Sapphire/NiAl System

The predicted longitudinal strength of the Sapphire/NiAl system at both room temperature and 649°C (1200°F) is summarized for both models and compared with the experimental data in Table 17. The measured strengths are substantially lower than the predicted strengths since the NiAl-matrix composites contained a large number of broken fibers after processing.

Table 17 - Longitudinal strength results for Sapphire/NiAl system

Sapphire/NiAl system (31% v/o)			
	Longitudinal strength, MPa (ksi)		
Temp, C (F)	Rule of mixtures	Curtin	Experiment
21 (70)	642.6 (93.2)	959.5 (139.2)	222.7 (32.3)
			116.5 (16.9)
649 (1200)	310.3 (45.0)	648.0 (94.0)	183.5 (26.6)

Since the interfacial friction is not a well-characterized parameter, the variation of the strength predicted by the Curtin model versus interfacial friction is shown in Figure 59. The predicted longitudinal stress-strain curves are shown together with the experimental results in Figure 60.

3.4.3.2 Sapphire/NiAlFe System

The predicted longitudinal strength of the Sapphire/NiAlFe system at both room temperature and 649°C (1200°F) is summarized for both models and compared with the experimental data in Table 18. The rule-of-mixtures under-predicts the strength, particularly at room temperature. However, the Curtin model, which includes the fiber fracture statistics does a better job of predicting the strengths.

Table 18 - Longitudinal strength results for Sapphire/NiAlFe system

Sapphire/NiAlFe system (15% v/o)			
	Longitudinal strength, MPa (ksi)		
Temp, C (F)	Rule of mixtures	Curtin	Experiment
21 (70)	761.9 (110.5)	935.7 (135.7)	977.0 (141.7)
			991.5 (143.8)
649 (1200)	287.5 (41.7)	374.1 (54.3)	313.7 (45.5)
			309.6 (44.9)

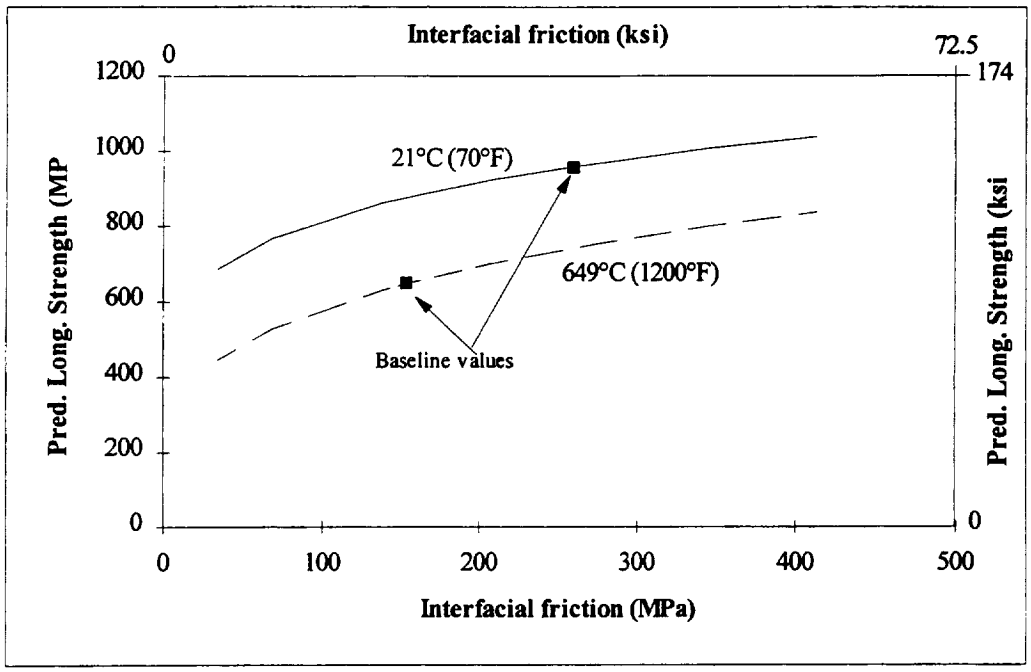

Figure 59 - Effect of interfacial friction of predicted longitudinal strength of Sapphire/NiAl using Curtin model

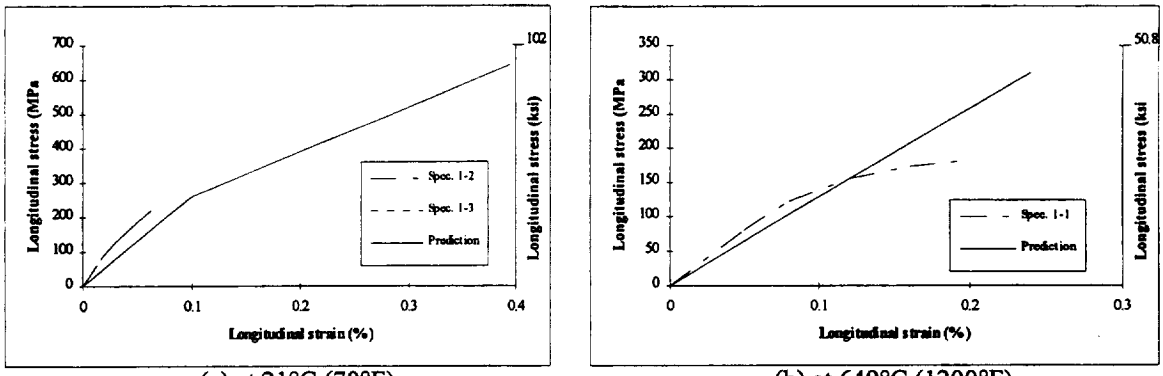

(a) at 21°C (70°F)

(b) at 649°C (1200°F)

Figure 60 - Comparison of predicted and experimental longitudinal stress-strain response of Sapphire / NiAl

Since the interfacial friction is not a well-characterized parameter, the variation of the strength predicted by the Curtin model versus interfacial friction is shown in Figure 61.

The predicted longitudinal stress-strain curves are shown together with the experimental results in Figure 62.

3.4.4 Transverse Behavior

The Aboudi model was used to predict the transverse stress-strain response of the composite systems. The ultimate transverse strength was predicted using the appropriate equation, depending on whether the Aboudi model predicted fiber/matrix separation would occur prior to failure. For both models, the clamping stress was taken from the residual stress analyses. The results of these analyses are presented in this section.

3.4.4.1 Sapphire/NiAl System

For the NiAl-based system, both at room and elevated temperatures, the expression for transverse strength assuming a strong interface was less than the transverse stress required to cause debonding (unclamping). Thus, the strength was calculated based on this strong bond assumption, and the results for both temperatures are shown in Table 19. (Note that experimental data was only available at room temperature). The strength model agreed quite well with the higher data point.

Table 19 - Transverse strength results for Sapphire/NiAl system

Sapphire/NiAl system (31% v/o)		
	Transverse strength, MPa (ksi)	
Temp, C (F)	**Prediction**	**Experiment**
21 (70)	58.2 (8.4)	28.9 (4.2)
		59.2 (8.6)
649 (1200)	34.3 (5.0)	-----

The predicted transverse stress-strain response up to failure is shown for room and elevated temperature in Figure 63 along with the available experimental data. Since the Aboudi model does not model damage, the stress-strain curves diverge after the initial failure event in the experiment. But the initial moduli and ultimate loads show promising agreement.

3.4.4.2 Sapphire/NiAlFe System

For the NiAlFe-based system, both at room and elevated temperatures, the transverse stress required to cause debonding (unclamping) was less than the predicted transverse strength assuming a strong bond. Thus, the NiAlFe system appears to act like a conventional metal matrix composite, exhibiting bilinear behavior due to the interface separation. The strength was calculated based on the debond assumption (where the interface separation stress was determined from the residual clamping stress and the Aboudi model), and the results for both temperatures are shown in Table 20. (Note that

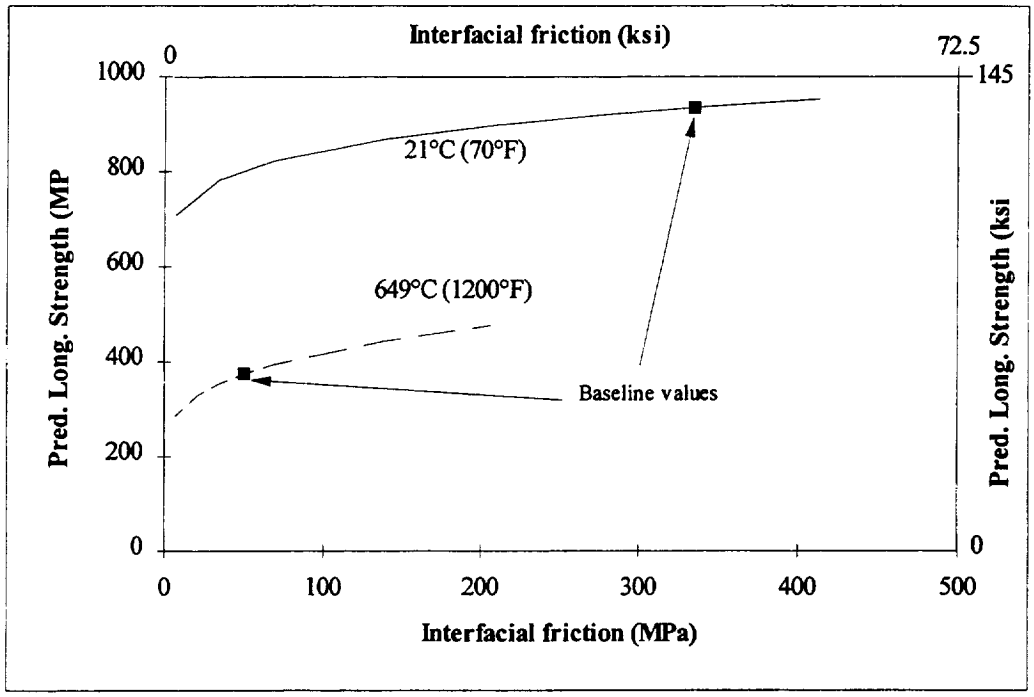

Figure 61 - Effect of interfacial friction of predicted longitudinal strength of Sapphire/NiAlFe using Curtin model

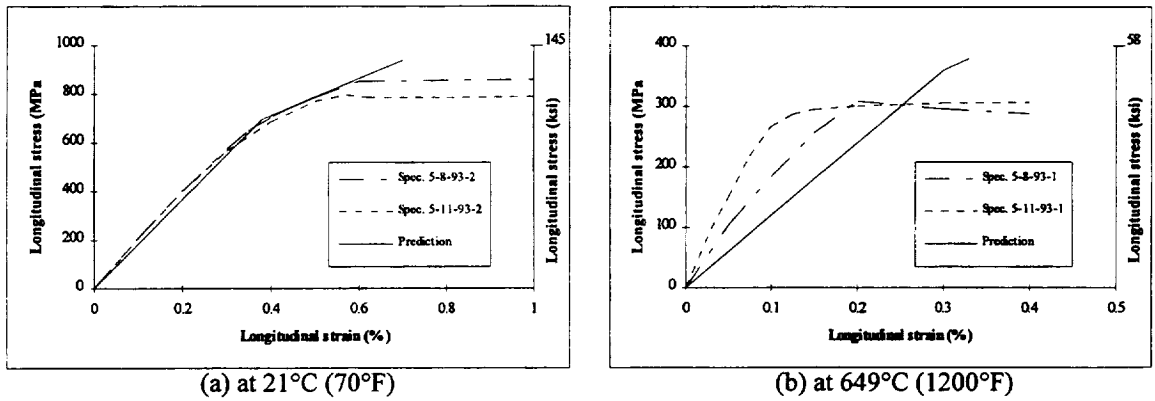

(a) at 21°C (70°F)

(b) at 649°C (1200°F)

Figure 62 - Comparison of predicted and experimental longitudinal stress-strain response of Sapphire/NiAlFe

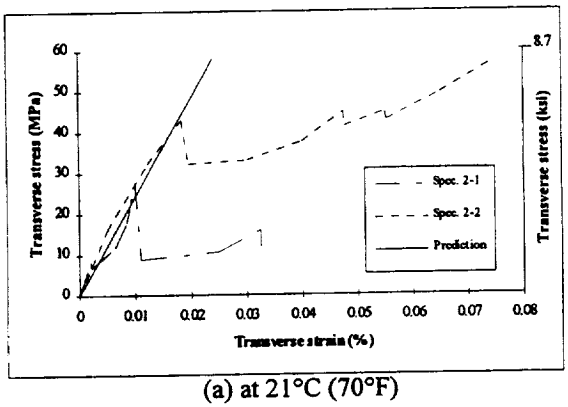

(a) at 21°C (70°F)

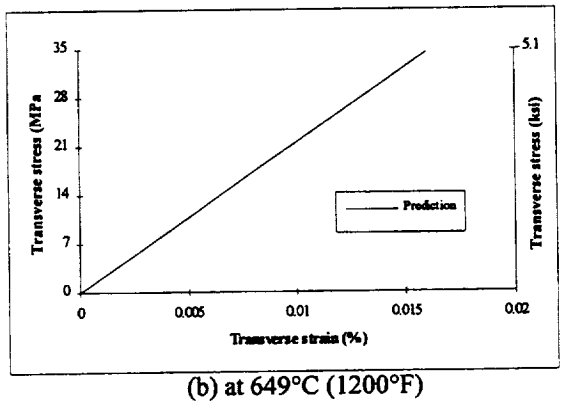

(b) at 649°C (1200°F)

Figure 63 - Comparison of predicted and experimental transverse stress-strain response of Sapphire / NiAl

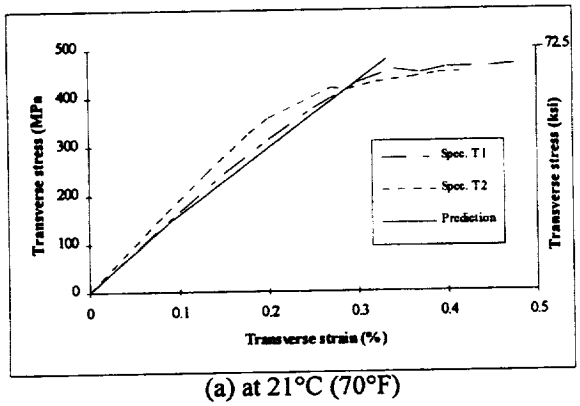

(a) at 21°C (70°F)

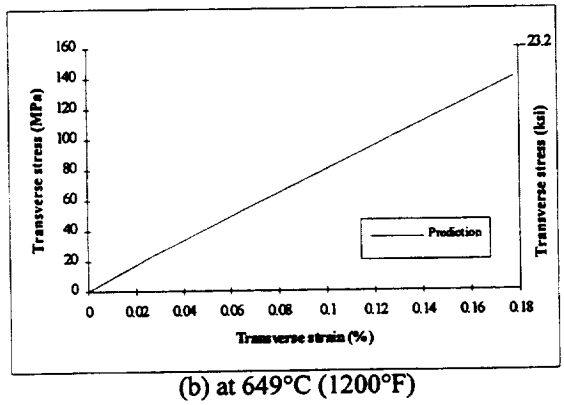

(b) at 649°C (1200°F)

Figure 64 - Comparison of predicted and experimental transverse stress-strain response of YSZ-coated Sapphire/NiAlFe

experimental data was only available at room temperature). The strength model agreed very well with the available data.

Table 20 - Transverse strength results for Sapphire/NiAlFe system

Sapphire/NiAlFe system (15% v/o)		
	Transverse strength, MPa (ksi)	
Temp, C (F)	Prediction	Experiment
21 (70)	478.2 (69.4)	470.4 (68.2)
		454.0 (65.9)
649 (1200)	140.2 (20.3)	-----

The predicted transverse stress-strain response up to failure is shown for room and elevated temperature in Figure 64 along with the available experimental data. Since the Aboudi model does not model damage, the stress-strain curves again diverge somewhat after the initial failure event in the experiment. But the general agreement between the prediction and the experiment is excellent.

Since the NiAlFe system appears to exhibit fiber-matrix separation under transverse loading, the transverse strength should be highly dependent on the separation stress. Using the Cooper-Kelly relation, the transverse strength was predicted for all possible values of the separation stress and the results are shown in Figure 65. (Note that the separation stress cannot exceed the predicted strength using the strong-bond assumption).

3.4.5 Fracture Toughness

The room temperature fracture toughness of each of the composite systems was predicted using the modified rule-of-mixtures approach as shown in Equation (21). The results are summarized here.

3.4.5.1 Sapphire/NiAl System

Since the NiAl matrix was fairly brittle, it was assumed that fiber bridging was a more likely energy absorption mechanism during fracture than local matrix plasticity. Both methods for predicting this effect were utilized, and the resulting predictions are compared with experimental data provided by GE in Table 21. Agreement with experiment was encouraging.

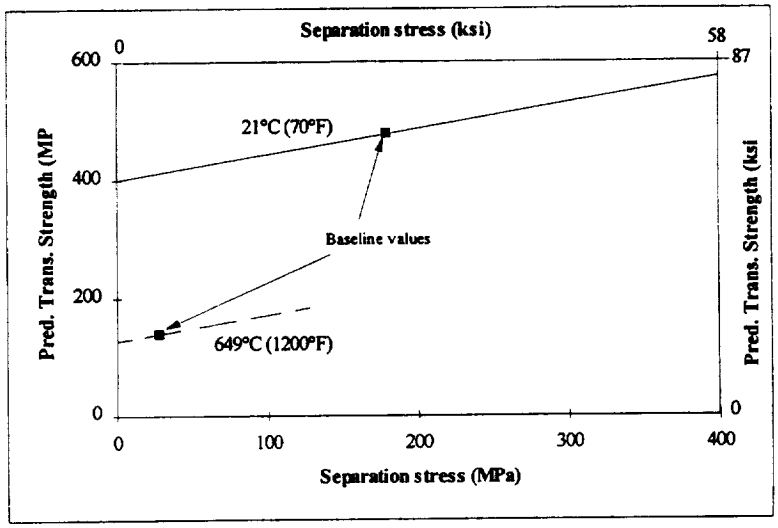

Figure 65 - Effect of separation stress on predicted transverse strength of Sapphire/NiAlFe

Table 21 - Predicted and experimental apparent fracture toughness of Sapphire/NiAl

Fracture toughness of Sapphire/NiAl, MPa$\sqrt{m}$ (ksi$\sqrt{in}$)		
M-C[8] bridging	P-T[9] bridging	Experiment
7.3-8.1 (6.7-7.3)	8.6-10.2 (7.9-9.2)	7.8 (7.1) 9.6 (8.8)

3.4.5.2 Sapphire/NiAlFe System

Since the NiAlFe matrix was fairly ductile, it was not clear whether fiber bridging or local matrix plasticity was a more likely energy absorption mechanism during fracture. So both mechanisms were considered. The resulting predictions are compared with experimental data provided by GE in Table 22. Agreement with experiment was again encouraging.

Table 22 - Predicted and experimental apparent fracture toughness of Sapphire/NiAlFe

Fracture toughness of Sapphire/NiAlFe, MPa$\sqrt{m}$ (ksi$\sqrt{in}$)			
M-C[8] bridging	P-T[9] bridging	P-T[9] plasticity	Experiment
48.0 (43.7)	51.0 (46.4)	58.4 (53.1)	51.7 (47.0) 61.5 (56.0) 61.3 (55.8) 55.4 (50.5)

3.4.6 Crack Growth Direction

The direction of crack extension out of a crack that is initially perpendicular to the fibers under uniaxial longitudinal loading was predicted using the Normal Stress Ratio (NSR) model. The crack was selected to be an arbitrarily small length [2.54 mm (0.1 in)]. The strength inputs to the model were taken from the experimental data.

3.4.6.1 Sapphire/NiAl System

For the baseline properties of the NiAl system, the predicted crack growth direction was ±73°. This crack behavior is shown schematically in Figure 66. This type of behavior is beneficial to composite toughness, as it should result in little fiber breakage and substantial crack deflection. Since the NiAl system behaved like a strongly bonded system in transverse loading, the predicted crack growth direction (which is highly dependent on transverse strength) should be fairly insensitive to interfacial effects.

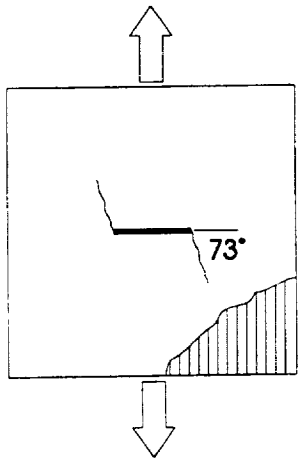

Figure 66 - Predicted direction of crack growth in Sapphire/NiAl composite

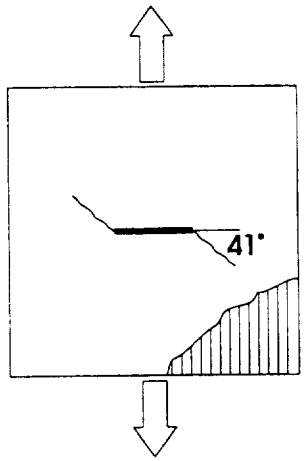

Figure 67 - Predicted direction of crack growth in Sapphire/NiAlFe composite

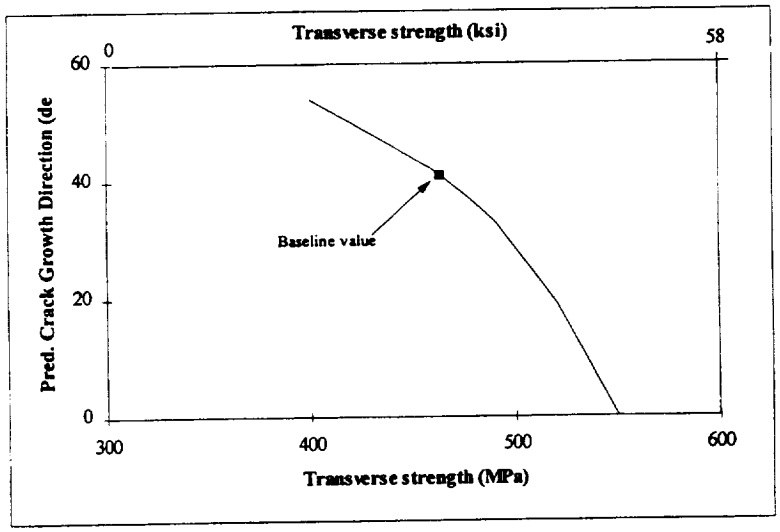

Figure 68 - Effect of varying transverse strength on predicted crack growth direction in Sapphire/NiAlFe

3.4.6.2 Sapphire/NiAlFe System

For the baseline properties of the NiAlFe system, the predicted crack growth direction was ±41°. This crack behavior is shown schematically in Figure 67. This type of behavior could result in a fair amount of fiber breakage, which is disadvantageous for developing composite toughness. Since the NiAlFe system appears to debond prior to transverse failure, the crack direction is fairly sensitive to interface strength. The variation of predicted crack growth direction with the range of expected transverse strengths (from immediate separation to no separation) is shown in Figure 68.

4. DISCUSSION

4.1 Fabrication/Material Quality Issues

The fibers in the samples from both the MMC systems appeared fragmented or at least weakened as-fabricated. The fiber digestion indicated typical fibers lengths considerably less than the full ingoing fiber length. The metallographic observations did not entirely support this observation. In metallographic sections, fiber breaks in the NiAlFe system could be seen (Figure 27), but fiber breaks were not apparent in the NiAl system (Figure 25). This combination of observations suggests that the fibers may not have been actually fractured but simply weakened by the consolidation. This hypothesis is supported by a larger body of experience from coated MMC in the NASA EPM program where it was proposed that twinning in the single crystal sapphire under the compressive thermal cooldown stresses would weaken the fiber in any subsequent tensile loading. The larger extent of fiber damage in the NiAlFe matrix composites tends to support the role of residual stresses, since the higher matrix strength and lower fiber fraction both contribute to higher fiber stress. Quantitatively, the axial fiber stress can be quite high, as shown by the residual stress modeling, Figure 57, with an axial fiber stress of nearly -900 MPa in the NiAlFe composites and nearly -300 MPa in the NiAl composites.

Certainly the observation of broken or weakened fibers in these samples should not be interpreted as an indictment of fabrication care or quality, since fabrication of uncoated sapphire fiber composites by both GE and NASA has produced good extracted fiber strengths. It is rather an indication of a generic fabrication issue associated with coated sapphire fibers in nickel-base matrices. While careful study beyond the scope of the present program is required to identify the exact causes and remedies for the problem, it is apparent that significant changes in materials or fabrication methods are required.

4.2 Model validation

The models selected for study in this program generally proved to be useful and capable of predicting at least the proper trend and magnitude of the property changes with constituent material changes. Comments on each of the models follows:

4.2.1 Residual stress

While finite element models have proven to be highly accurate in thermal stress modeling, little loss of accuracy is suffered and considerable convenience is obtained through the use of a concentric cylinder model. Actual measurement of residual stresses in nickel base systems has demonstrated either to be satisfactory. This is the only model that does not require an interface strength parameter, since the radial interface stresses from cooling from fabrication are compressive, the frictional forces generated make the interface behave as if it were well-bonded.

4.2.2 Matrix Cracking

The model of Lu et al. (1991) correctly predicted the lack of matrix cracking from cooldown in both systems. However, the systems chosen did not critically test the model

since they were relatively far from the critical levels predicted to be necessary for cracking. There is some ambiguity about how to incorporate the effect of plasticity, but it seems appropriate to use the actual (as relieved by plasticity) thermal stresses rather than the pseudo-elastic ones.

4.2.3 Longitudinal Strength

In order for the longitudinal strength models investigated to give reasonable correlation with the experimental values it was necessary to use degraded fiber strength values. Since these were not determined in this program, the data from Bowman (1993) on extracted sapphire fibers were used. Given the relatively short lengths and/or wide strength variation in the fibers it is not surprising that a statistical type model such as Curtin's compared more favorably the experimental data than did the Rule of Mixtures, which is applicable to continuous fiber systems. Even so, poor agreement with both models was obtained in the NiAl MMC's (Table 17). This suggests that failure was by more of a weak-link mode (early fiber failures lead to specimen fracture) than by the damage accumulation mode (multiple fiber breaks build up to a gradual loss of load-carrying capability) assumed by Curtin. It seems probable that the strong interfacial bonding in these composites would contribute to such behavior: in a brittle matrix system (NiAl) early matrix or fiber failures would tend to propagate unchecked through adjacent fibers, leading to low composite strength. Indeed, control of interface strengths to modest levels in ceramic composites is key to obtaining good tensile properties. In the more ductile matrix system (NiAlFe) matrix plasticity tends to reduce the local crack tip stress levels and inhibit rapid propagation of local cracks.

In this light it is somewhat surprising that the NiAl MMC do not have better high temperature strength where the matrix should be ductile. Part of the reason for the poor 650C longitudinal tensile strength of the NiAl system may lie in the observation of cleavage-like fracture behavior and general lack of evidence of ductility in the matrix. It is possible that the actual matrix material is less ductile/tough than assumed from the unreinforced matrix data used in the models. The source of such ductility degradation is unknown.

4.2.4 Transverse Strength

The transverse strength model gave good predictions of transverse strength for both materials assuming that the interface bond strength was weaker than the matrix (that is, the fiber carried no significant load). Note that studies in the NiAlFe system (Figure 64) suggested that the sensitivity of transverse composite strength to interfacial strength was not high, ranging from 400 MPa for an interface bond strength of 0 to 600 MPa for a bond strength of 400 MPa. However, the application of weak bond models to transverse strength is contrary to the fractographic observation of good bonding in the tested transverse samples, and the high interface strengths obtained in pushout testing. Since the transverse tension fracture paths were observed to pass through and not around the fibers, it appears likely that fiber fracture was the initiation event for transverse fracture; i.e., that the fibers failed first, eliminating their load carrying capability. These early failures may be related to edge cutting damage in specimen preparation. The specimen

load would then be thrown onto the remaining matrix cross section, so that the model of Equation (18) still applied, although for different reasons than originally anticipated.

4.2.5 Toughness

The toughness of these systems appeared to be dominated by the matrix toughness, and this was reflected in the model predictions. Due to the relatively small fiber volume fractions (large matrix fractions) this is not surprising. In the NiAl system only a modest (approximately 2-4 MPa$\sqrt{m}$) contribution from fiber pullout was predicted. This is due to the high interfacial shear strengths and short predicted pullout lengths. In the NiAlFe system, the addition of fiber pullout to the bulk matrix toughness contribution still fell short of the observed toughness, suggesting an additional contribution due to localized matrix plasticity. Better detailed observations and measurements of the fracture process are required in order to effectively sort out and quantify the contributions to toughness in these systems.

4.2.6 Crack Direction

The crack direction model showed the poorest agreement with experiment of all the models investigated. Both material systems were predicted to show significant deviations from 0^o, but in fact did not. Part of this discrepancy may have been due to the chevron notch geometry which constrains the crack to lie within the notch plane more strongly than assumed by the model. Also, the model used the bulk transverse strengths in determining the crack angle, and the transverse strength may be artificially degraded by fiber edge damage not present at the notch tip.

4.3 Guidance From Models For Material Development

4.3.1 Matrix Properties

Recommendations for matrix ductility, strength, and toughness can be inferred from predictions of the models examined in this program. Matrix ductility effects enter most discernibly through the residual stress and matrix cracking models. Sufficient matrix ductility is required to accumulate the residual thermal strains without cracking. Since the matrix residual strain is of the order $\Delta\alpha\Delta T$, and for sapphire and these matrices $\Delta\alpha \approx 6 \times 10\text{-}6/^oC$ and $\Delta T \approx 1200^oC$, the total thermal strain to be accommodated is about 0.75%. In actuality the local strains will be somewhat higher (due to concentrations) and strains from mechanically imposed loads also have to be tolerated. In titanium matrix composites the $\Delta\alpha\Delta T$ is about 0.6% while experimentally it has been observed than a matrix ductility of about 2.5% is actually required to suppress cracking and give full mechanical strength. Applying this empirical concentration factor of 4 to the nickel-base systems suggests that a matrix ductility of 3% is required for full composite strength.

Matrix strength requirements follow from the transverse strength models examined. In the weakly bonded or weak fiber strength models, transverse composite strength is expected to be about 1/2 that of the matrix. Since matrix strength generally decreases with increasing temperature, the matrix strength at peak (use) temperature will govern. This strength will be dictated by application and material layup. In nominally

unidirectionally loaded structures, most of the load will be carried in the fiber direction, but some nominal load carrying capability will be required for transverse and shear loads. Based on experience with polymer and carbon matrix composites, transverse or shear strengths below 35 MPa (5 ksi) give rise to significant problems in attachment. Thus the minimum matrix strength should be no less than 70 MPa (10 ksi). This strength value should be based on creep or fatigue strengths if these failure modes are the limiting ones in application.

Resistance to thermal cyclic fatigue also places requirements on matrix strength because if the matrix cycles inelastically during thermal excursions in use, then it is likely that the matrix will undergo fatigue failure. The tendency for cyclic yielding will be controlled by a combination of room temperature and elevated temperature yield strengths, so that approximately,

$$\Delta\alpha\Delta T \approx (\sigma_{RT}^{y} + \sigma_{ET}^{y})/E$$

Since $\Delta\alpha\Delta T$ = .6% for a use temperature of 1000C, E = 170 GPa, and σ_{ET}^{y} = 70 MPa (from above), this indicates that σ_{RT}^{y} needs to be $\geq$ 950 MPa (140 ksi).

Matrix toughness appears to be the dominant portion of composite toughness for well-bonded systems, so matrix toughness needs to be high enough to be adequate toughness for the application requirements. This in turn will be influenced by stress level and expected flaw size, but in view of the potential for occasional broken fibers in the composite, the expected flaw size should be at least equivalent to two adjacent broken fibers. In weak interface systems (not tested here), matrix toughness should be less important although still desirable.

4.3.2 Interface Properties

Definition and achievement of the proper interface for high temperature MMC remains a key issue. Prior work has demonstrated the inadequacies of weakly bonded interfaces in sapphire-reinforced NiAl MMC. The present program examined the behavior of strongly bonded interfaces in sapphire-reinforced NiAl and NiAlFe. That strong bonding was achieved by the introduction of a PVD YSZ coating is demonstrated by the high fiber push out strengths (170 to 330 MPa at RT and approximately 75% of that at 650C) and lack of interface separation in transverse tensile testing. Indeed, the strength levels achieved may be too strong, in terms of allowing some crack deflection capability for toughening. There is little to be gained from having the interfacial strength significantly greater than the matrix strength, since then the load transfer characteristics are limited by the matrix rather than the interface. The most stringent interface requirements probably come from the transverse strength requirements, since interfacial debonding will lead to loss of transverse strength. The interface is subjected to tension in this condition, and to achieve full matrix properties, the interface must be slightly stronger than the matrix. For the matrix strength requirements given above, this translates to an interface tensile strength of about 70 MPa (10 ksi) to achieve full transverse strength at peak temperature. (Strengths at lower temperatures may be less

than optimal with this interface strength, but usually the material properties are limiting at maximum temperature.) Since elevated temperature transverse tension tests were not performed in this study, it has not been verified here whether such interface strength levels could lead to adequate high temperature transverse composite strength. However, work in the EPM program has demonstrated improved transverse strength in ductile matrices with well bonded interfaces.

Interfacial shear strengths could actually be lower than those for tension since the lower shear strength can be somewhat compensated for in longitudinal tensile properties by a longer load transfer distance. Such a characteristic should be beneficial for toughness, however, it is unclear how the interface would be tailored to produce such a characteristic.

Additionally, of course, the interface has other requirements imposed by processing and long time stability: thermodynamic compatibility with the fiber, especially, and the matrix to a lesser degree, and oxidation resistance. These requirements severely limit the choice of interface coating materials.

4.3.3 Fiber Properties

While fiber properties were not the focus of this study, some hitherto unnoticed sapphire fiber characteristics have turned out to be important in the behavior of the materials fabricated here. The fiber must be capable of withstanding the residual compressive thermal stresses generated in cooling form fabrication (approximately 2400 MPa for a matrix with a RT yield strength of 1000 MPa) without damage. Alternatively, (and more beneficially) a fiber material with a higher thermal expansion must be identified to lower the thermal stresses on both the fiber and matrix. Also, to achieve transverse strength properties equivalent to those of the matrix, the fiber must have transverse strength equivalent to that of the matrix, at least at the peak temperature where properties are likely to be most limiting.

5. SUMMARY AND CONCLUSIONS

Based on the results presented in this report, a number of observations and recommendations can be made:

- The concentric cylinder model was useful for investigating the overall residual stress state of a composite after processing. This type of analysis was indispensable for gaining knowledge about interfacial clamping stress.

- The matrix cracking model used in this program appeared to provide accurate predictions regarding the integrity of fabricated composites. However, some clarity is needed regarding how to handle matrices which exhibit plastic response during cooldown.

- Rule-of-mixtures strengths should be attainable in a nickel-base composite provided there is not a large amount of induced fiber breakage. The longitudinal strength model should incorporate the statistical fiber strength properties, especially incorporating fiber strength after fabrication processing. The Curtin model appeared to be acceptable given the appropriate input data.

- The Cooper-Kelly equations for transverse strength provided accurate predictions. Knowledge of the fiber-matrix separation stress or fiber fracture stress was required, and can be obtained from experiment or estimated from the residual stress predictions.

- The Aboudi model was effective for predicting the stress-strain response of nickel-base composites. The model is only applicable in its current form until the first failure event. If the whole stress-strain curve is required, it may be necessary to modify the model to include damage effects.

- A modified rule-of-mixtures approach for predicting fracture toughness appeared to work quite well. It was necessary to incorporate additional energy-absorbing mechanisms to complete the calculation. This required some a priori knowledge of how the composite will fracture.

- The Normal Stress Ratio model was not a good indicator of how the composite strength parameters affected the tendency of cracks to deflect parallel to the fibers. The poor agreement of predictions and data may have resulted from the highly constrained chevron notch geomtery used.

- Considerable fiber damage was produced in consolidating these composites, similar to that experienced in other programs. The resistance of the fiber to thermal and mechanical processing stresses and/or the thermal expansion mismatch needs to be

significantly improved in order for nominal Rule of Mixtures longitudinal strengths to be achieved.

- A strong interface was achieved with the PVD YSZ coating applied to the fibers. While a moderately strong interface appears to be necessary for achieving acceptable mechanical properties, such benefits could not be demonstrated due to the fiber damage developed in these materials.

6. REFERENCES

Aboudi, J., "Elastoplasticity Theory for Composite Materials," *Solid Mechanics Archives*, Vol. 11, No. 3, 1986, pp. 141-183.

Bodner, S.R., "Review of a Unified Elastic-Viscoplastic Theory," in *Unified Constitutive Equations for Plastic Deformation and Creep of Engineering Alloys*, A.K. Miller (Ed.), Elsevier Applied Science Publishers, 1986.

Bowman, R.R., Noebe, R.D., and Darolia, R, "Mechanical Properties and Deformation Mechanisms of NiAl", *HITEMP Review 1989*, NASA CP 10039, Oct. 1989, pp. 47-1 to 47-15.

Bowman, R.R., Noebe, R.D., Doychak, J., Crandall, K.S., and Locci, I.E., "Effect of Interfacial Properties on the Mechanical Behavior of NiAl Based Composites", *HITEMP Review 1991*, NASA CP 10082, Oct. 1991, pp. 43-1 to 43-14.

Bowman, R.R, Misra, A.K., and Locci, I.E., "Unresolved Technical Barriers to the Development of a Structurally Viable Al_2O_3/NiAl Composite," *HITEMP Review 1993*, NASA CP 19117, Oct. 1993, pp. 57-1 to 57-12.

Buczek, M.B. and Herakovich, C.T., "Direction of Crack Growth in Fibrous Composites," *Mechanics of Composite Materials 1983*, AMD-58, (Dvorak, ed), ASME, 1983, pp. 75-82.

Cooper, G.A. and Kelly, A., "Role of the Interface in the Fracture of Fiber-Composite Materials," *Interfaces in Composites*, ASTM STP-452, ASTM Symposium, San Francisco, 23-28 June 1968.

Curtin, W.A., "Ultimate Strengths of Fibre-Reinforced Ceramics and Metals," *Composites*, Vol. 24, No. 2, 1993, pp. 98-102.

Hecker, S.S., "Elastic-Plastic Analysis of Composite Cylinders in Axial Tension," Ph.D. Thesis, Case Western Reserve University, 1968.

Lekhnitskii, S.G., *Theory of Elasticity of an Anisotropic Elastic Body*, Holden-Day Inc., San Francisco, 1963.

Lu, T.C., Yang, J., Suo, Z., Evans, A.G., Hecht, R., and Meherabian, R., "Matrix Cracking in Intermetallic Composites Caused by Thermal Expansion Mismatch," *Acta Metall. Mater.*, Vol. 39, No. 8, 1991, pp. 1883-1890.

Marshall, D.B. and Cox, B.N., "Tensile Fracture of Brittle Matrix Composites: Influence of Fiber Strength," *Acta Metallurgica*, Vol. 35, No. 11, 1987, pp. 2607-2619.

Nimmer, R.P., "Fiber-Matrix Interface Effects in the Presence of Thermally Induced Residual Stresses", *J. of Composites Techn ology and Research*, Vol. 12, 1990, pp. 65-75.

Noebe, R.D., Bowman, R.R., Cullers, C.L., and Raj, S., "Flow and Fracture of Binary NiAl with Prospects for Future Alloy Development", *HITEMP Review 1990*, NASA CP 10051, Oct. 1990, pp. 20-1 to 20-19.

Petrasek, D.W, "High Temperature Engine Materials Intermetallic Matrix Composites", *HITEMP Review 1988*, NASA CP 10025, Nov. 1988, pp.67-82.

Phillips, D.C. and Tetelman, A.S., "The Fracture Toughness of Fibre Composites," *Composites*, Sept. 1972, pp. 216-223.

Watson, G.K., Pickens, J.W., Noebe, R.D., Brindley, P.K., and Draper, S.L., "Intermetallic Matrix Composite Fabrication Development", *HITEMP Review 1988* NASA CP 10025, Nov. 1988, pp.215-223.

Williams, T.O., and Pindera, M-J, *Multiple Concentric Cylinder Model (MCCM) User's Guide*, NASA CR 195299, April 1994.

Wright, P.K., Sensmeier, M.D., Kupperman, D., and Wadley, H., "Thermal Stress Effects in Intermetallic Matrix Composites," *HITEMP Review 1991*, NASA CP 10082, Oct. 1991, pp. 45-1 to 45-14.

APPENDICES

Appendix I - Stress Intensity Solution for Chevron Notched Bend Specimen

The notched bend test data have been reduced to fracture toughness values, using a stress intensity solution for the non-standard chevron notched four point bend specimen estimated from the literature. Munz, et al (1) present a solution, partly in graphical form, for a chevron notched four point bend specimen using the straight-through crack approach:

$$K = (Y^*P)/(B\sqrt{W}) \quad (1)$$

where:

$$Y^* = Y[(\alpha_1-\alpha_0)/(\alpha_m - \alpha_0)]^{1/2} \quad (2)$$

$$Y = \{(S_1-S_2)/W\}\{3\sqrt{\alpha_m}/(2[1-\alpha_m]^{3/2}\} \times \{1.989-1.326\alpha_m-[3.49-0.68\alpha_m+1.35\alpha_m^2][\alpha_m][1-\alpha_m]/[1+\alpha_m]^2\} \quad (3)$$

$$\alpha_m = a_m/W, \text{ etc.} \quad (4)$$

and B is the width, W the height, a_0 and a_i the notch depths, S_1 is the major span, S_2 is the minor span, and P the maximum load as shown in Figure 3. a_m is the crack size at maximum load, which is found analytically by determining the α which minimzes Y. Munz shows α_m to be approximately 0.492 for $\alpha_0 = 0.083$ and $\alpha_1 = 0.668$, the nominal notch geometry used. When this value of α_m is substituted into Equations 3 and 2, Y* becomes 13.1.

Munz also presents an alternative solution to the same problem using the slice model. For these conditions, the slice model gives a Y* which is 20% lower for these conditions, or: Y* = 10.9. Without knowing which solution is more accurate, the two results were averaged:

$$Y^* = 12.0$$

This value of Y* was used to calculate the material toughness from Equation 1. These results are presented in Tables 8 and 12 in Sections 3.3.2 and 3.3.3.2, respectively.

Appendix 2 - Input Properties Used in Analyses

Sapphire Fiber

The properties of the Sapphire fibers as used in the modeling work are summarized below. The elastic and thermal properties were supplied by GE, while the statistical parameters are inferred from Bowman (1993).

Elastic modulus:
@ 21°C (70°F) 413.7 GPa (60.0 Msi)
@ 982°C (1800°F) 405.4 GPa (58.8 Msi)
@ 1316°C (2400°F) 346.8 GPa (50.3 Msi)
(Linearly interpolated at intermediate temperatures)

C.T.E. (instantaneous)

$$\alpha(\text{m/m/°C}) = 5.85\times10^{-6} + 8.250\times10^{-9}\,T - 3.440\times10^{-12}\,T^2$$
(where T in °C)

$$\alpha(\text{in/in/°F}) = 3.169\times10^{-6} + 2.584\times10^{-9}\,T - 5.898\times10^{-13}\,T^2$$
(where T in °F)

Fiber diameter: 127 μm (0.005 in)

Mean fiber strength:	As-received	@ 21°C (70°F)	3275 MPa (475 ksi)
		@ 649°C (1200°F)	2000 MPa (290 ksi)
	Degraded	@ 21°C (70°F)	1724 MPa (250 ksi)
		@ 649°C (1200°F)	793 MPa (115 ksi)
Weibull modulus: (L_o=2.54 cm [1 in])	As-received	@ 21°C (70°F)	8.8
		@ 649°C (1200°F)	4.1
	Degraded	@ 21°C (70°F)	4.2
		@ 649°C (1200°F)	2.5

NiAl Matrix

The elastic, thermal and yield properties used for the NiAl system were supplied by GE and are summarized in Table A.2-1. Linear interpolation was used between the temperatures shown.

Table A.2-1 - Elastic, thermal, and yield properties used for NiAl matrix

NiAl Matrix Properties				
Temp, °C (°F)	**E, GPa (Msi)**	**ν**	**α_{tan}, 1/°C (1/°F)**	**σ_y, MPa (ksi)**
21 (70)	193.1 (28.00)	0.3133	12.82 (7.12)	157.2 (22.8)
127 (260)	188.7 (27.37)	0.3156	13.37 (7.43)	133.8 (19.4)
227 (440)	184.6 (26.78)	0.3177	13.88 (7.71)	122.0 (17.7)
327 (620)	180.6 (26.19)	0.3199	14.36 (7.98)	115.1 (16.7)
427 (800)	176.4 (25.59)	0.3220	14.83 (8.24)	104.8 (15.2)
527 (980)	172.4 (25.00)	0.3242	15.26 (8.48)	102.0 (14.8)
627 (1160)	168.2 (24.40)	0.3263	15.68 (8.71)	95.2 (13.8)
727 (1340)	164.2 (23.81)	0.3285	16.09 (8.94)	82.1 (11.9)
827 (1520)	160.1 (23.22)	0.3306	16.45 (9.14)	80.0 (11.6)
927 (1700)	156.0 (22.62)	0.3328	16.81 (9.34)	77.2 (11.2)
1027 (1880)	151.9 (22.03)	0.3349	17.15 (9.53)	66.2 (9.6)
1538 (2800)	6.9 (1.00)	0.3459	18.50 (10.28)	6.9 (1.0)

Fracture toughness: @21°C (70°F) 4.4-6.6 MPa$\sqrt{m}$ (4-6 ksi $\sqrt{in}$)

Plasticity parameters: (Bodner model)

@21°C (70°F)
Z_0 = 227.5 MPa (33 ksi)
Z_1 = 248.2 MPa (36 ksi)
n = 10, m = 75, D_0 = 1

@649°C (1200°F)
Z_0 = 110.3 MPa (16 ksi)
Z_1 = 131.0 MPa (19 ksi)
n = 10, m = 75, D_0 = 1

NiAlFe Matrix

The elastic, thermal and yield properties used for the NiAlFe system were supplied by GE and are summarized in Table A.2-2. Linear interpolation was used between the temperatures shown.

Table A.2-2 - Elastic, thermal, and yield properties used for NiAlFe matrix

NiAlFe Matrix Properties				
Temp, °C (°F)	**E, GPa (Msi)**	**ν**	**α_{tan}, 1/°C (1/°F)**	**σ_y, MPa (ksi)**
21 (70)	141.3 (20.50)	0.32	4.61 (2.56)	592.3 (85.9)
204 (400)	141.3 (20.50)	0.32	11.12 (6.18)	542.6 (78.7)
427 (800)	133.1 (19.30)	0.32	14.80 (8.22)	471.6 (68.4)
538 (1000)	115.5 (16.75)	0.32	15.34 (8.52)	347.5 (50.4)
649 (1200)	71.0 (10.30)	0.32	15.88 (8.82)	198.6 (28.8)
871 (1600)	46.9 (6.80)	0.32	10.87 (6.04)	42.1 (6.1)
1316 (2400)	6.9 (1.00)	0.32	7.27 (4.04)	6.9 (1.0)

Fracture toughness: @21°C (70°F) 56.27 MPa$\sqrt{m}$ (51.21 ksi $\sqrt{in}$)

Plasticity parameters: @21°C (70°F) Z_0 = 655.0 MPa (95 ksi)
(Bodner model) Z_1 = 930.8 MPa (135 ksi)
n = 10, m = 75, D_0 = 1

@649°C (1200°F) Z_0 = 241.3 MPa (35 ksi)
Z_1 = 275.8 MPa (40 ksi)
n = 10, m = 75, D_0 = 1

Composite Systems

Some of the models required certain input parameters for the composite system in addition to the constituents.

The major Poisson's ratio, ν, of the composite was assumed to be 0.25 for any case. The longitudinal strength model required the interfacial friction. GE provided fiber push-out test data for the room temperature values, and the elevated temperature values were ratioed from these based on the residual clamping stress calculations. The final values used in the models were:

Sapphire/NiAl system: @21°C (70°F) τ = 260 MPa (37.7 ksi)
@649°C (1200°F) τ = 154 MPa (22.3 ksi)

Sapphire/NiAlFe system: @21°C (70°F) τ = 335 MPa (48.6 ksi)
@649°C (1200°F) τ = 50 MPa (7.3 ksi)

REPORT DOCUMENTATION PAGE

Form Approved
OMB No. 0704-0188

1. AGENCY USE ONLY (*Leave blank*)	2. REPORT DATE	3. REPORT TYPE AND DATES COVERED
	July 1995	Final Contractor Report

4. TITLE AND SUBTITLE

The Effect of Interface Properties on Nickel Base Alloy Composites

5. FUNDING NUMBERS

WU-505-63-12
C-NAS3-26501

6. AUTHOR(S)

M. Groves, T. Grossman, M. Sensmeier, and K. Wright

7. PERFORMING ORGANIZATION NAME(S) AND ADDRESS(ES)

GE Aircraft Engines
Cincinnati, Ohio

8. PERFORMING ORGANIZATION REPORT NUMBER

E-9769

9. SPONSORING/MONITORING AGENCY NAME(S) AND ADDRESS(ES)

National Aeronautics and Space Administration
Lewis Research Center
Cleveland, Ohio 44135-3191

10. SPONSORING/MONITORING AGENCY REPORT NUMBER

NASA CR-198363

11. SUPPLEMENTARY NOTES

Project Manager, S.M. Arnold, Structures Division, NASA Lewis Research Center, organization code 5220, (216) 433-3334.

12a. DISTRIBUTION/AVAILABILITY STATEMENT

Unclassified - Unlimited
Subject Category 24

This publication is available from the NASA Center for Aerospace Information, (301) 621-0390.

12b. DISTRIBUTION CODE

13. ABSTRACT ***(Maximum 200 words)***

This program was performed to assess the extent to which mechanical behavior models can predict the properties of sapphire fiber/nickel aluminide matrix composites and help guide their development by defining improved combinations of matrix and interface coating. The program consisted of four tasks: 1) selection of the matrices and interface coating constituents using a modeling-based approach; 2) fabrication of the selected materials, 3) testing and evaluation of the materials; and 4) evaluation of the behavior models to develop recommendations. Ni-50Al and Ni-20Al-30Fe (a/o) matrices were selected which gave brittle and ductile behavior, respectively, and an interface coating of PVD YSZ was selected which provided strong bonding to the sapphire fiber. Significant fiber damage and strength loss was observed in the composites which made straightforward comparison of properties with models difficult. Nevertheless, the models selected generally provided property predictions which agreed well with results when fiber degradation was incorporated. The presence of a strong interface bond was felt to be detrimental in the NiAl MMC system where low toughness and low strength were observed.

14. SUBJECT TERMS

Composites; Interfaces; Residual stresses

15. NUMBER OF PAGES

90

16. PRICE CODE

A05

17. SECURITY CLASSIFICATION OF REPORT	18. SECURITY CLASSIFICATION OF THIS PAGE	19. SECURITY CLASSIFICATION OF ABSTRACT	20. LIMITATION OF ABSTRACT
Unclassified	Unclassified	Unclassified	